CONSTRUCTION MATERIALS CONSULTANTS, INC.

Pyrrhotite Epidemic in Eastern Connecticut – A Case Study From Ellington, CT

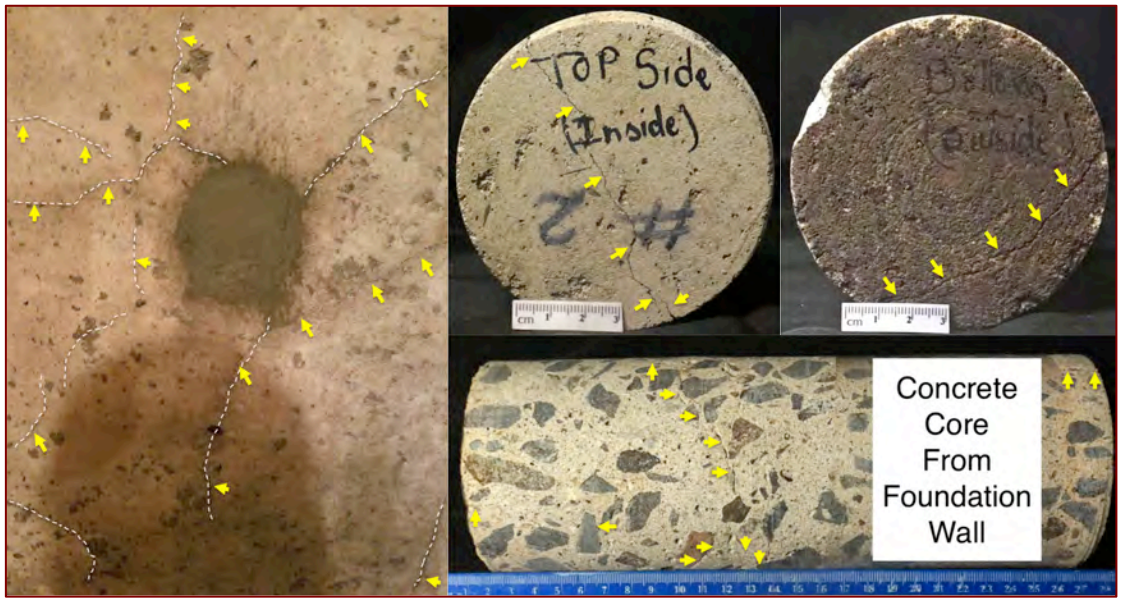

Cracking & Crumbling of A Residential Concrete Foundation In Ellington, Connecticut

January 2018
CMC Interim Report

TABLE OF CONTENTS

EXECUTIVE SUMMARY

Widespread outbreak of deterioration of many residential concrete foundations due to oxidation of an iron sulfide mineral 'pyrrhotite' in the quarried aggregate stones has occurred in the state of Connecticut with many thousands of homes being affected. Pyrrhotite (from Greek *pyrrhos* i.e. flame-colored or redness) commonly occurs in many mafic igneous, sedimentary, and metamorphic rocks, or in high temperature hydrothermal and replacement veins as a minor accessory mineral having a chemical formula of $Fe_{1-x}S$, where x varies from 0 to 0.125. It is commonly associated with pyrite (FeS_2) but is distinguished by its bronze rather than brass color of pyrite, its lower hardness, decomposition in HCl (Deer et al., 2008), lower S/Fe ratio, and weakly magnetic nature. All these features along with X-ray diffraction of rocks containing both iron sulfide minerals help to determine the pyrrhotite content, whereas XRF analysis of rocks determine the sulfur (as SO_3) content from all iron sulfide minerals. Currently, much of the information available on pyrrhotite-related concrete deterioration in northeastern Connecticut is limited to news media but the cause of deterioration has been attributed by an investigation conducted at the University of Connecticut (Wille and Zhong, 2016) as oxidation of pyrrhotite present in the coarse aggregate in the presence of moisture and oxygen in concrete. Manifestation of the damage has taken as much as 10 to 20 years. Typical visual deterioration is in the form of map cracking, some causing deformation of the wall, reddish-brown discoloration as rust stains, whitish formation of sodium sulfate salts (thenardite and mirabilite) in the vicinity of surface cracking, and in some severe cases crumbling of concrete. Most of the damage to date has been linked to aggregates supplied from one square-shaped quarry (Becker's quarry) in Willington, CT that sits in a weathered hydrothermal vein of metamorphic rocks containing significant pyrrhotite mineralization. The geology in the vicinity of the quarry is made up of metamorphic rocks predominately from two to three formations consisting predominantly of foliated schists and gneissic rock, granofels, and foliated quartz diorite. Quartz, plagioclase or oligoclase are primary minerals with micas, and noted are garnet and pyrrhotite as common accessory minerals. Most findings of concrete deterioration around the world due to pyrrhotite oxidation, including the ones in northeastern Connecticut (e.g., Moum and Rosenqvist 1959 from Norway, Tagnit-Hamou, et.al. 2005 and Rodrigues et al. 2012 from Canada, Oliveira, et al. 2014 from Spain, and Wille and Zhong, 2016 from USA) indicated the following two-stage mechanisms of distress due to: (a) primary expansions associated with oxidation of pyrrhotite in the presence of oxygen, moisture, and high pH in concrete to form ferric oxy-hydroxides, e.g., ferrihydrite [$Fe(OH)_3$] causing cracking of the unsound aggregates, followed by (b) secondary expansions from internal sulfate attacks by the sulfates released from pyrrhotite oxidation to cement hydration and carbonation products forming secondary ettringite and thaumasite, respectively causing further cracking in the paste. The former expansion is contributed from the pyrrhotite-bearing aggregates, whereas, the latter expansion is contributed from internal sulfate attacks within the confined spaces of the released sulfate-contaminated hydrated cement paste.

In light of this known problem of pyrrhotite in concrete aggregate from around the world, and particularly from the Becker's quarry in CT, and the resulting distress in many residential foundations in northeastern Connecticut, the observed map cracking and reported crumbling of a residential concrete foundation wall in Ellington, Connecticut i.e. within the known zone of 'pyrrhotite epidemic' has steered renewed concern of: (a) whether or not the deteriorated concrete foundation contains pyrrhotite in its aggregate, and, if detected, (b) if pyrrhotite has played the primary role for the observed cracking and crumbling as in the case of other cracked foundations.

As a result, a 10 in. long and 4 in. diameter concrete core drilled from over a visible map crack through the entire thickness of the foundation wall was retrieved, and provided for investigations of all possible causes for cracking, including the possible presence of pyrrhotite in concrete, and, its potentially deleterious role in concrete deterioration. Pyrrhotite's presence along with overall condition of concrete and aggregates were examined by detailed petrographic examinations (optical microscopy) *a la* ASTM C 856, whereas possible roles of pyrrhotite, its potential oxidation products and sulfate levels, and microstructures of deteriorated concrete around pyrrhotite-bearing aggregates are examined by scanning electron microscopy and energy-dispersive X-ray microanalysis (SEM-EDS) of multiple thin sections of concrete (*a la* ASTM C 1723), X-ray diffraction (XRD) and X-ray fluorescence (XRF) of multiple pyrrhotite-bearing coarse aggregate particles extracted from the concrete, and ion chromatography (IC *a la* ASTM D 4327) of extracted aggregate particles digested in a strong oxidant of 35% hydrogen peroxide solution for several days in an accelerated oxidation test, then diluted in distilled water to

determine levels of sulfates released by these aggregates in relation to a control aggregate without any iron sulfide mineral. Detection of pyrrhotite by optical microscopy and XRD, along with detection of its oxidation products by SEM-EDS and XRD, reaction microstructures and evidence of distress by SEM-EDS, and measurement of release of sulfate levels by IC have provided a good assessment of potential role of pyrrhotite in causing the observed distress.

Petrographic examinations have determined the concrete to be made using: (a) crushed stone coarse aggregate, which is a mixture of a predominant dark gray metamorphic garnetiferous quartzo-feldspathic and micaceous gneiss and a subordinate light brown quartz-feldspar-mica gneiss (having a higher quartz content than the dark gray gneiss) both having a nominal maximum size of $^{3}/_{4}$ in. (19 mm) showing the typical gneissose texture of alternating bands of quartz-albitic feldspar and micaceous (mostly biotite and less muscovite) minerals that often contain pyrope garnet poikiloblast; (b) natural siliceous sand fine aggregate having a nominal maximum size of $^{3}/_{8}$ in. (9.5 mm) and containing major amounts of quartz and quartzite, and subordinate amounts of feldspar, mica, ferruginous rock, and mafic minerals; (c) a hardened paste of Portland cement as the sole cementitious component having an estimated cement content of 6 to $6^{1}/_{2}$ bags per cubic yard and an estimated water-cement ratio (*w/c*) of 0.45 to 0.50, and (d) an estimated air content of 6 to 7 percent; the concrete is air-entrained.

Petrographic examinations detected severe cracking in the foundation wall core that is not only visible on both exposed faces of the wall, but also extended all throughout the entire thickness of the core (and foundation wall). Cracks are random, up to 1 mm in width, tapered down from the exposed faces of the wall to depths of 20 to 50 mm at least in the core examined, transected and/or circumscribed the crushed gneiss coarse aggregate particles, and shown pattern that cannot be formed by typical concrete shrinkage or settlement of the wall but more likely due to a chemical deterioration in line with the suspected expansions from oxidation of pyrrhotite-bearing aggregates and subsequent possible internal sulfate attack by the released sulfates in concrete. Irrespective of the mechanism(s), such severe and pervasive cracking of the wall is judged to be the reason for the reported crumbling of the foundation.

As mentioned, petrographic examinations detected two types of crushed gneiss coarse aggregate particles – (a) a dominant dark gray crushed gneiss that contains alternating bands of quartz-feldspar and micaceous (mostly biotite less muscovite) minerals (defining the gneissose texture) and pyrope garnet poikiloblast, and lesser quartz than the other (b) less predominant light brown crushed gneiss. Both gneiss types contained iron sulfide minerals (but more common in the predominant dark gray gneiss particles) as small equant to irregular-shaped to elongated particles with characteristic metallic luster appearance and optically opaque natures. Multiple lapped cross sections of core show many such iron sulfide inclusions mostly concentrated in the dark gray crushed gneiss and lesser in light brown coarse aggregate (probably due to more oxidation of sulfide in the latter) throughout the entire depths of the cross sections. Clearly, abundant iron sulfide mineralization in the quarried stone coarse aggregate is established in the concrete, as was reportedly found in many other foundations from the northeast CT that has shown pyrrhotite-oxidation related cracking.

XRD analyses of coarse aggregate particles extracted from the core have confirmed the iron sulfide minerals to be pyrrhotite, along with ferrihydrite as its oxidation product, which are, again, in line with previous findings from other deteriorated foundations (Wille and Zhong, 2016). XRD and XRF studies of both crushed gneiss types showed characteristic difference in mineralogy and chemistry between these types, e.g., having higher quartz in lighter brown particle, higher pyrrhotite in darker gray particles, higher iron oxide and sulfate in dark gray particle in XRF, etc. As high as in excess of 10 percent sulfur (SO_3) is detected in the dark gray crushed gneiss coarse aggregate, which is 10 times higher than the minimum 1 percent SO_3 limit by mass of aggregates established in many codes and guidelines. Light brown crushed gneiss showed 2 percent sulfur. XRD analyses showed as high as 8 percent pyrrhotite in the predominant dark gray crushed gneiss coarse aggregate.

Microcracking within many pyrrhotite-bearing crushed gneiss coarse aggregates due to pyrrhotite oxidation, often extending from unsound aggregates to paste is the first sign of distress due to primary expansion of unsound aggregate *per se* that are distinct in numerous photomicrographs of thin sections. Many times, microcracks simply followed the micaceous bands in gneiss due to the internal plane of weakness along the micaceous bands of gneissose-textured rock. The gneissose texture of crushed gneiss coarse aggregate particles consisting of

alternating bands of denser quartzo-feldspathic minerals and flaky (cleavable) biotitic mica provided additional inherent planes of weaknesses (foliation) in the aggregate that are susceptible to develop cracking along the internal planes of weakness along the biotite bands during expansions from pyrrhotite oxidation. As a result, a lot of cracks within the gneiss coarse aggregate particles are found along the weak bands of mica flakes. In many particles, however, no such preferential path of aggregate cracking is noticed.

Petrographic examinations also detected abundant secondary ettringite crystallization lining or filling many air voids and occasionally lining some microcracks that are indicative of prolonged presence of moisture in the concrete during service, which is an essential pre-requisite for pyrrhotite oxidation. It also indicates availability of sulfates for ettringite crystallization, which, however, may or may not have necessarily derived from pyrrhotite oxidation since ettringite-filled air-voids are a very common microstructural feature in a concrete exposed to moisture without even any iron sulfide contaminant. Any Portland cement concrete exposed to moisture during service forms secondary ettringite deposits lining and filling air voids. To establish the source of secondary ettringite i.e. from Portland cement's sulfate and/or from oxidation of pyrrhotite-bearing aggregates require determination of sulfate levels in concrete i.e. if the level is higher than that expected from a typical Portland cement concrete where sulfate (as SO_3) content in cement is around 3 weight percent i.e. giving about 0.45 percent sulfate in concrete for a usual cement content of 15 percent by mass of a normal weight concrete. Excess sulfate in concrete above 0.45 percent from cement's contribution would then correspond to the pyrrhotite-aggregate source if no other sulfate source were present. To determine the sulfate (SO_3) level of bulk concrete, a thin slice of concrete was sectioned through the entire length of the core traversing the full thickness of the foundation wall and pulverized for XRF analysis, which showed 1.45 percent bulk sulfate (SO_3) by weight of concrete, which is more than 3 times sulfate than that normally contributed from Portland cement. Clearly, some of the secondary ettringite crystallization in air-voids and microcracks were derived from sulfates other than Portland cement having the most likely source from oxidation of pyrrhotite in coarse aggregate.

To establish secondary expansion of paste from internal sulfate attacks by reactions between sulfates released from pyrrhotite oxidation and cement hydration products, microstructural evidence for expansion of the sulfate-contaminated hydrated cement paste has to be established. A common microstructural evidence of paste expansion commonly attributed to delayed ettringite formation (DEF) in many steam-cured precast concrete elements is gaps or separations around aggregates due to direct expansion of paste relative to aggregate (Jana 2008), where widths of the gaps are usually proportional to the size of the aggregates around which the gaps are formed from paste expansion. Optical microscopy did not detect many such gaps around aggregates, or, similar features as found in many cracked precast concrete members deteriorated by delayed ettringite formation. Another feature common in sulfate attacks from internal or external sulfates is ettringite filled cracks, which is seen in the present concrete, especially in the interior cracked regions. Therefore, the possibility of paste expansion from an internal sulfate attack by reactions between excess (i.e. beyond cement's contribution) sulfates released from pyrrhotite oxidation and cement hydration products are diagnosed both by optical microscopy and subsequently by SEM-EDS.

However, the most interesting microstructural feature detected is poorly crystalline (perhaps some colloidal form) secondary ettringite in the confined (or relatively less dense) areas of paste than the well-formed acicular or fibrous secondary ettringite in voids or cracks. The former type i.e. poorly crystalline secondary ettringite in paste areas (called ettringite infested paste, EIP) are judged to be the breeding grounds for internal sulfate attack that have caused secondary expansion of paste, and associated cracking. The main mechanism of paste expansion from internal sulfate attack is judged to be not so much due to precipitation of secondary ettringite in voids and cracks but more due to formation of poorly crystalline ettringite in relatively confined areas in paste. Ettringite-lined voids or cracks are most probably the result not the cause of internal sulfate attack, whereas poorly crystalline ettringite in confined areas of paste (EIP) are the direct cause for expansion and cracking of paste and around aggregate-paste interfaces. EIP is directly responsible for high sulfate content of paste detected in SEM-EDS studies described below, which is the more powerful evidence for internal sulfate attack than simple secondary ettringite-filled cracks.

SEM-EDS studies found well-developed secondary ettringite crystallization mostly in air-voids and only occasionally in microcracks including in gaps around aggregates and at aggregate-paste interfaces, which are

more common microstructures of other DEF-distressed concretes. Most of the microcracks are empty, and gaps around aggregates due to paste expansion are not as frequent as in other DEF-affected concretes. However, EDS analyses of sulfate contents of paste are in the range of 4 to 6.5% (as SO_3), which are noticeably higher than less than 1% sulfate (SO_3) commonly found in the paste of a normal Portland cement concrete prepared using a Portland cement containing 3 percent sulfate at a similar water-cement ratio and cement content of the present core but containing no iron sulfide contaminant.

Clearly, high sulfate content of paste detected from EDS analyses is consistent with the ettringite-infested paste found in thin section photomicrographs during optical microscopy, as well as overall high bulk sulfate (SO_3) content of concrete, indicating sulfate release from pyrrhotite oxidation. SEM-EDS analyses found three different optically opaque iron species in gneiss, e.g., iron sulfide (pyrrhotite), oxidation products of pyrrhotite measured in the EDS as iron oxide (determined in XRD as ferrihydrite), and iron-titanium oxide (rutile and ilmenite). High sulfate content of paste, detection of poorly crystalline ettringite infested paste (EIP), high bulk sulfate content (1.45%) of concrete, yet the absence of abundant secondary ettringite in many microcracks and gaps around aggregates except more profuse crystallization in air-voids – all these chemical and microstructural features indicate that perhaps microcracking due to paste expansion by internal sulfate attack occurred from poorly crystallized ettringite or perhaps in a colloidal form within the confined spaces in paste i.e. in EIP which is not as frequently diagnosed even in SEM as in other DEF-affected concretes having well-crystallized delayed ettringite in cracks, gaps, and voids.

Therefore, this study shows clear microstructural evidence of (a) primary expansion of concrete due to oxidation of pyrrhotite in crushed gneiss coarse aggregate causing cracking within the unsound aggregate particles often extending into paste, and (b) secondary expansion of paste due to formation of poorly crystalline (perhaps also colloidal formed) secondary ettringite in relatively confined areas in sulfate-contaminated paste (called ettringite infested paste) that are the breeding ground for internal sulfate attack causing paste expansion and associated cracking. Relatively well-developed secondary ettringite in voids and few in cracks are judged to be the consequence of exposure of ettringite infested paste (EIP) to moisture during service causing dissolution and precipitation of secondary ettringite in open spaces.

In accelerated pyrrhotite oxidation test, multiple dark gray and light brown crushed gneiss coarse aggregate particles are extracted from the core, cleaned of adhered paste remains, crushed, then immersed in a 35% hydrogen peroxide (strong oxidant) solution for several days. Sulfates released from aggregates to the filtrates are measured (as SO_4^{-2}) in an anion exchange chromatograph. Two sets of each aggregate are measured at several days for two-week period. All particles show noticeable release of sulfates as opposed to no sulfate released from a control gneiss aggregate containing no pyrrhotite. The high pH environment of Portland cement concrete is also known to enhance pyrrhotite oxidation (Divet and Davy 1996).

All these studies have confirmed and provided clear mechanisms of the common consensus that the observed cracking and reported crumbling of concrete foundation wall is due to: (a) oxidation of pyrrhotite in crushed garnetiferous quartzo-feldspathic gneiss coarse aggregate particles in the presence of oxygen and moisture during service in concrete with the formation of ferrihydrite causing expansion of the unsound aggregates and formation of cracks from unsound aggregates to paste, which was then followed by (b) additional expansion in the paste from reactions between sulfates released from pyrrhotite oxidation and cement hydration products (internal sulfate attack) and formation of poorly crystalline or perhaps colloidal ettringite within the confined spaces in paste. Microcracks from the primary expansion of unsound aggregates are more frequent in this core than that from secondary expansion of paste by internal sulfate attack.

Based on this comprehensive case study, the following conclusions are drawn:

1. Observed cracking and reported crumbling of concrete foundation wall is determined to be due *oxidation of unsound pyrrhotite grains in crushed garnetiferous quartzo-feldspathic and biotitic gneiss coarse aggregate* particles in the presence of oxygen and moisture during service in concrete.

2. The host rock for pyrrhotite mineralization used as coarse aggregate in concrete is the predominant dark gray garnetiferous quartzo-feldspathic and biotitic gneiss having alternating bands of quartz-feldspar and micaceous (mostly biotite) minerals and garnet poikiloblast (i.e. containing inclusions) and lesser amounts of light brown gneiss having more quartz and less pyrrhotite than the dark gray stones. Amount of pyrrhotite grains, however, varied widely amongst different crushed gneiss particles, irrespective of the host rock mineralogy.

3. Sulfur (as SO_3) contents in the pyrrhotite-bearing crushed gneiss aggregates are from *2 percent in light brown gneiss to as high as 10 percent in predominant dark gray gneiss particles*, or perhaps even higher, giving a *total bulk sulfate (SO_3) content of 1.45 percent in the concrete, which is more than 3 times than sulfate in a normal Portland cement concrete without any iron sulfide contaminant*. As high as 8 percent pyrrhotite is found from XRD analysis of dark gray gneiss indicating significant pyrrhotite mineralization in the dark gray gneiss used as coarse aggregate.

4. Oxidation of pyrrhotite has formed *ferrihydrite* with an expansion of unsound crushed gneiss coarse aggregate causing extensive cracking in many particles having cracks extending from the affected particles to paste. The typical gneissose texture of quarried aggregates has facilitated crack formation during expansion due to the presence of inherent planes of weakness along the micaceous bands in gneiss. Reddish brown rust stain found in many distressed foundations are due to pyrrhotite (and also pyrite) oxidation and formation of iron oxy-hydroxides (e.g., goethite, limonite) and ferrihydrites. The present core, however, does not show any rusty brown discoloration from pyrrhotite oxidation, or popout from expansion of near-surface unsound pyrrhotite.

5. Evidence of pyrrhotite oxidation is confirmed from: (a) detection of ferrihydrite in XRD, and, (b) from SEM-EDS studies of lower than stoichiometric S/Fe ratio of many pyrrhotite grains (mostly <0.50) indicating advanced oxidation. Microstructural evidence of oxidation-related expansion of unsound aggregate is found from extensive cracking of many of these crushed gneiss coarse aggregate particles often extending into the paste.

6. Pyrrhotite oxidation has readily released sulfates and contaminated the Portland cement paste as detected from high (4 to 6.5%) sulfate contents in the SEM-EDS analyses of paste as opposed to normal less than 1% sulfate found in the paste of a Portland cement concrete containing no iron sulfide contaminants. Ready release of sulfate has promoted internal sulfate attack and subsequent secondary expansion of paste with additional cracking.

7. To determine the potential for release of sulfate in an oxidizing environment, five crushed gneiss coarse aggregate particles were carefully removed from the core, cleared of all adhered paste, crushed, and immersed in a strong oxidation (35% hydrogen peroxide) solution for various days, then filtered, diluted by distilled water, and the filtrates were then tested for sulfate contents by Ion chromatography. Results showed significant release of sulfate mostly within 3 days of immersion, even after service in concrete.

8. Sulfates released from pyrrhotite oxidation have reacted with cement hydration products (e.g., calcium hydroxide, calcium aluminate hydrate, calcium monosulfoaluminate) and formed poorly crystallize or perhaps colloidal form of ettringite within the confined spaces in paste with the resultant secondary expansion of paste and additional cracking within the paste and around aggregate-paste interfaces. Presence of excess sulfates, moisture, and open spaces of air-voids and cracks – all three conditions have facilitated dissolution and precipitation of well-crystallized fibrous secondary ettringite in voids and occasionally in cracks that were visible in optical microscopy and SEM analyses.

9. Evidence of internal sulfate attack in paste came first from the paste chemistry i.e. (a) very high sulfate (SO_3) content of paste from SEM-EDS studies, and then from various microstructural evidences in optical and scanning electron microscopy, e.g., (b) ettringite-infested paste containing poorly crystalline (perhaps some colloidal) form of ettringite, (c) well-formed secondary ettringite crystallization in aggregate-paste interfaces, microcracks, and air-voids, often due to moisture-induced dissolution of ettringite from ettringite-infested confined areas of paste and precipitation of relatively well-formed ettringite in voids and cracks, and (d) gaps between aggregates due to expansion of paste (more common in many other concrete distresses due to internal sulfate attack than the present one).

10. Relative roles of primary expansion of unsound aggregates due to pyrrhotite oxidation and secondary expansion of paste due to internal sulfate attack in the overall distress of foundation depend on various factors, e.g., proportion of pyrrhotite (and total available sulfate), moisture condition during service, consolidation and degree of impermeability of concrete to moisture ingress, etc.

11. In light of the observed severe cracking of the foundation wall all throughout the thickness, and its anticipated progress with potential worsening of condition with time, replacement of the wall is the only viable option with particular emphasis to avoid use of any aggregate from the subject quarry or elsewhere that contains pyrrhotite, at least anywhere near the amounts that have caused the cracking.

12. If the pyrrhotite-bearing crushed gneiss coarse aggregate found in this concrete was indeed from the Becker's quarry in Ellington, CT (as reported for other foundations undergoing similar pyrrhotite-oxidation-related distress), then due to the known geology of pyrrhotite mineralization in the hydrothermal vein in which this quarry is situated, and its known devastating effects when used in concrete from case studies of multiple homes (Wille and Zhong 2016) including the present one, use of crushed stone from this quarry for concrete aggregate should be abandoned, or should only be used after extensive evaluation of aggregates for the presence of pyrrhotite (e.g., from magnetic test, total sulfur test from XRF, XRD detection of pyrrhotite amount) and its potential release of sulfate in an accelerated oxidation test of aggregates.

13. Aggregate to be used in a new foundation from other quarries must be evaluated for the possible presence of any unsound constituents, including iron sulfide minerals, e.g., (a) from XRD analysis of quarried stones to detect the amount and speciation of iron sulfide minerals present, (b) from XRF analysis to detect the total sulfur (as SO_3) content of quarried stones, (d) from accelerated oxidation test to detect the rate and level of sulfates that can be released from aggregates, and (e) even from a magnetic test to separate weakly magnetic pyrrhotite grains from other non-magnetic iron sulfide minerals.

14. Since there is no industry specification on the threshold pyrrhotite limit above which potential for oxidation-related distress can occur, and, in fact as low as 0.3% pyrrhotite by mass of aggregate in the host rock has reportedly shown severe distress in concrete (e.g., in Quebec Canada), the best solution is to avoid aggregates containing pyrrhotite for its known damaging affects without further laboratory verification of its potential unsoundness in concrete (e.g., from expansion of mortar bar or concrete prism tests similar to those used for ASR-expansion).

INTRODUCTION

Reported herein are the results of detailed laboratory studies of a hardened concrete core reportedly retrieved from an existing foundation wall of a residential home located in Ellington, Connecticut. The concrete wall has reportedly shown *visible cracking* and *crumbling* that has warranted the investigation.

BACKGROUND INFORMATION

Figure 1 shows the Google street view of the subject house in Ellington, CT. Background information provided indicates "crumbling" of the foundation wall and associated visible cracking mostly as map cracking.

Due to the well-known widespread occurrences of similar map cracking in many residential foundation walls in the neighboring areas and towns from an alleged iron sulfide mineral, pyrrhotite ($Fe_{1-x}S$, x varies from 0 to 0.125) present as a minor constituent in the crushed stone coarse aggregate used in those concretes, it was also requested to determine the possible presence of pyrrhotite in this concrete core, and whether or not pyrrhotite, if detected, has caused the reported cracking and crumbling of the wall.

Figure 1: Google Street View of the subject house in Ellington, Connecticut.

FIELD PHOTOGRAPHS

Map Cracking in Concrete Foundation Wall

Figure 2: Field photographs showing cracking of the foundation wall, and the location on the wall from where the core for the present study was reportedly retrieved.

Figure 2 shows field photographs of the foundation wall that has exhibited random and closed polygonal-shaped map cracking. Figure 2 also shows location of the concrete core provided for this study from over a visible crack on the wall. From the total full-length retrieved thickness of the core, which is 10 in., as well as evidence of through depth cracking in the core, the foundation wall is determined to be 10 in. thick that has shown severe internal cracking. The observed cracking in the core is in conformance to the cracking of the foundation wall, which could also lead to the reported crumbling of concrete.

PURPOSE OF PRESENT INVESTIGATION

Based on the background information, the purposes of the present investigation, therefore, are to determine: (a) the composition, quality, and overall condition of concrete in the wall as represented by the core; and particularly (b) detection of any possible physical or chemical deterioration of concrete that may have contributed to the reported cracking or spalling of the foundation wall; and (c) detection of any pyrrhotite presence in the concrete aggregates, and, if such mineral has caused the reported distress due to its known deleterious effects on durability of concrete from other studies in the region.

METHODOLOGIES

OPTICAL MICROSCOPY (FOR OVERALL CONDITION OF CONCRETE AND AGGREGATES)

The core was tested and examined by following the methods of ASTM C 856 "Standard Practice for Petrographic Examination of Hardened Concrete." Details of petrographic examinations and sample preparation are described in Jana (2006). The steps of petrographic examinations include (Jana 2006):

i. Visual examinations of the core, as received to trace all visible cracks;
ii. Low-power stereomicroscopical examinations of as-received, saw-cut and freshly fractured sections, and lapped cross sections of core for evaluation of concrete composition, condition, extent of cracking, detection of iron sulfide minerals, etc.;
iii. Low-power stereomicroscopical examinations of air content and air-void system of concrete as well as detection of iron sulfide minerals (amount and distribution) in the lapped cross sections;
iv. Examinations of oil immersion mounts in a petrographic microscope for mineralogical compositions of specific areas of interest;
v. Examinations of un-treated and fluorescent-dye-mixed (to highlight open spaces, cracks, etc.) epoxy-impregnated treated lapped cross sections of concrete in a stereomicroscope for detailed compositional and microstructural analyses;
vi. Examinations of blue dye-mixed (to highlight open spaces, cracks, etc.) epoxy-impregnated large area (50 mm × 75 mm) thin sections of concrete in a stereomicroscope and a petrographic microscope for detailed compositional and microstructural analyses;
vii. Photographing sample as received, and during preparation with a digital camera and a flatbed scanner;
viii. Photomicrographs of four (4) full-length lapped cross sections and seven (7) thin sections of core taken with stereomicroscope and petrographic microscope, respectively to provide detailed compositional, microstructural, and mineralogical information of concrete;
ix. Detailed compositional, mineralogical, and microstructural examinations of concrete in a petrographic microscope from thin sections;
x. Selection of areas of interest in the thin sections for subsequent examinations in scanning electron microscope;
xi. A Nikon Eclipse 600 POL petrographic microscope attached to a Jenoptik Progres GRYPHAX high-resolution digital camera were used for petrographic examinations and collecting photomicrographs of thin sections of concretes (Figure 3). A Nikon SMZ-10A stereomicroscope (Figure 3) and an Olympus SZH stereo zoom microscope (equipped with transmitted polarizing light facilities) were used for examinations of fresh fractured and lapped sections and transmitted-light examinations of thin sections, respectively.

Figure 3: Optical Microscopy: Left - A Nikon Eclipse E600 POL polarizing (petrographic) microscope at left with reflected, transmitted, polarized-light, and fluorescent-light capabilities; Middle – An Olympus SZH reflected/transmitted/polarized-light Stereozoom microscope; and Right – A Nikon SMZ-10A Stereozoom microscope. All microscopes are equipped with Jenoptik Gryphax and Lumenera Infinity digital cameras.

X-RAY DIFFRACTION (FOR MINERALOGY OF UNSOUND AGGREGATE, IDENTIFICATION OF IRON SULFIDE PHASES & THEIR OXIDATION PRODUCTS)

A few crushed stone coarse aggregate particles containing metallic-lustered iron sulfide minerals (as detected from the core as received, and from its lapped cross section) were extracted from the core, pulverized, and used for X-ray diffraction to determine the sulfide species in the aggregate.

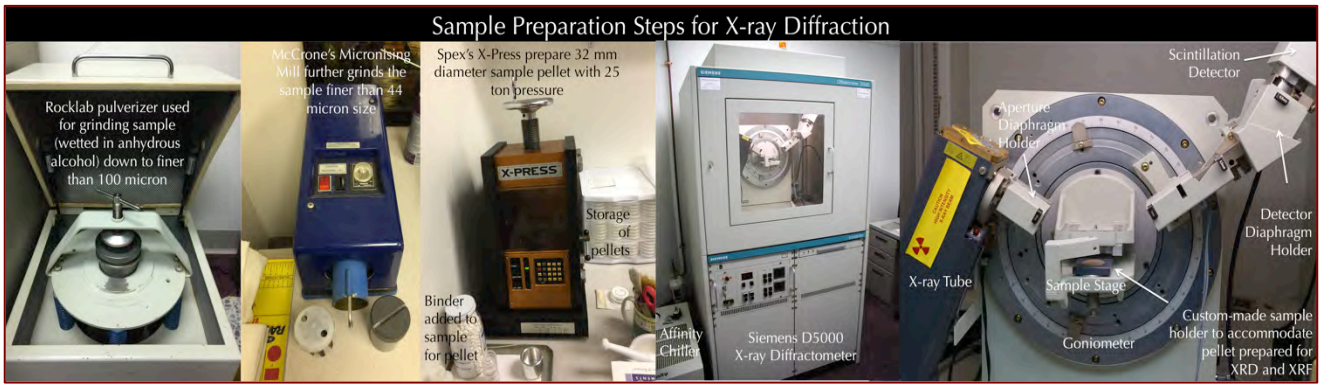

Figure 4: XRD: Siemens D5000 X-ray diffractometer and MDI Jade search/match software used for determination of mineralogical compositions of extracted concrete aggregates. Left to right: Rocklab pulverizer for initial grinding of aggregate with anhydrous alcohol; McCrone micronizing mill for final grinding; Spex 25-ton press for pellet preparation; Siemens D5000 X-ray diffractometer; and custom-made sample holder to place a 32-mm diameter pellet on sample stage.

A Rocklab pulverizer was used to grind the extracted aggregate particles down to finer than 100 microns. Usually, a few drops of anhydrous alcohol are added to reduce decomposition of any hydrous phases from the heat generated from grinding. Approximately 10 grams of sample was ground first in the Rockland pulverizer, from which about 8.0 grams of sample was selected, mixed with three binder tablets (total binder weight of 0.6 grams, for a fixed binder proportion of 7.5%), the mixture is then further ground in Rocklab pulverizer and in a McCrone micronizing mill down to finer than 44 micron size. Approximately 7.0 grams of binder-mixed pulverized sample thus prepared was weighed into a stainless steel die to prepare the sample pellet. A 25-ton Spex X-press was used to prepare 32 mm pellet from the pulverized sample. The same pellet is used for XRD to determine the mineralogy and XRF to determine the chemical composition.

X-ray diffraction was carried out in a Siemens D5000 Powder diffractometer (θ-2θ goniometer, Figure 4) employing a long line focus Cu X-ray tube, divergent and anti-scatter slits fixed at 1 mm, a receiving slit (0.6 mm), diffracted and incident beam Soller slits (0.04 rad), a curved graphite diffracted beam monochromator, and a sealed proportional counter. Generator settings used are 40 kV and 30mA. Sample was placed in a custom-made circular sample holder and excited with the copper radiation of 1.54 angstroms. Tests were scanned at 2θ from 4° to 64° with a step of 0.02° 2θ integrated at 1 sec. step^{-1} dwell time.

The resulting diffraction patterns were collected by DataScan 4 software of Materials Data, Inc. (MDI), analyzed by Jade software of MDI with ICDD PDF-4 (Minerals 2017) diffraction data. Phase identification, and quantitative analyses were carried out with MDI's Search/Match, Easy Quant, and Rietveld modules, respectively.

SCANNING ELECTRON MICROSCOPY AND ENERGY-DISPERSIVE X-RAY SPECTROSCOPY (SEM-EDS) (FOR MICROSTRUCTURE & COMPOSITION OF DETERIORATED CONCRETE & UNSOUND AGGREGATE)

Products of oxidation of iron sulfide minerals and associated possible secondary ettringite/thaumasite reaction products and reaction microstructures were examined in detail by SEM-EDS. Procedures for SEM examinations are described in ASTM C 1723.

Polished and gold-palladium coated thin sections of core already examined by optical microscopy were selected for SEM-EDS studies and examined in a Cambridge CamScan Series II scanning electron microscope equipped with a backscatter detector, a secondary electron detector, and x-ray fluorescence spectrometer (Figure 5) to observe pyrrhotite or other potentially unsound constituents in concrete and aggregate and their effect on the performance and durability of concrete, as well as evidence of internal sulfate attack and secondary ettringite formation in the paste from released sulfate.

Figure 5: SEM-EDS: Cambridge CamScan Series II Scanning Electron Microscope and 4Pi Revolution software, backscatter detector, secondary electron detector, and energy-dispersive X-ray fluorescence spectrometer used for microstructural and microchemical analyses of concrete and aggregate.

ENERGY-DISPERSIVE X-RAY FLUORESCENCE SPECTROSCOPY (ED-XRF) (FOR OXIDE COMPOSITION & SULFUR (SO_3) LEVEL OF UNSOUND AGGREGATE & CONCRETE)

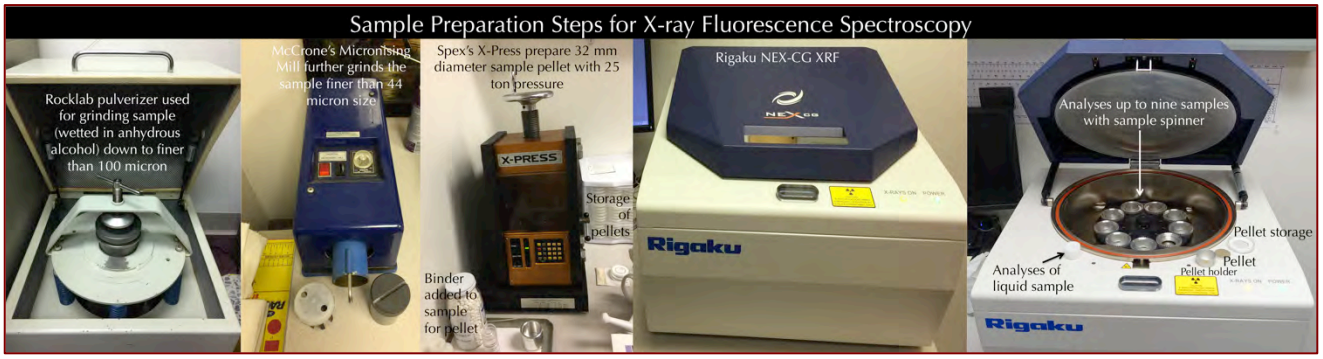

Figure 6: XRF: Rigaku NEX-CG bench-top ED-XRF unit used for bulk chemical compositions of aggregates.

An energy-dispersive bench-top X-ray fluorescence unit from Rigaku Americas Corporation (NEX-CG, Figure 6) was used for determination of bulk chemical (oxide) composition and sulfur (as SO_3) content of unsound

aggregate particles, and concrete. The instrument is calibrated by using various certified (CCRL, NIST, GSA, and Brammer) reference standards of rocks. The sample pellet prepared for X-ray diffraction is used for X-ray fluorescence studies as well. The main focus of this analysis was to determine the sulfur content (as SO_3) in the aggregate particles as well as sulfate content (as SO_3) in concrete.

ION CHROMATOGRAPHY (FOR RELEASED SULFATES FROM UNSOUND AGGREGATES)

Pyrrhotite-bearing coarse aggregate particles extracted from the core were pulverized to pass No. 20 sieve, then digested in a hydrogen peroxide (35%) solution for various days for accelerated oxidation, then filtered through 0.45-micron micro-filter paper under vacuum.

The filtrate was then diluted to 250 mL with distilled water to be analyzed by Metrohm's 861 Advanced Ion Chromatograph (Figure 7) for determination of released sulfates from oxidation of sulfides.

Procedures followed in Ion chromatography are described in ASTM D 4327 "Standard Test Method for Anions in Water by Chemically Suppressed Ion Chromatography." The IC was calibrated against six (6) different custom-made Metrohm anion standard solutions having sulfate from 0.1-ppm to 100-ppm levels.

Figure 7: IC: Metrohm 861 Advanced IC used for analysis of sulfate released from aggregate.

SAMPLE

PHOTOGRAPHS, IDENTIFICATION, INTEGRITY, AND DIMENSIONS

Figure 8 shows the exposed opposite ends of the core in the left column, representing opposite surfaces of the foundation wall (darker end is for the outside wall surface), and, the side views of the core in the right column, representing the total wall thickness. The core is 10 in. (255 mm) in total length, which is also the thickness of the wall at the core location, and $3^1/_2$ in. (90 mm) in nominal diameter.

END SURFACES

The opposite end surfaces of core (wall) are smooth flat formed surfaces of wall with the major cracks visible on both surfaces (Figure 8, left column). The smooth gray surface is the inside, and darker end is the outside surface of the wall.

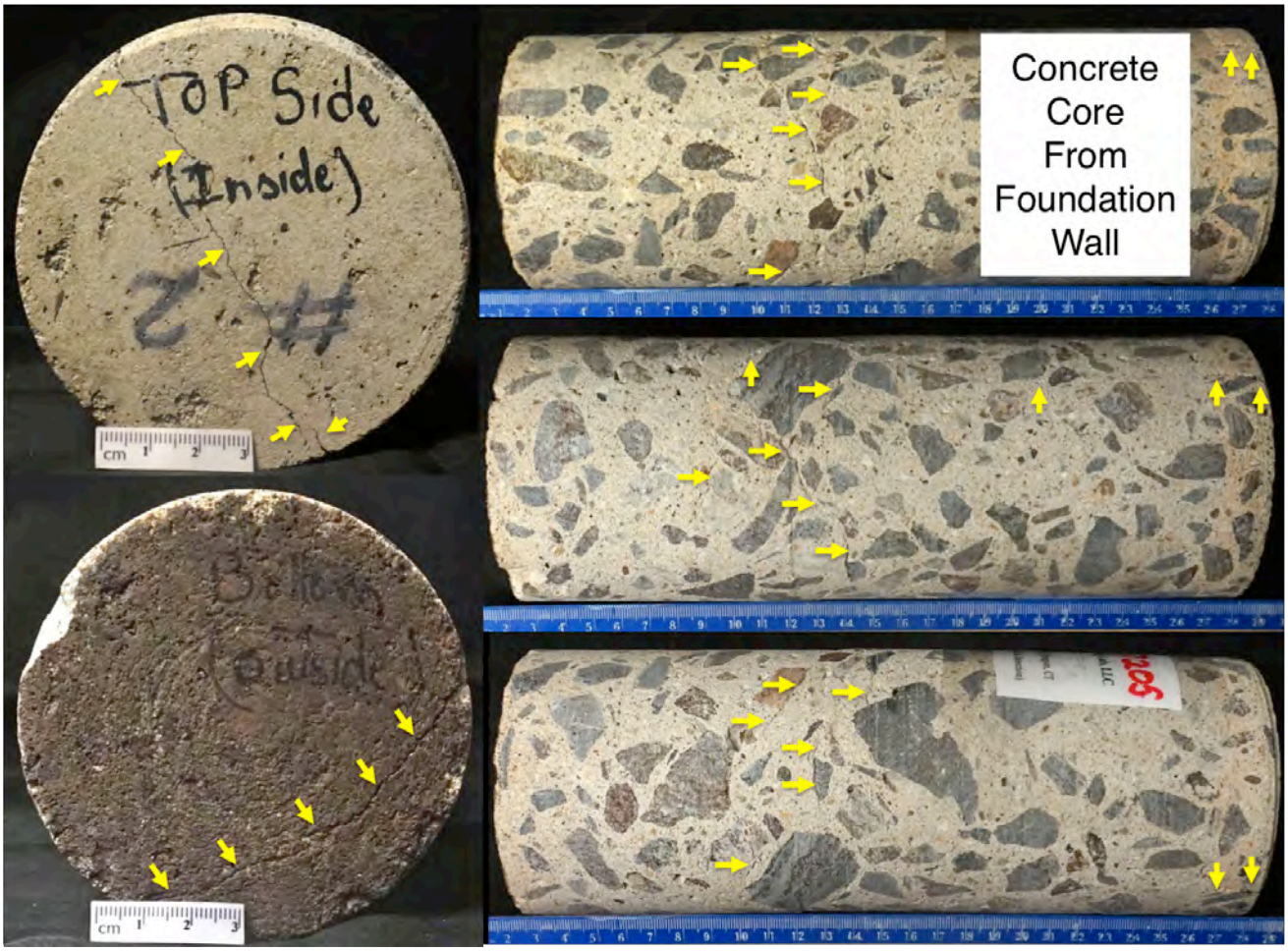

Figure 8: Shown are the formed end surfaces (left), and three cylindrical side views of the core (right), as received. Arrows in the right column indicate major cracks visible on the cylindrical side surfaces of the core, both parallel and perpendicular to the end surfaces. The core was rolled over a flatbed scanner to get three photos of the cylindrical surface.

CRACKING & OTHER VISIBLE DISTRESS

The core contains a major crack perpendicular to the end surfaces extending through the thickness of the core, and many other fine visible cracks that are marked with arrows on the end and cylindrical surfaces (Figure 8). Despite the visible cracks, the core was received in intact condition.

EMBEDDED ITEMS

There is no evidence of any fibers or other embedded items found in the core.

RESONANCE

The core has a ringing resonance, when hammered.

LABORATORY STUDIES

EXTENSIVE CRACKING IN LAPPED CROSS SECTIONS OF CORE

Figures 9 through 12 show four lapped cross sections of the core with the main purpose of highlighting all visible and invisible cracks after recognizing the cracks with the help of a stereo-microscope, tracing the cracks either with a black marker pen (Figures 9 and 11), or after treating the lapped sections with fluorescent dye-mixed epoxy and thereafter viewing under a short wave length ultraviolet light in a dark room (Figure 12).

Figure 10 shows the cracks that are already detected and marked with a black marker pen in Figure 9 but retraced the cracks again in red with the purpose of just showing the cracks for their abundance and distribution all throughout the length of the core, indicating extension of cracking through the full thickness of the foundation wall.

All lapped cross sections show extensive cracking of concrete in the foundation wall. Figures 9 through 12 show three types of cracks:

(a) One, visible on the end surfaces, oriented perpendicular to the exposed surfaces, and extended to depths of 20 mm to as deep as 50 mm;
(b) Second, are interior cracks situated away from end surfaces but in the body of the core that are short, discontinuous, transected and circumscribed the aggregate particles, and show patterns that are indicative of their formation at the hardened state of concrete;
(c) The third one is the major visible crack at the mid-depth location (marked in white dashed line in Figure 9), which was probably a pre-existing microcrack but re-activated during the coring operations to become macro crack.
(d) Image analyses of just the cracks in Figure 10 showed approximately 4.7 to 4.9 percent cracking in the two lapped sections.

Figure 12 shows fluorescent dye-mixed epoxy-impregnated lapped cross sections of core, where air-voids, cracks, and porous areas of paste were highlighted when viewed in a short-wave length ultraviolet light due to greater absorption of fluorescent epoxy compared to aggregates and denser areas of paste. Extensive cracking in the interior portion of the core (wall) is clear from this fluorescent epoxy treatment. Vertical cracks at the exposed surface ends of core (wall), horizontal cracks oriented parallel to the core ends, as well as many diagonal and random cracks are seen.

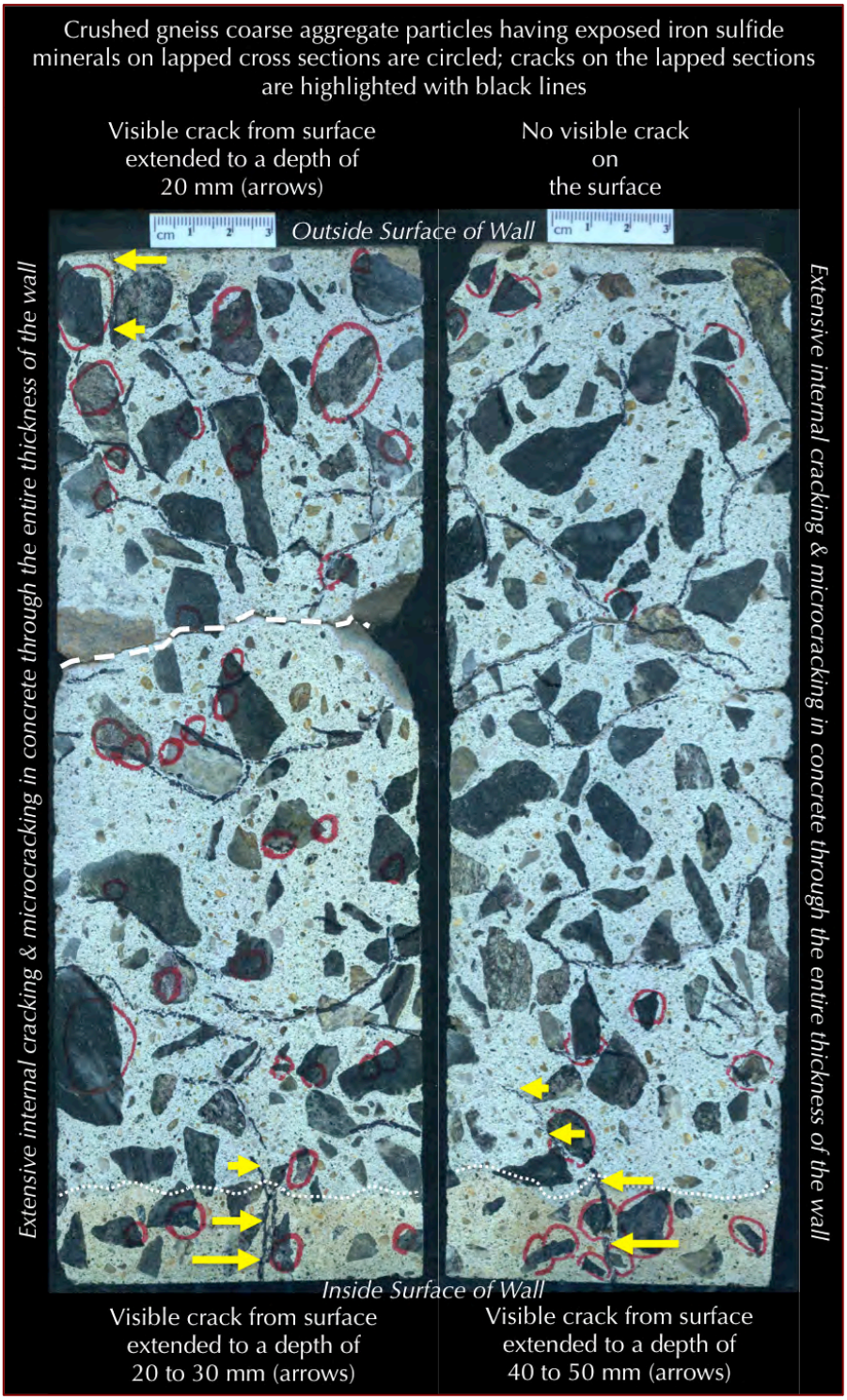

Figure 9: Lapped cross sections of the core showing: (a) extensive cracking all throughout the depth of the core (i.e. thickness of the wall) many of which are highlighted by black lines (see also Figure 10), (b) iron sulfide minerals in crushed stone coarse aggregate particles that show characteristic metallic luster, many of which are circled in red, (c) beige discoloration of concrete at the exposed surface ends due to atmospheric carbonation (white dotted line shows depth of advancement of carbonation into concrete), (d) visible surface cracking from both ends of the core (wall) that have extended to depths of 20 to 40 mm (marked by arrows at the ends), (e) a major crack at the middle probably formed from a pre-existing crack during coring and sectioning, and (f) the good grading and well-distribution of the crushed stone coarse aggregate particles.

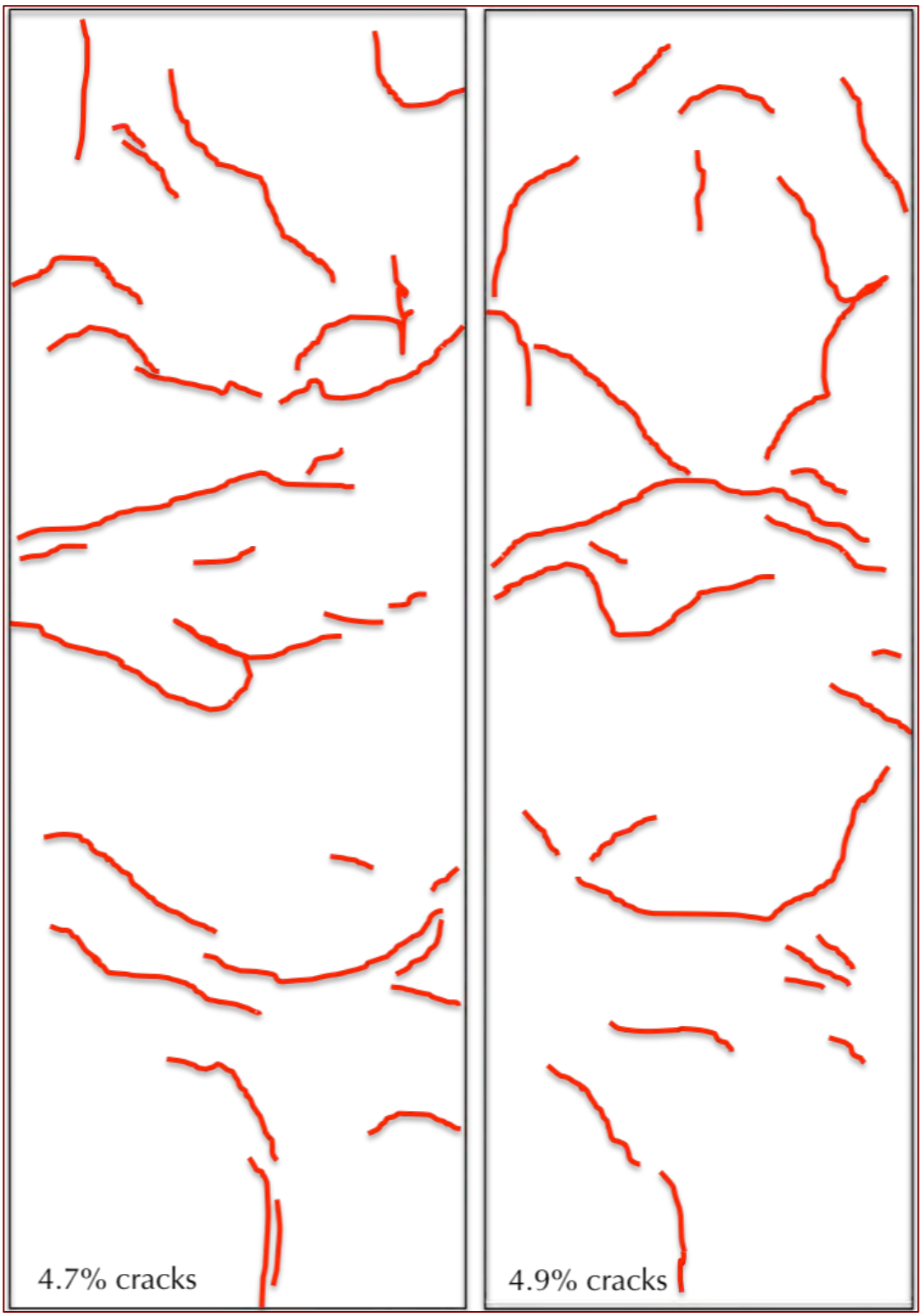

Figure 10: Crack traces and approximate crack volumes (calculated from ImageJ) on lapped cross sections of core from Figure 9 where cracks traced in black ink on the lapped sections are highlighted in this Figure in red. Individual cracks were first identified with the help of a Stereozoom microscope and traced on the lapped surface in black ink pen while examining under the microscope, thereafter cracks were re-marked in red for this Figure.

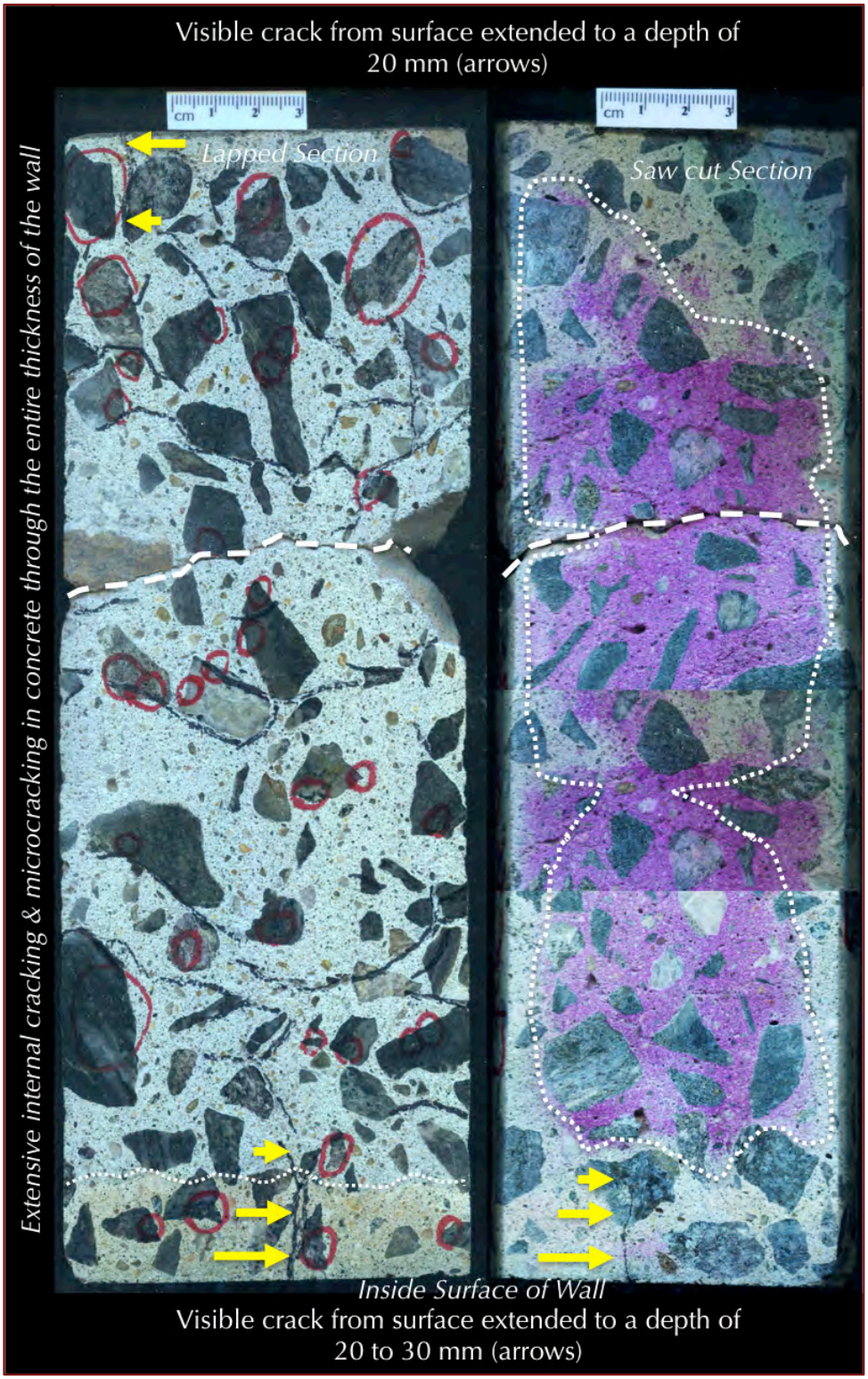

Figure 11: Lapped cross sections of the core showing the same features found in the previous Figure (in the left column), and corresponding extent of carbonation on the opposite saw-cut section after treatment with phenolphthalein alcoholic solution where carbonated portion remains colorless whereas non-carbonated interior turned pink (mostly within the dotted lines). Enclosed within red circles in the left column are iron sulfide minerals detected in crushed stone coarse aggregate particles; many visible cracks are traced in black ink.

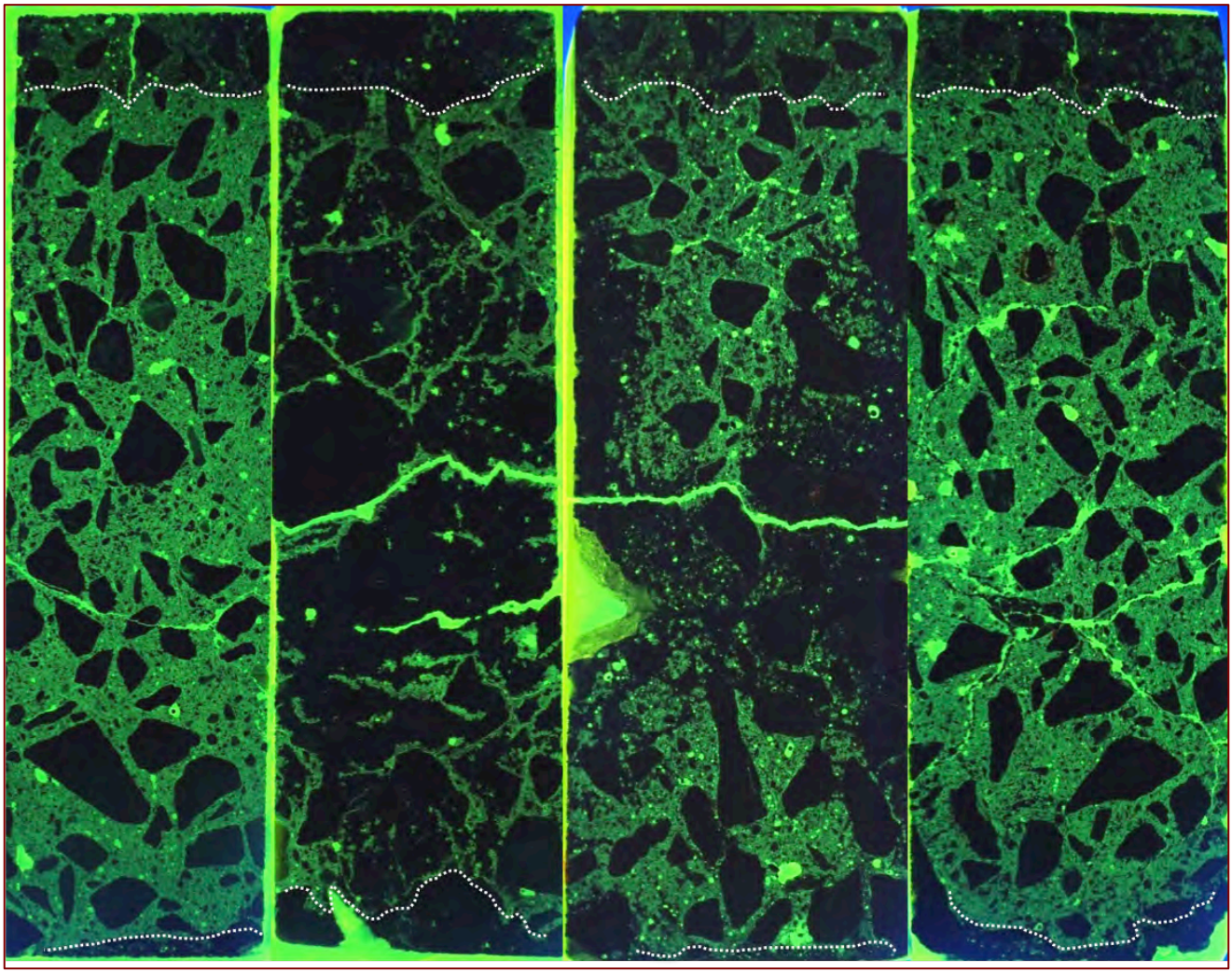

Figure 12: Lapped cross sections of core after treatment with a fluorescent dye-mixed epoxy and viewed in a short wavelength ultraviolet light in a dark room where cracks, air-voids, and open sapces and porous areas of concrete are highlighted in green to greenish-yellow (latter mostly in cracks and voids) as opposed to darker toned denser areas.

Figure 11 shows a saw-cut section before lapping but after treatment with phenolphthalein alcoholic solution to show non-carbonated nature of the interior concrete where the treated section turned pink in the right column of Figure 11 but carbonated portion remained beige to light grey color tone of paste. The dotted lines in Figure 11 enclosed the interior non-carbonated concrete from the carbonated end surface regions at the interior and exterior surfaces of the wall. Depth of carbonation is marked from beige discoloration of paste especially visible along the inside surface of the wall where carbonation has extended to a distance of 20 to 30 mm (marked by white dotted line parallel to the inside surface in Figures 9, 11, 12, and 13. Densification of paste due to carbonation at the exposed ends of the core (foundation Wall) is clear in these fluorescent sections.

IRON SULFIDE MINERALS IN CRUSHED GNEISS COARSE AGGREGATE

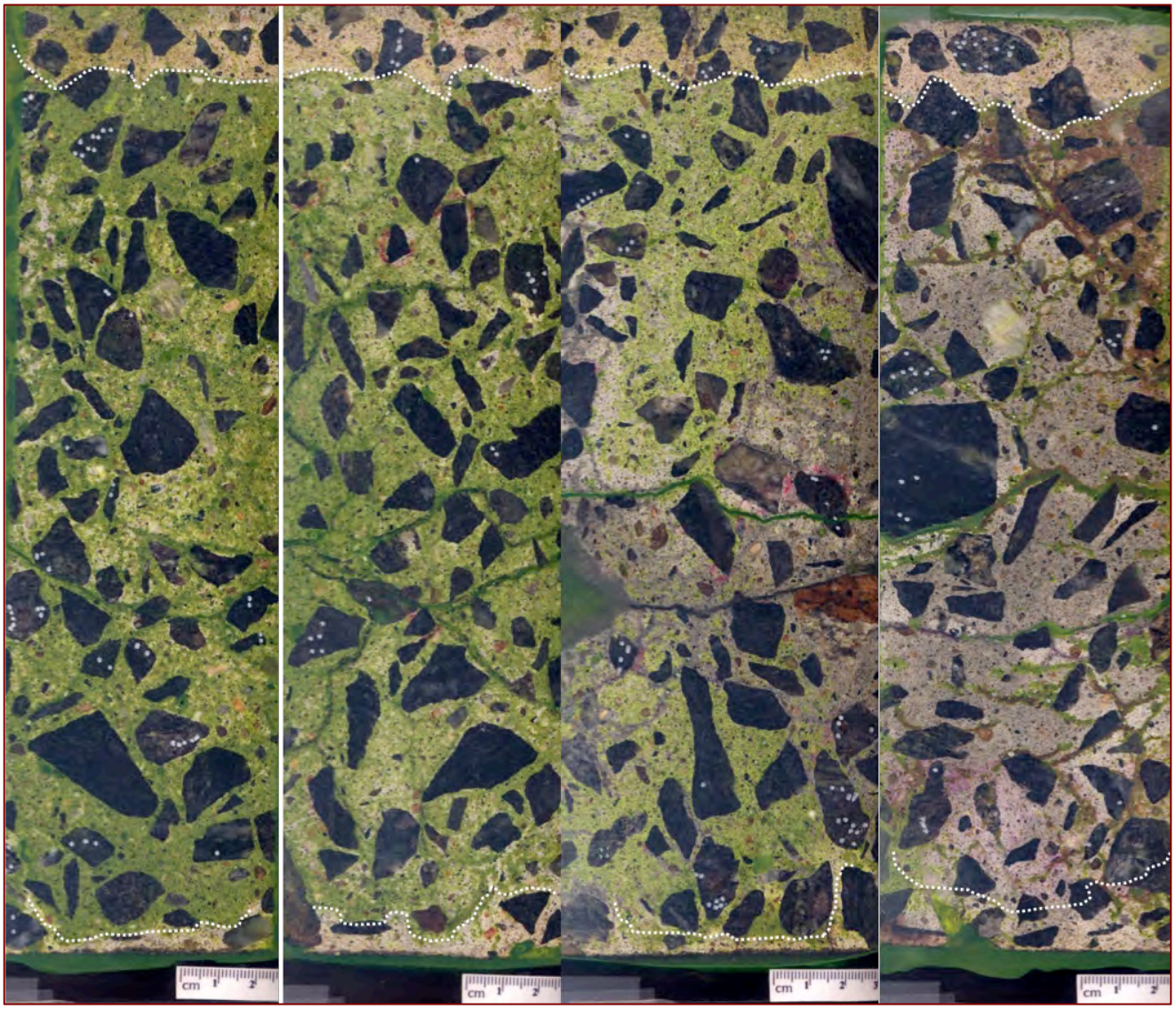

Figure 13: Lapped cross sections of core after treatment with a fluorescent dye-mixed epoxy and scanned on a flatbed scanner. Shown in this Figure are the amount and distirbution of iron sulfide (pyrrhotite) inclusions in crushed stone coarse aggregate where individual pyrrhotite grains are highlighted with a small silver 'dot.' Pyrrhotite-bearing aggregate particles are highlghted in red circles in Figure 9, but in this Figure they are first detected with the help of a stereo-microscope and then highlighted with a silver marker pen.

Small silver 'dots' marked on crushed stone coarse aggregate particles in the lapped cross sections of core in Figure 13 indicate significant amounts of iron sulfide minerals (detected from XRD to be pyrrhotite). Another interesting feature in Figure 13 is relative densification of paste along the beige discolored carbonated end surface regions of core causing lesser absorption of florescent dye compared to more porous (hence absorptive) interior body of concrete. Carbonation has apparently densified the concrete along the end surfaces but did not protect the surfaces from developing visible cracks due to internal expansion of concrete in the wall, as discussed later.

PHOTOMICROGRAPHS OF IRON SULFIDE MINERALS IN CRUSHED GNEISS COARSE AGGREGATE

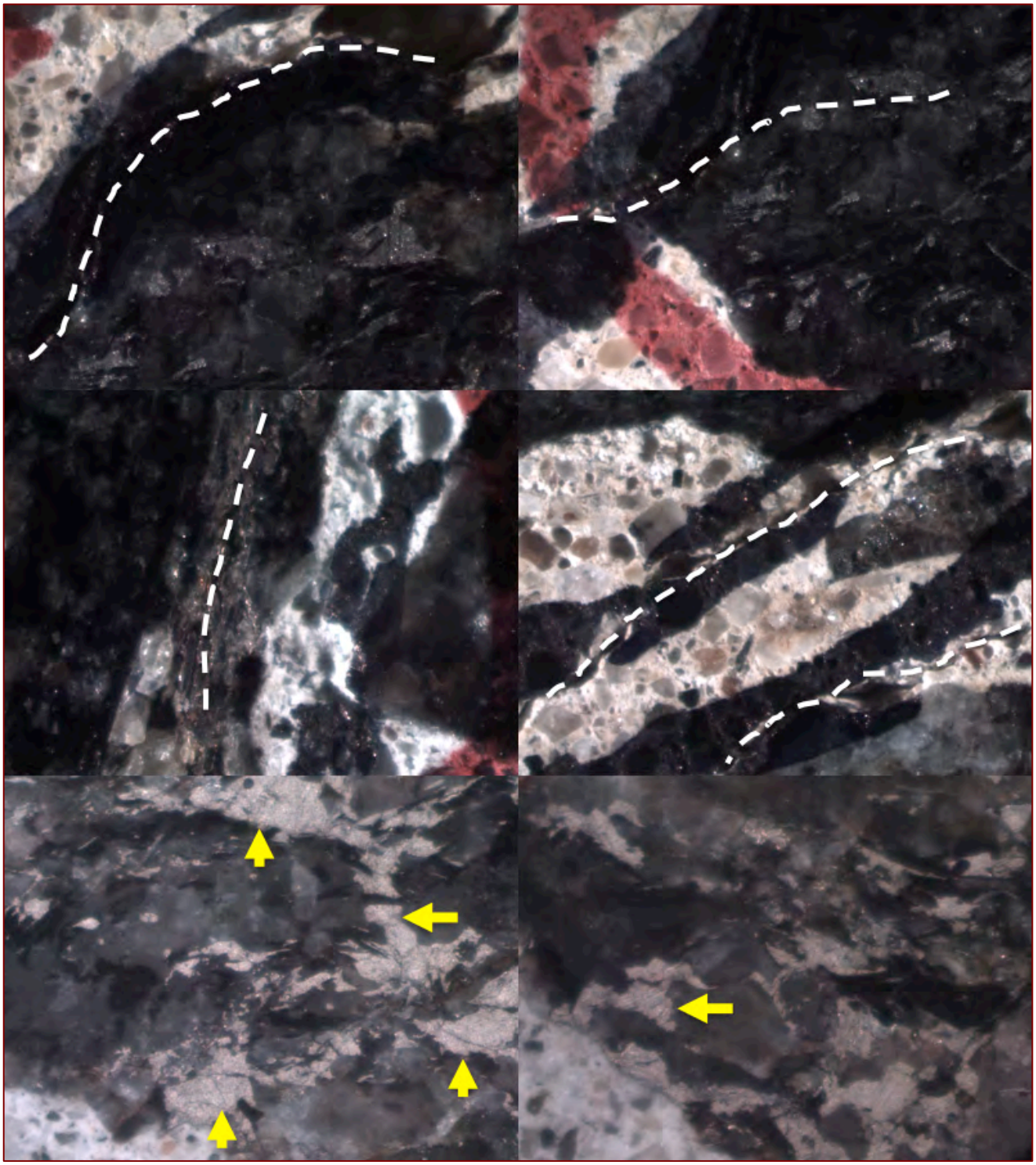

Figure 14: Photomicrographs of lapped cross section of core showing some iron sulfide minerals within crushed gneiss coarse aggregate particles that are identified by characteristic golden yellow metallic luster (some are marked with arrows), and some visible cracking in coarse aggregates (white dashed lines). Field width of each photo is 9 mm.

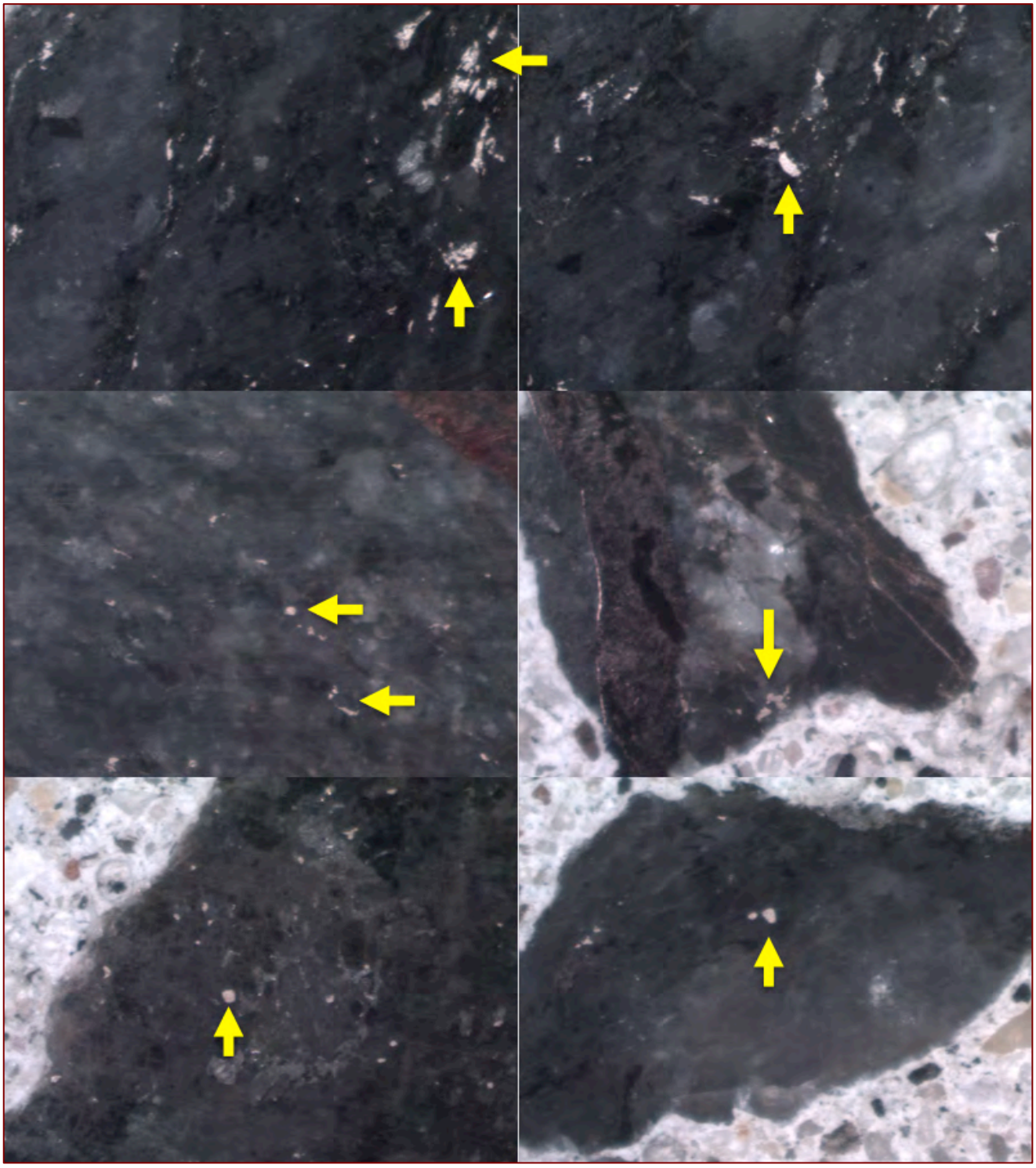

Figure 15: Photomicrographs of lapped cross section of core showing some iron sulfide minerals within crushed gneiss coarse aggregate particles that are identified by characteristic golden yellow metallic luster (some are marked with arrows). Field width of each photo is 9 mm. Amount of pyrrhotite is estimated to be 0.4 to 2.4 percent by volume of individual aggregate particles on lapped cross section (calculated by Image J).

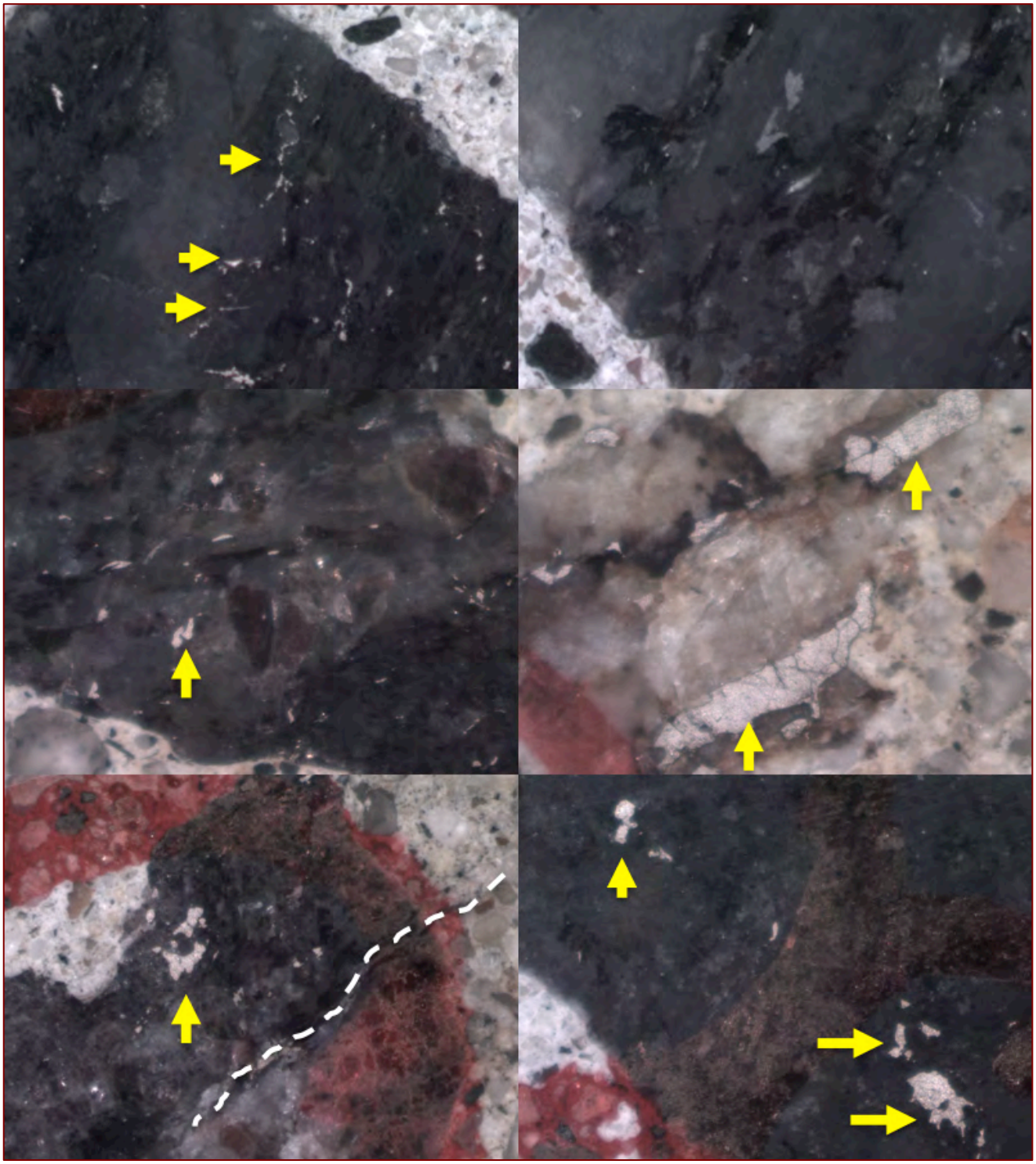

Figure 16: Photomicrographs of lapped cross section of core showing some iron sulfide minerals within crushed gneiss coarse aggregate particles that are identified by characteristic golden yellow metallic luster (some are marked with arrows), and some visible cracking in coarse aggregates (white dashed lines). Field width of each photo is 9 mm.

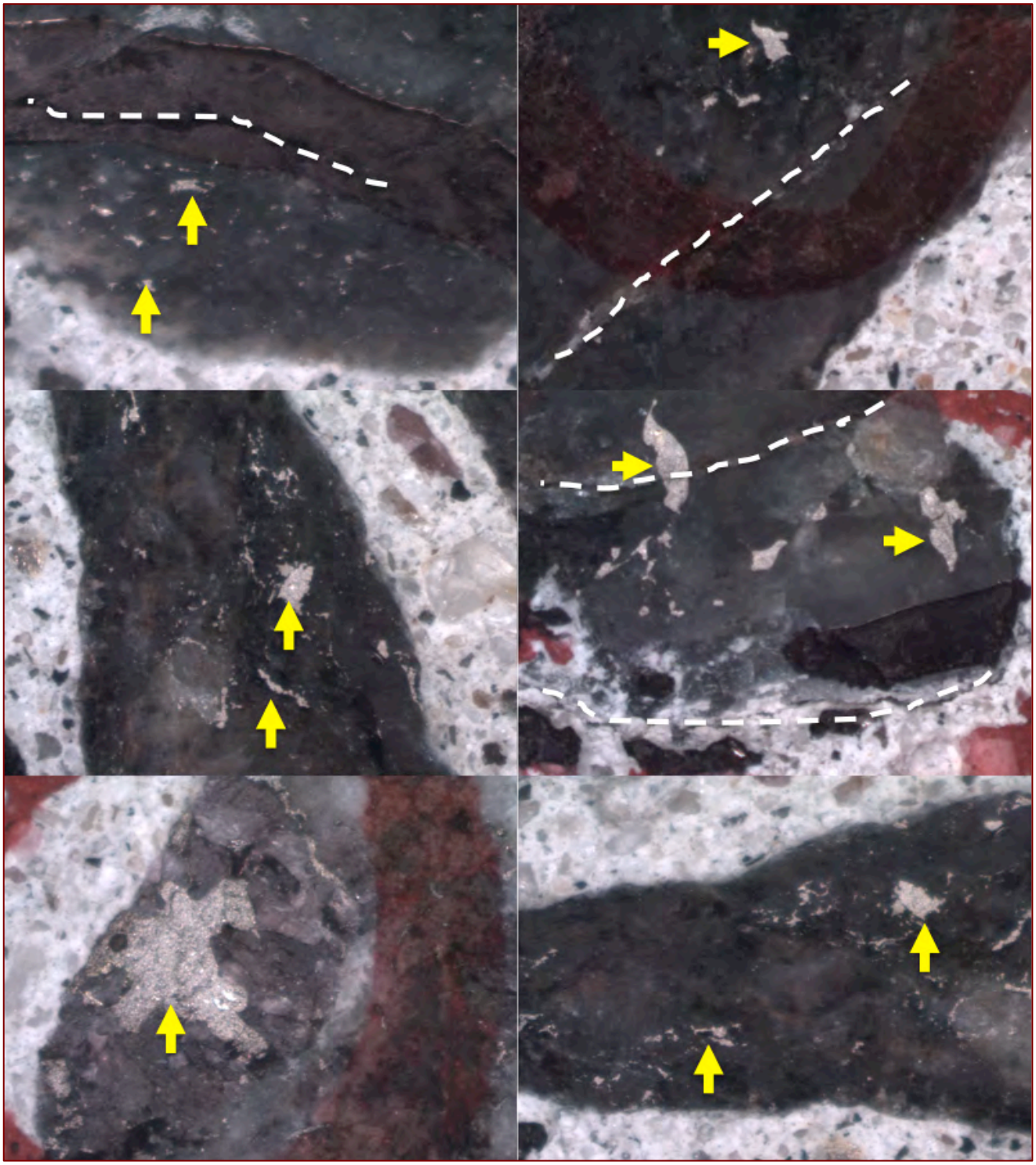

Figure 17: Photomicrographs of lapped cross section of core showing some iron sulfide minerals within crushed gneiss coarse aggregate particles that are identified by characteristic golden yellow metallic luster (some are marked with arrows), and some visible cracking in coarse aggregates (white dashed lines). Field width of each photo is 9 mm. Amount of pyrrhotite is estimated to be 0.4 to 2.4 percent by volume of individual aggregate.

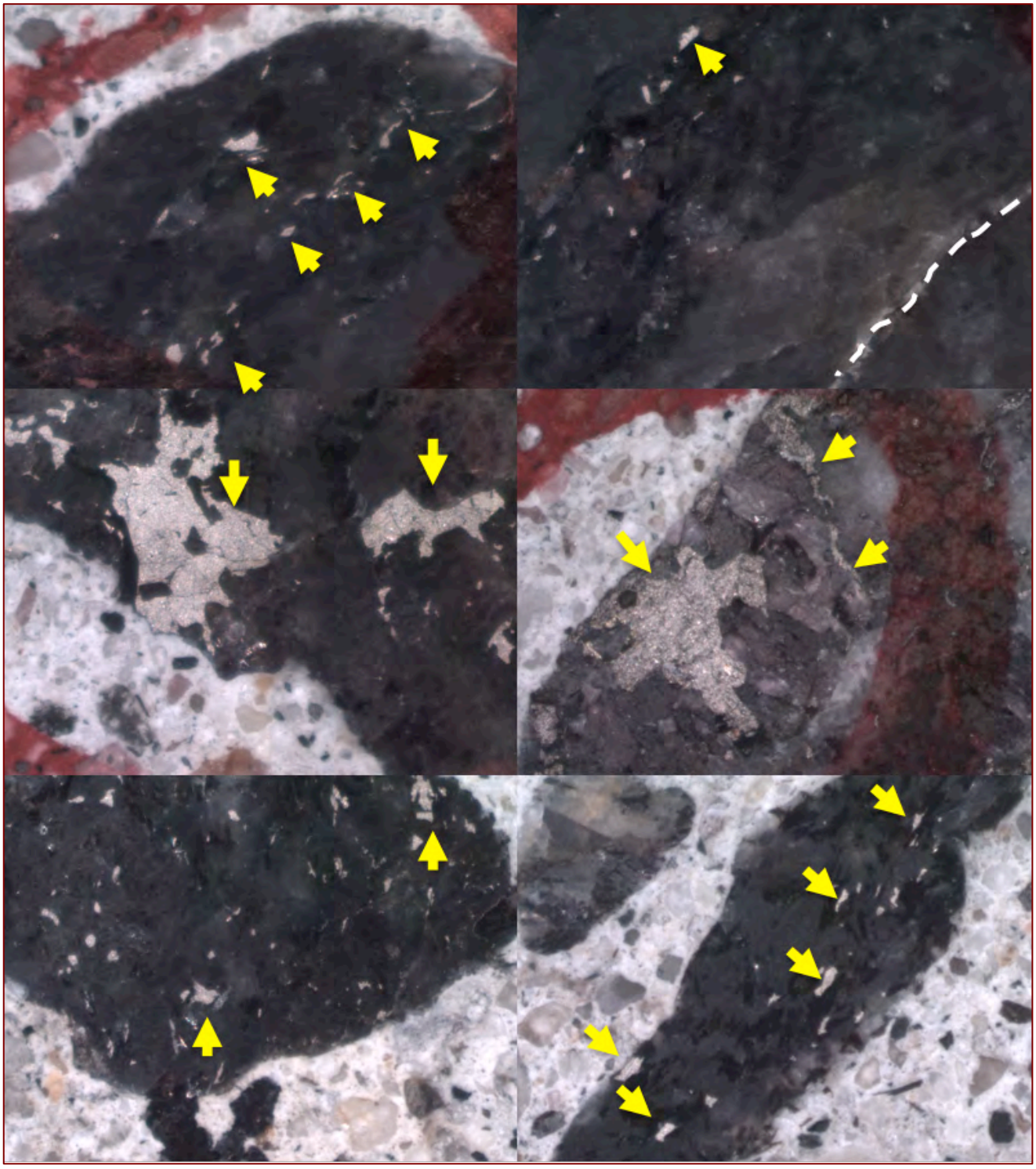

Figure 18: Photomicrographs of lapped cross section of core showing some iron sulfide minerals within crushed gneiss coarse aggregate particles that are identified by characteristic golden yellow metallic luster (some are marked with arrows), and some visible cracking in coarse aggregates (white dashed lines). Field width of each photo is 9 mm. Amount of pyrrhotite is estimated to be 0.4 to 2.4 percent by volume of individual aggregate.

PHOTOMICROGRAPHS OF LAPPED CROSS SECTIONS

Figure 19 shows six (6) photomicrographs of lapped cross section of the core from various depths, taken by using a stereomicroscope to depict the overall air-entrained nature of concrete.

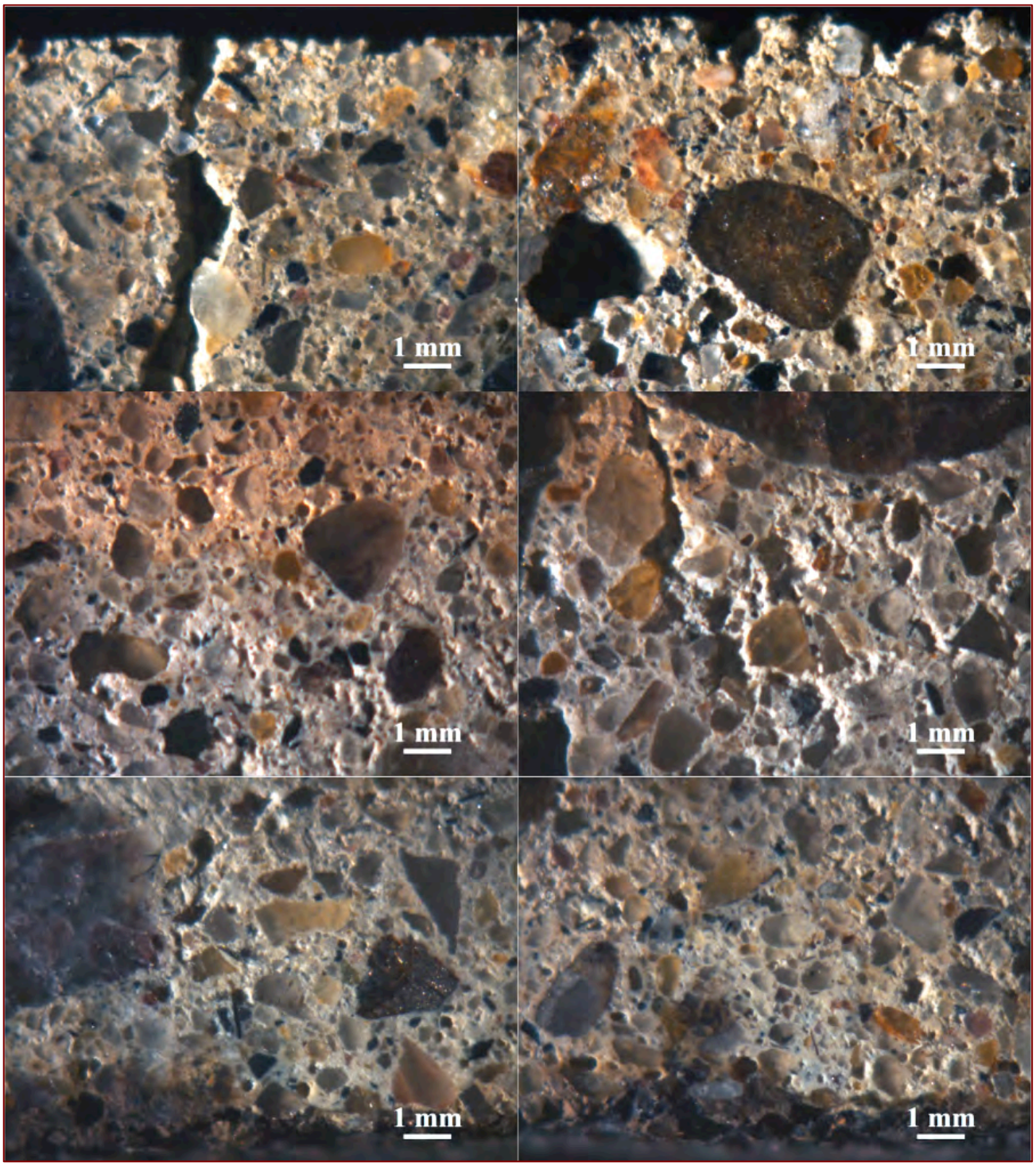

Figure 19: Photomicrographs of lapped cross section showing the air-entrained nature of concrete and many fine to coarse spherical and irregularly-shaped air-voids. Beige-toned paste areas are carbonated.

THIN SECTIONS

Figures 20 and 21 show blue dye-mixed epoxy-impregnated thin sections of the core prepared from various areas of the core. Thin Section Nos. 1 and 2 in Figure 20 are from the core end representing the inside surface of the wall where a vertical crack from the exposed face of the inside surface to a depth of 40 to 50 mm is distinct. Thin Section No. 3 Figure 20 is from the core end representing the outside surface of the wall where a vertical crack from the exposed face of the inside surface to a depth of 20 to 30 mm is distinct. The white dotted lines on residues of thin sections mark the carbonated ends of concrete from the non-carbonated interiors. The boxed area in a crushed stone coarse aggregate in Thin Section No. 1 shows alternating bands of darker and lighter colored minerals that is typical in a metamorphic gneiss defining the gneissose texture.

Figure 21 shows four more thin sections, Nos. 4 through 7 from one end of the core through depth to the opposite end. Equipments used for preparation of thin section and polished sections are shown in Figure 21.

PHOTOMICROGRAPHS OF THIN SECTIONS

Figures 22 through 25 show photomicrographs of thin sections in plane (left columns) and crossed (right columns) polarized lights in a transmitted-light Stereozoom microscope that show the major and micro cracks highlighted by blue epoxy, dark opaque grains of iron sulfide minerals in aggregates (some are marked by yellow arrows), gneiss coarse aggregate (some are marked by 'G'), quartz sand fine aggregate that are distinct in crossed polarized light modes, and typical gneissose texture of crushed gneiss coarse aggregate particles. Figure 25 shows alternating bands of quartzo-feldspathic and micaceous minerals defining the typical gneissose texture of gneiss.

Figures 26 through 29 show Thin Section No. 1 in a petrographic microscope showing crushed gneiss coarse aggregate having alternating bands of quartzo-feldspathic and micaceous minerals, dark opaque iron sulfide minerals, poikiloblastic garnet grains with mineral inclusions in gneiss. Figures 30 and 31 show similar microstructural features in Thin Section Nos. 2 and 3, respectively.

Cracking of Unsound Crushed Gneiss – Figures 22, 24, 28, 29, 30 all show cracked gneiss particles.

Ettringite Infested Paste (EIP) – Breeding Ground for Internal Sulfate Attack - Figures 32 to 36 show an interesting microstructural feature where confined areas of paste are often dominated by poorly crystalline (or perhaps some colloidal form) secondary ettringite, that are marked as ettringite infested paste (EIP). These confined areas of paste are the breeding grounds for deleterious secondary ettringite formation and associated expansions for secondary expansion of concrete and associated distress. These poorly crystallized ettringite from confined areas of paste became well developed fibrous or acicular-formed crystals when located in open spaces like air-voids or cracks.

Figures 37 through 40 show similar features e.g., EIP, cracked gneiss, microcracking in aggregates to paste, etc.

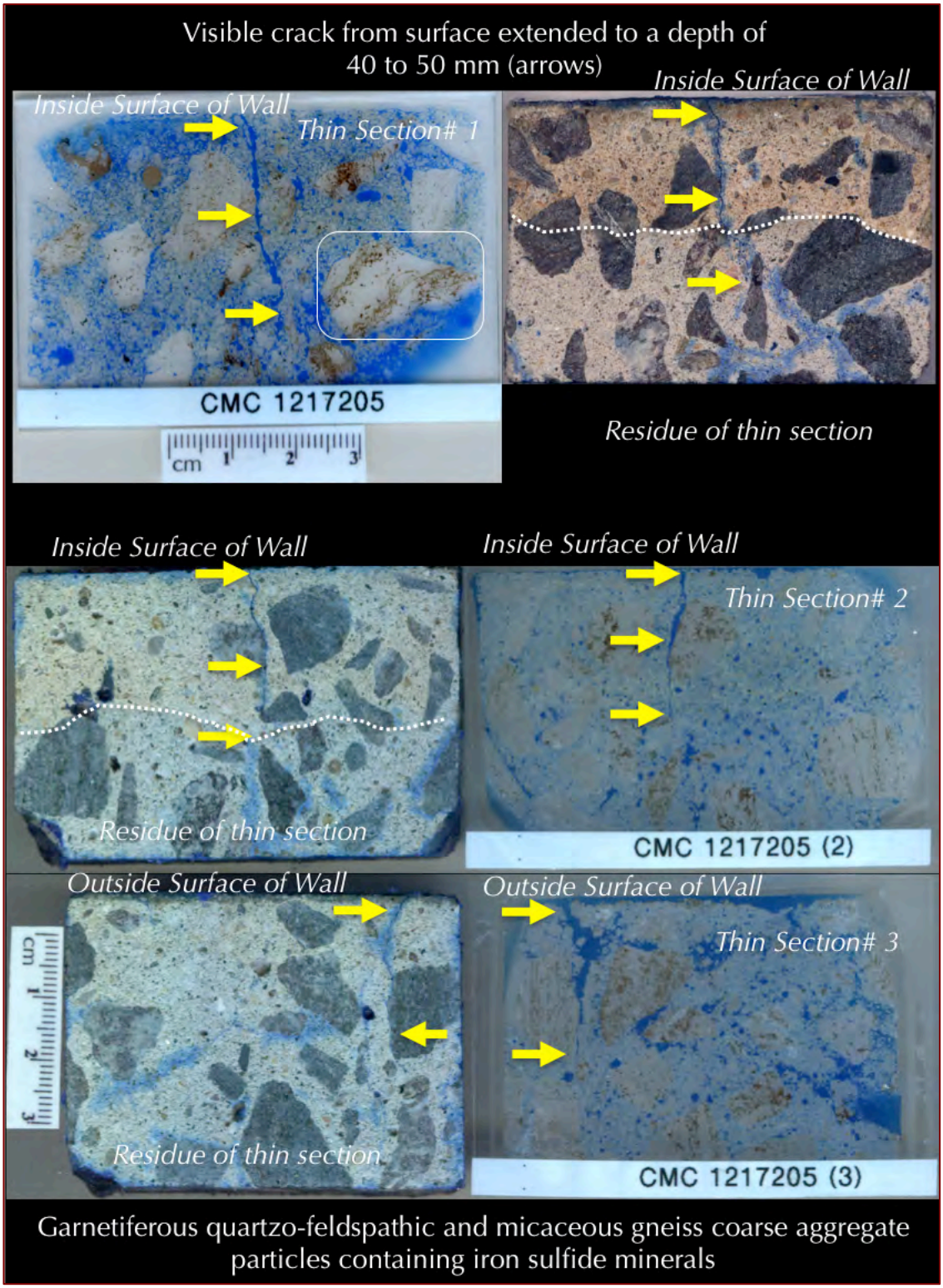

Figure 20: Blue dye-mixed epoxy-impregnated thin sections (30 micron thickness) of the core taken from inside and outside surfaces of the wall showing extension of visible map cracking from the opposite surfaces of the wall to the interior concrete (arrows) as well as depths of carbonation (marked as white dotted lines) and other cracks in concrete that are highlighted by the blue epoxy. The boxed coarse aggregate particle in the top thin section clearly shows alternate banding of light-colored quartzo-feldspathic and dark brown colored biotite bands defining the gneissose texture common in these crushed gneiss coarse aggregate particles.

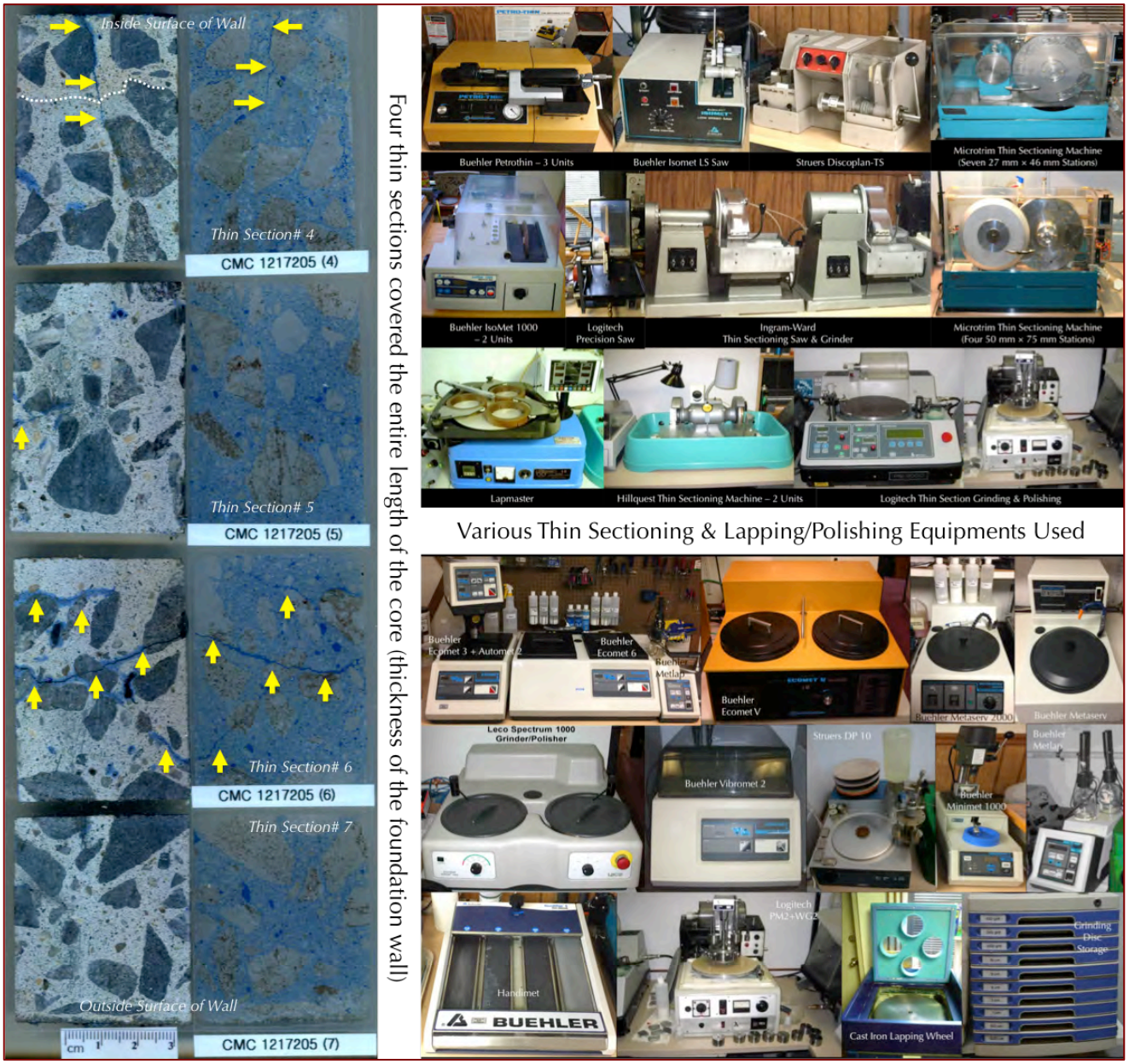

Figure 21: Four additional blue dye-mixed epoxy-impregnated thin sections (right column, 30 micron thickness) and corresponding residues left from thin sections (left column) from a full-depth cross section of the core taken from the inside through depth to the outside surface of the core/wall showing extension of visible map cracking from the opposite surfaces of the wall to the interior concrete (arrows) as well as depths of carbonation (marked as white dotted lines) and other cracks in concrete that are highlighted by the blue epoxy.

Also shown at right are various thin sectioning and grinding/polishing equipments used for preparation of thin sections of concrete.

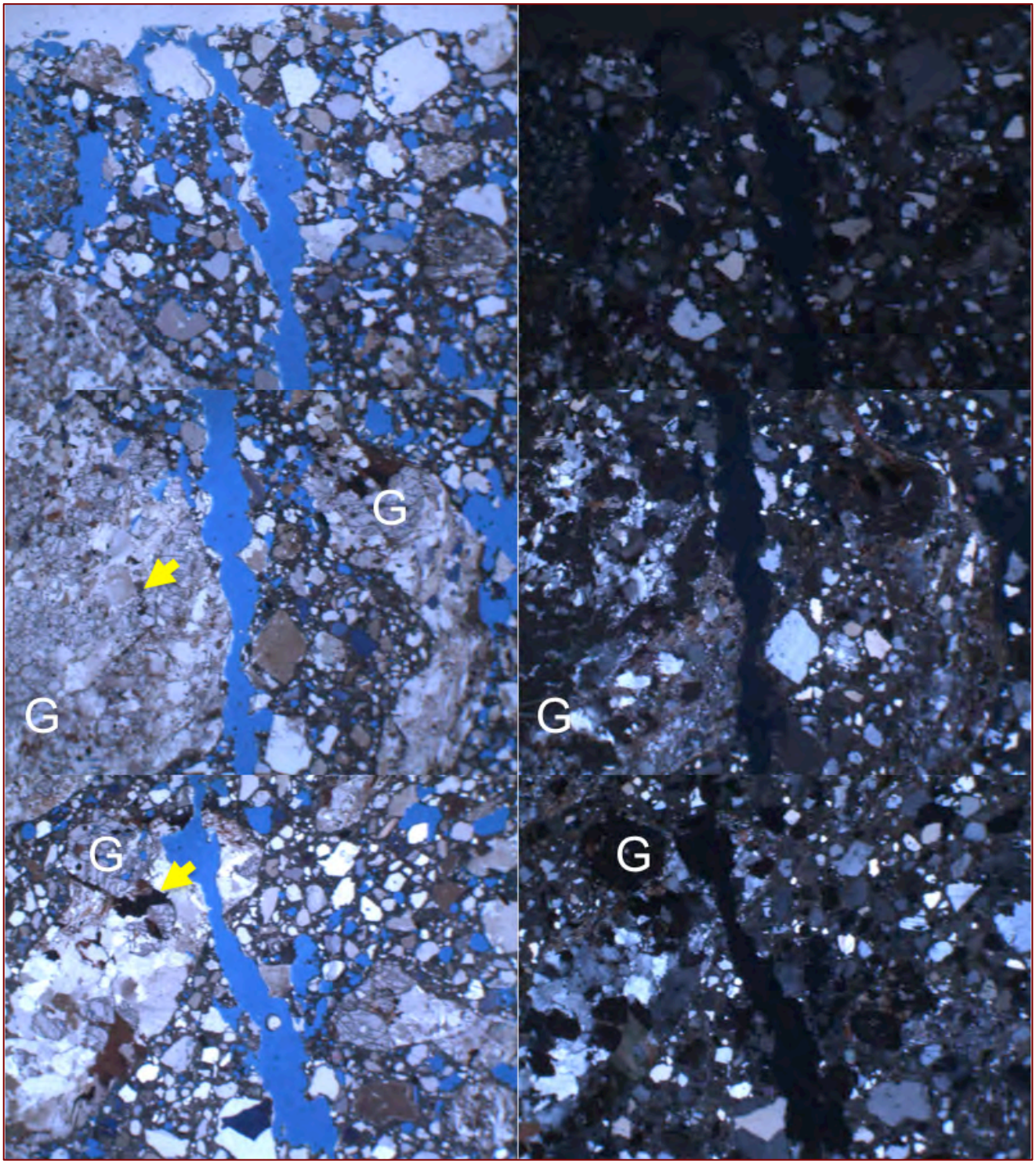

Figure 22: Photomicrographs of blue dye-mixed epoxy-impregnated Thin section (#1) of concrete showing: (a) visible cracking highlighted by blue epoxy, (b) garnetiferous gneiss crushed stone coarse aggregate having alternating bands of quartzo-feldspathic and micaceous minerals (some garnet grains are marked in 'G' that are optically isotropic), and siliceous sand fine aggregate. Left colum photos were taken in PPL and right column ones in corresponding XPL modes in a transmitted-light stereo-zoom microscope. A few dark opaque iron sulfide and oxide are marked with yellow arrows. Field width of each photo is 12 mm.

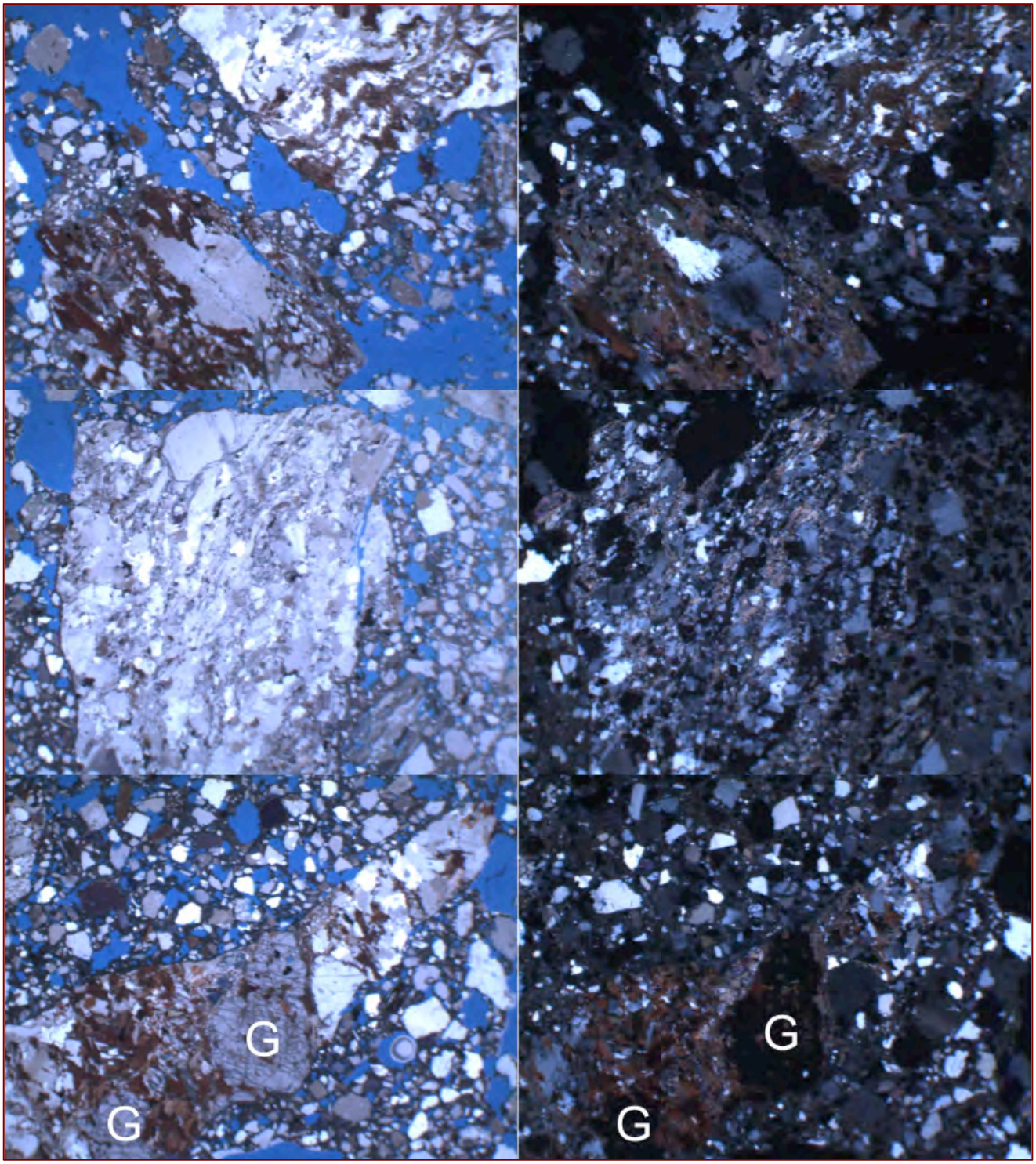

Figure 23: Photomicrographs of blue dye-mixed epoxy-impregnated Thin section (#2) of concrete showing: (a) visible cracking highlighted by blue epoxy, (b) garnetiferous gneiss crushed stone coarse aggregate having alternating bands of quartzo-feldspathic and micaceous minerals (some garnet grains are marked in 'G' that are optically isotropic), and siliceous sand fine aggregate. Left colum photos were taken in PPL and right column ones in corresponding XPL modes in a transmitted-light stereo-zoom microscope. Field width of each photo is 12 mm.

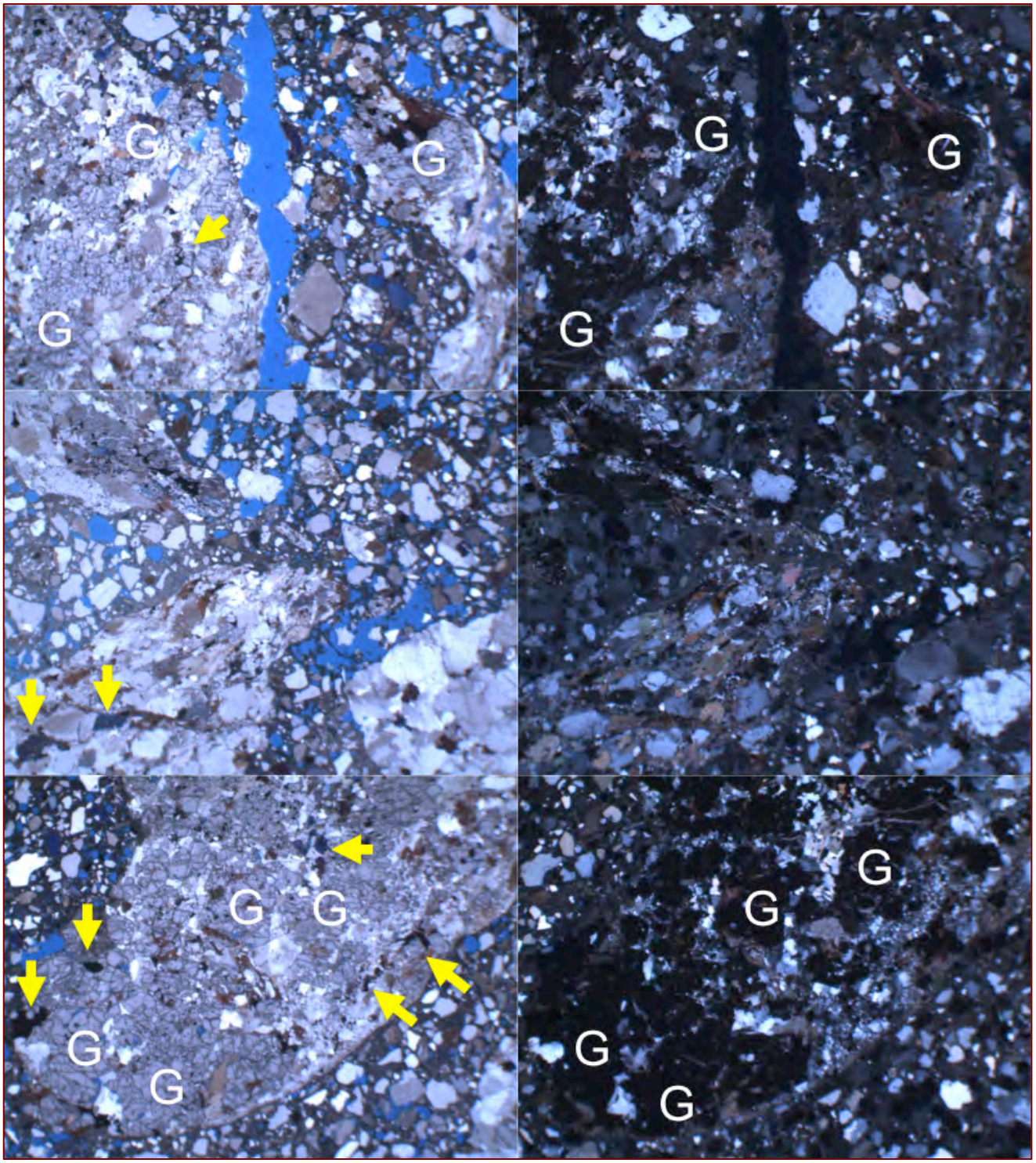

Figure 24: Photomicrographs of blue dye-mixed epoxy-impregnated Thin section (#3) of concrete showing: (a) visible cracking highlighted by blue epoxy, (b) garnetiferous gneiss crushed stone coarse aggregate having alternating bands of quartzo-feldspathic and micaceous minerals (some garnet grains are marked in 'G' that are optically isotropic), and siliceous sand fine aggregate. Left column photos were taken in PPL and right column ones in corresponding XPL modes in a transmitted-light stereo-zoom microscope. A few dark opaque iron sulfide and oxide are marked with yellow arrows. Field width of each photo is 12 mm.

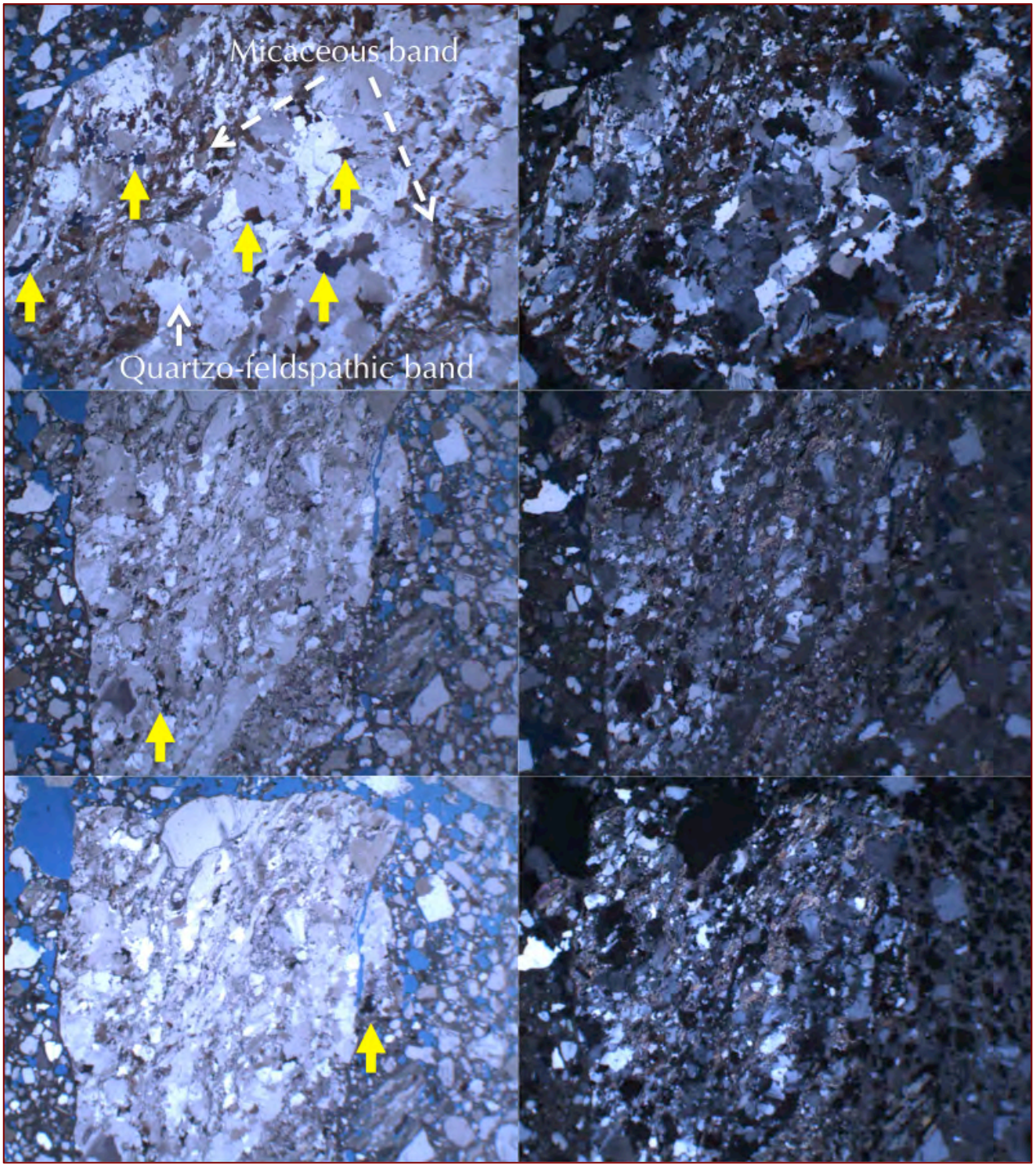

Figure 25: Photomicrographs of blue dye-mixed epoxy-impregnated Thin section (#4) of concrete showing: (a) visible cracking highlighted by blue epoxy, (b) garnetiferous gneiss crushed stone coarse aggregate having alternating bands of quartzo-feldspathic and micaceous minerals (some garnet grains are marked in 'G' that are optically isotropic), and siliceous sand fine aggregate. Left column photos were taken in PPL and right column ones in corresponding XPL modes in a transmitted-light stereo-zoom microscope. A few dark opaque iron sulfide and oxide are marked with yellow arrows. Field width of each photo is 12 mm.

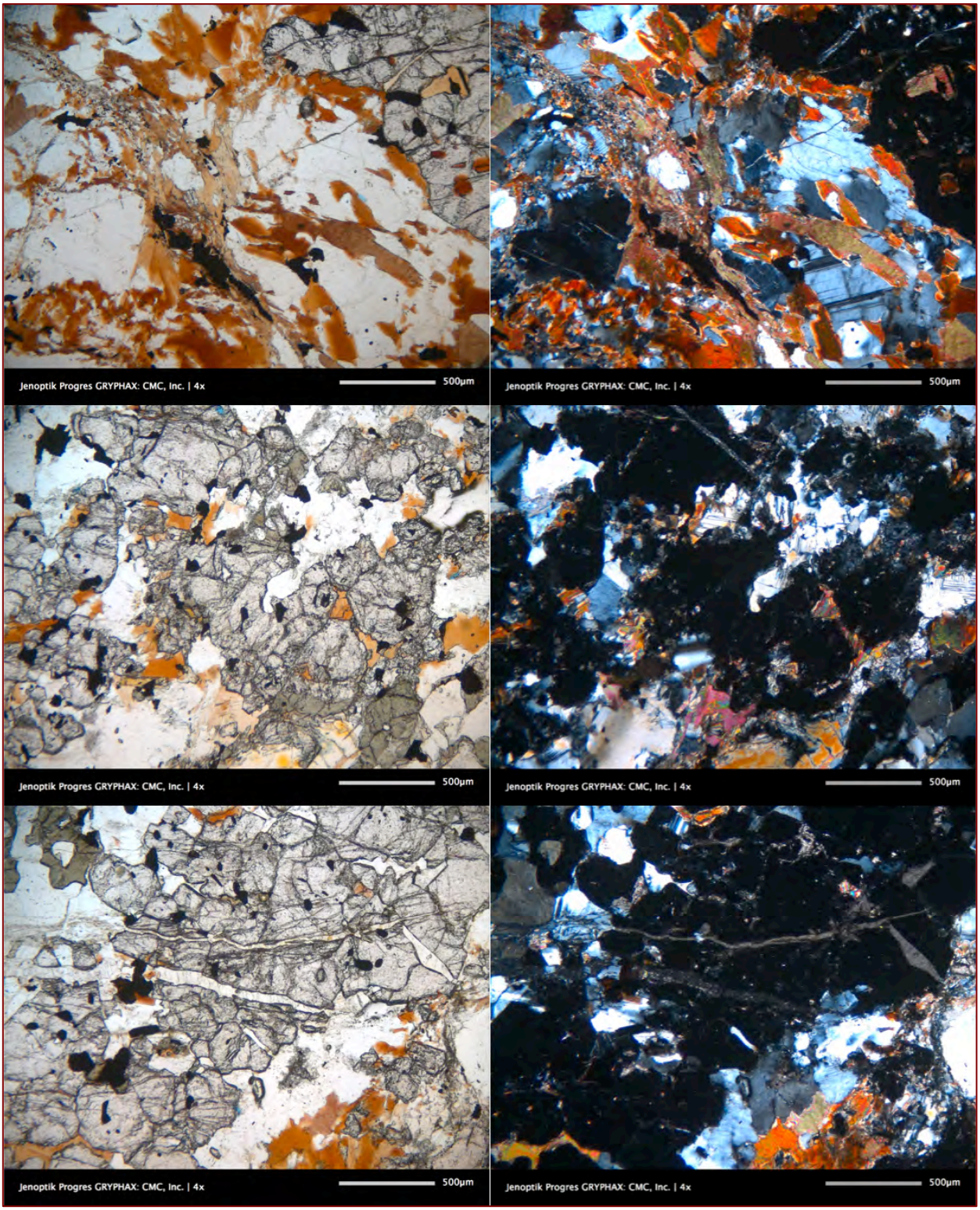

Figure 26: Thin Section# 1: Pyrrhotite-bearing quartz-feldspar-biotite-garnet gneiss coarse aggregate having gneissose texture characterized by alternate bands of quartzo-feldspathic and micaceous minerals, and optically isotropic garnet porphyroblasts caught in the middle of bands (often containing surrounding minerals). Pyrrhotite grains and oxidation products of pyrrhotite occur as small equant opaque phases scattered as inclusions in garnet or along biotite flakes, or as isolated accessory phase.

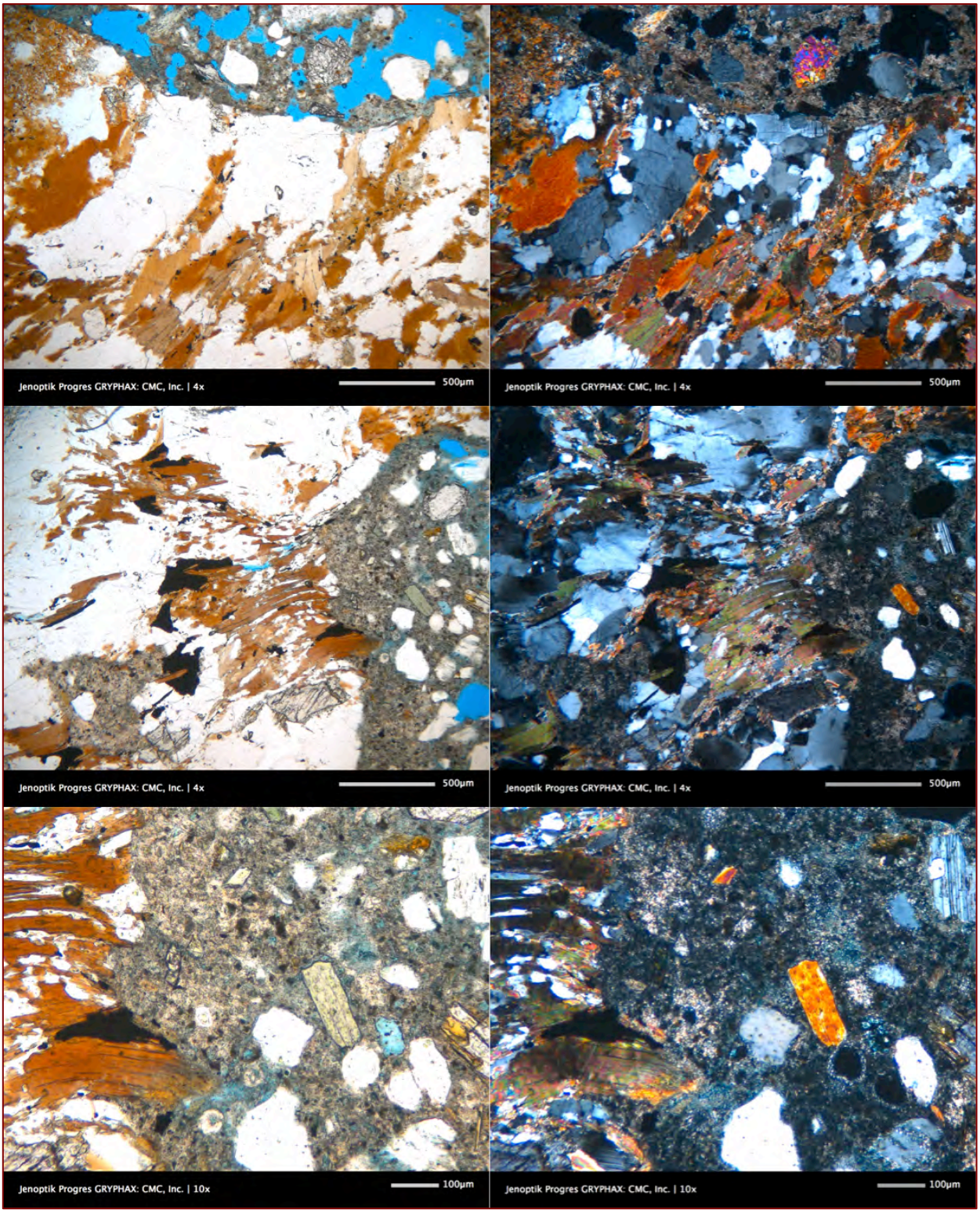

Figure 27: Thin Section# 1: Pyrrhotite-bearing quartz-feldspar-biotite-garnet gneiss coarse aggregate having gneissose texture characterized by alternate bands of quartzo-feldspathic and micaceous minerals. Pyrrhotite grains and oxidation products of pyrrhotite occur as small equant opaque phases scattered as inclusions in garnet or along biotite flakes, or as isolated accessory phase.

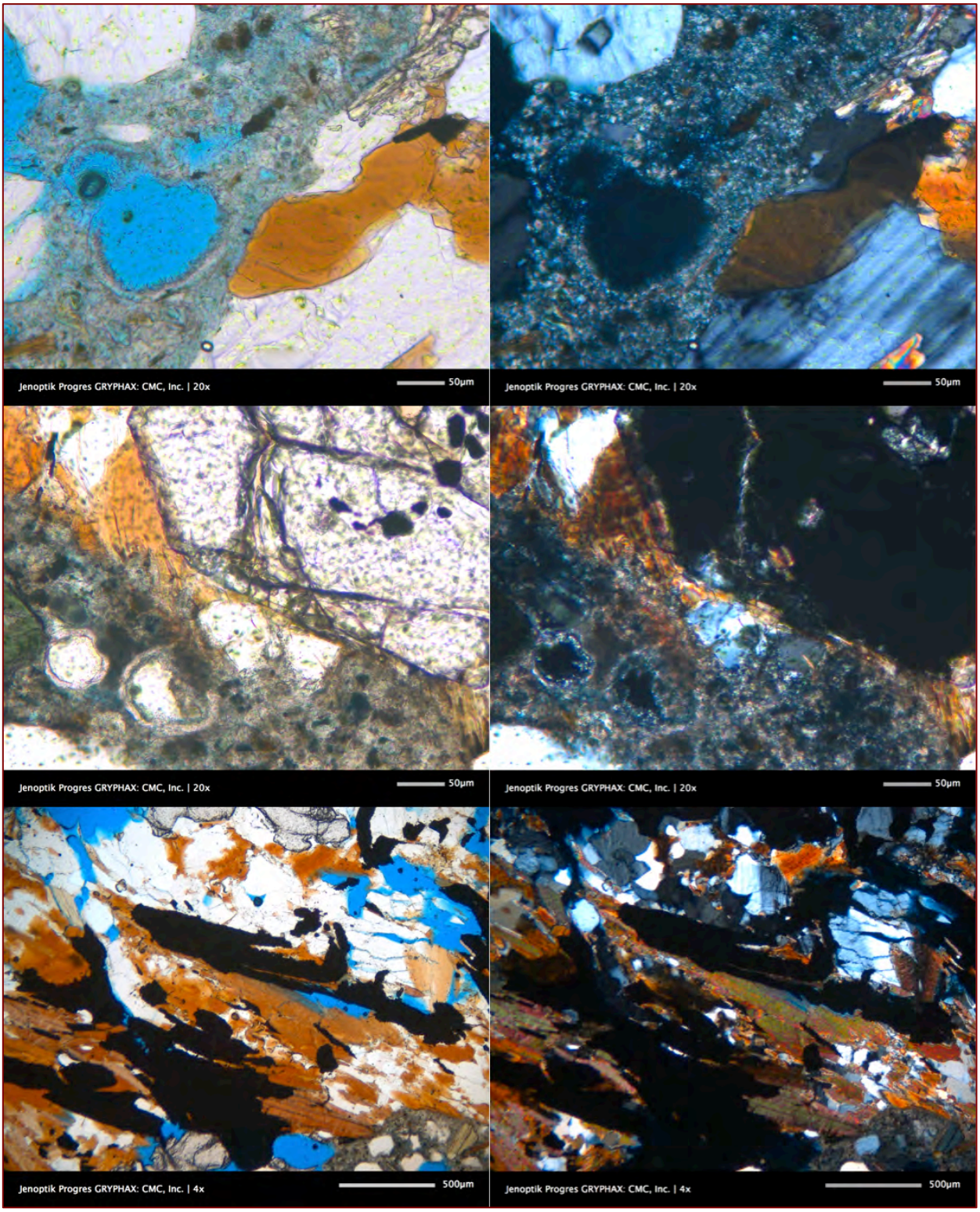

Figure 28: Thin Section# 1: Pyrrhotite-bearing quartz-feldspar-biotite-garnet gneiss coarse aggregate having gneissose texture characterized by alternate bands of quartzo-feldspathic and micaceous minerals, and optically isotropic garnet porphyroblasts caught in the middle of bands (often containing surrounding minerals). Pyrrhotite grains and oxidation products of pyrrhotite occur as small equant opaque phases scattered as inclusions in garnet or along biotite flakes, or as isolated accessory phase.

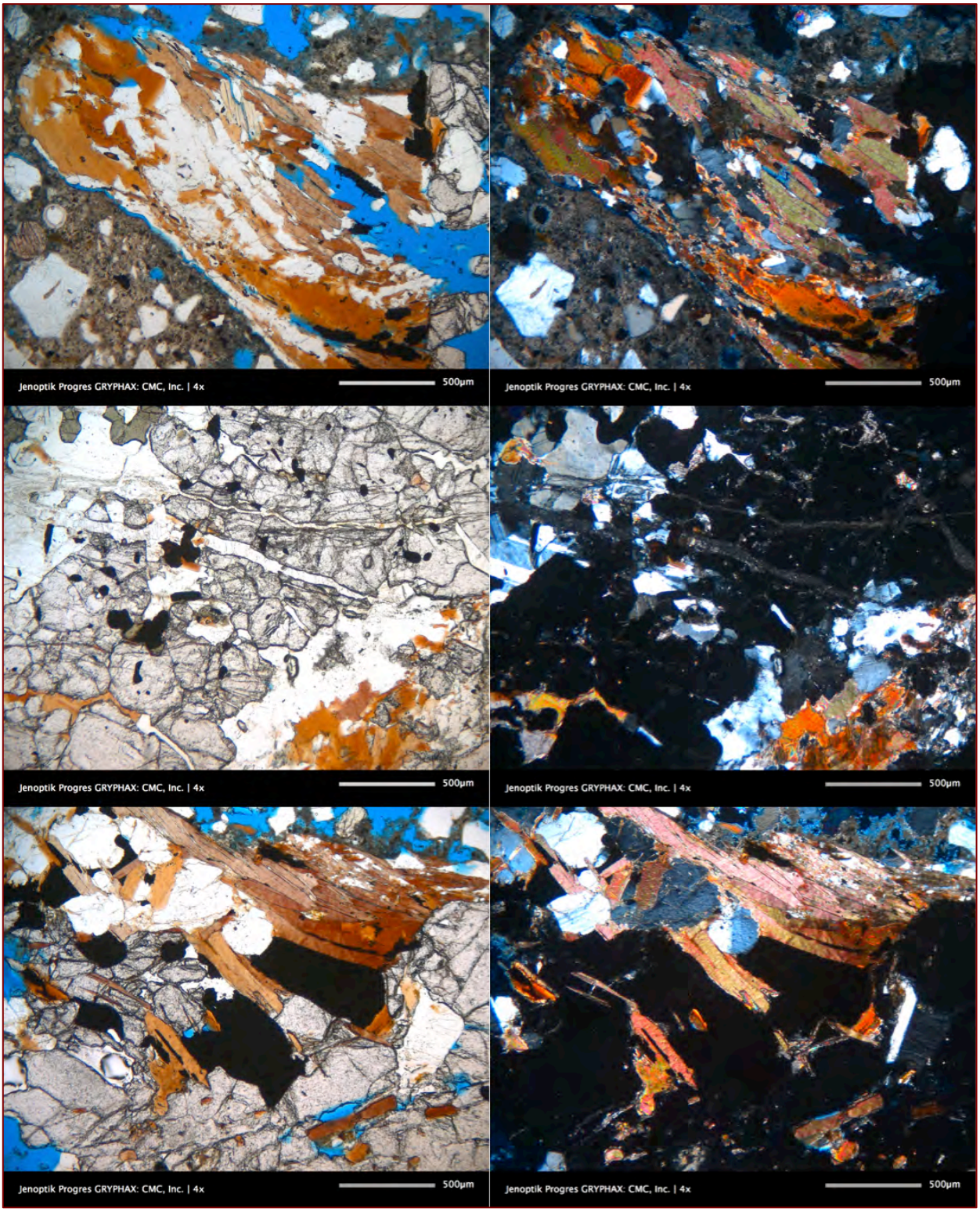

Figure 29: Thin Section# 1: Pyrrhotite-bearing quartz-feldspar-biotite-garnet gneiss coarse aggregate having gneissose texture characterized by alternate bands of quartzo-feldspathic and micaceous minerals, and optically isotropic garnet porphyroblasts caught in the middle of bands (often containing surrounding minerals). Pyrrhotite grains and oxidation products of pyrrhotite occur as small equant opaque phases scattered as inclusions in garnet or along biotite flakes, or as isolated accessory phase.

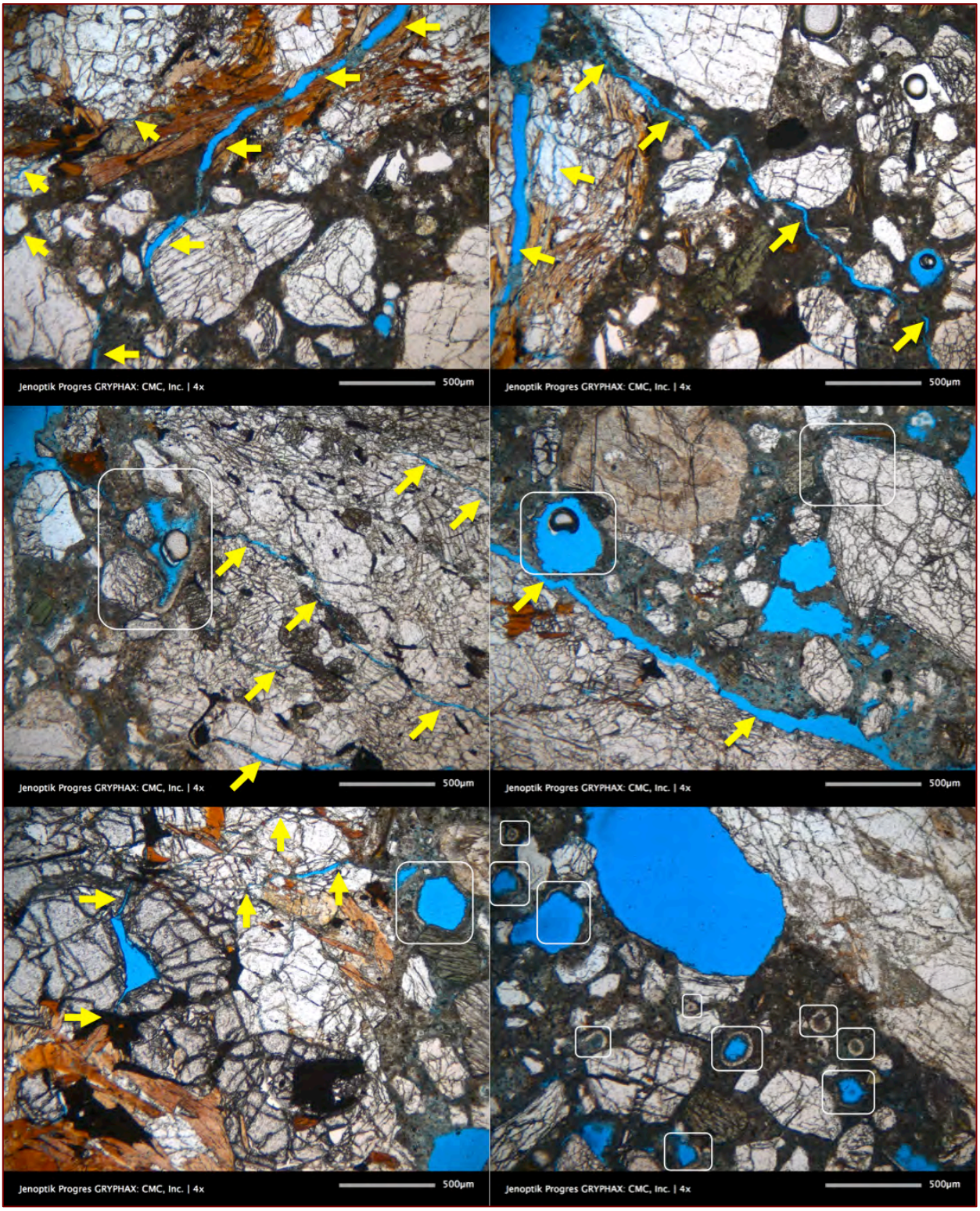

Figure 30: Thin Section# 2: Microcracking in and around concrete aggregate particles shown by arrows and secondary ettringite crystallization lining the air-voids shown by boxed areas.

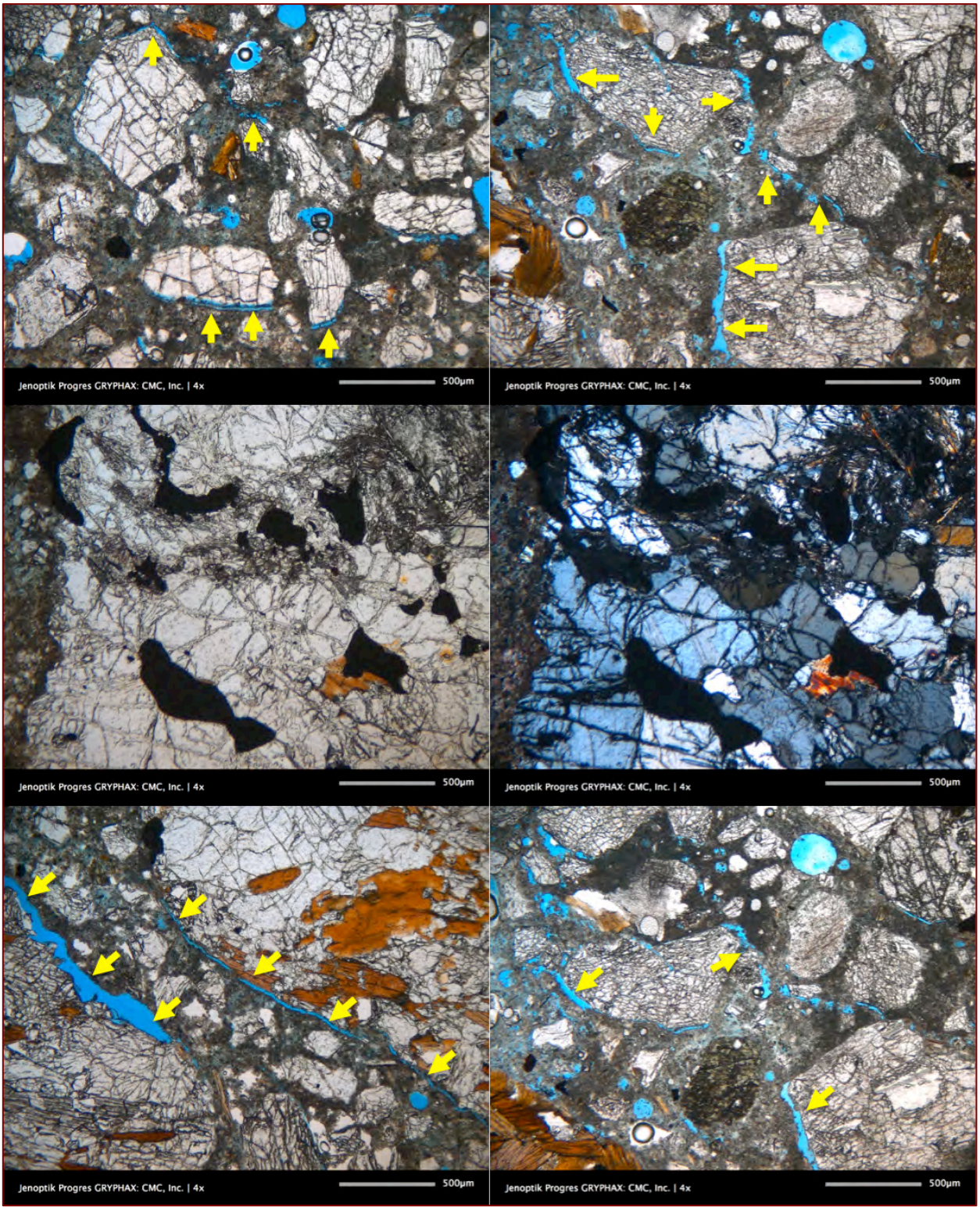

Figure 31: Thin Section# 3: Microcracking in and around concrete aggregate particles shown by arrows.

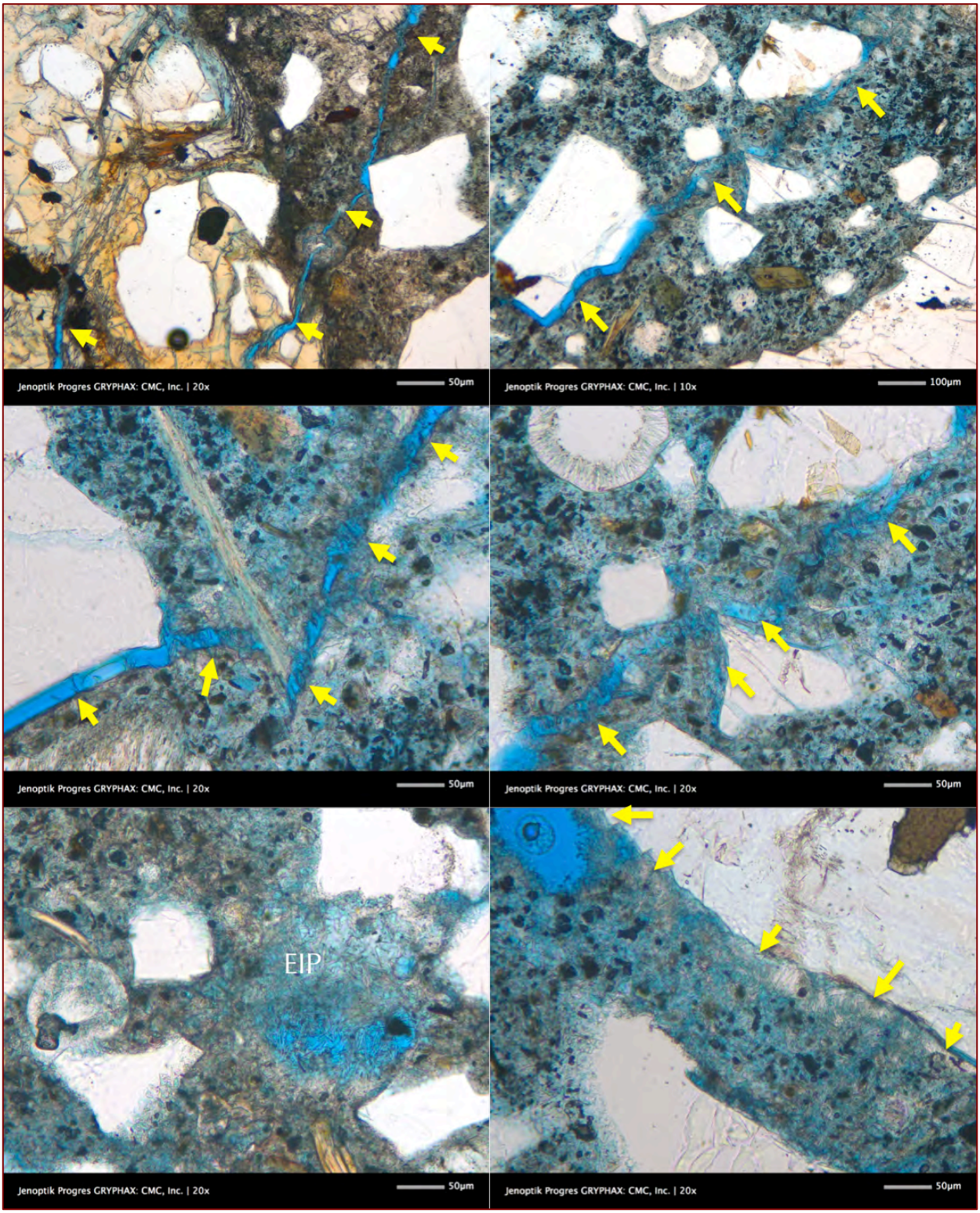

Figure 32: Thin Section# 4: Microcracking in and around concrete aggregate particles shown by arrows. Notice secondary ettringite crystallization in cracks as well as poorly crystalline secondary ettringite formation in paste, called ettringite infested paste (EIP) that are the breeding grounds for internal sulfate attack due to deleterious poorly crystalline ettringite formation in confined spaces in paste to cause expansion.

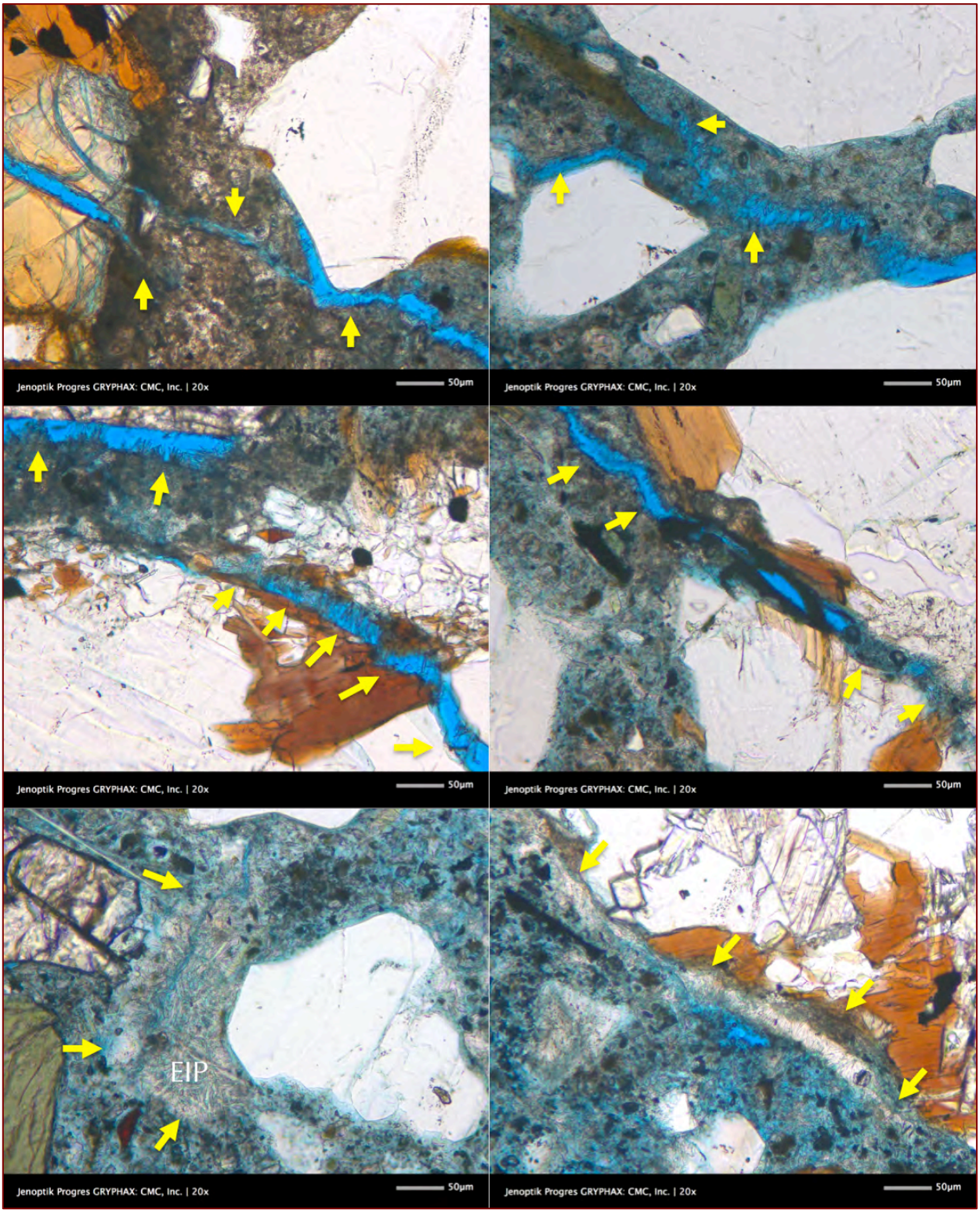

Figure 33: Thin Section# 4: Microcracking in and around concrete aggregate particles shown by arrows. Notice secondary ettringite crystallization in cracks as well as poorly crystalline secondary ettringite formation in paste, called ettringite infested paste (EIP) that are the breeding grounds for internal sulfate attack due to deleterious poorly crystalline ettringite formation in confined spaces in paste to cause expansion.

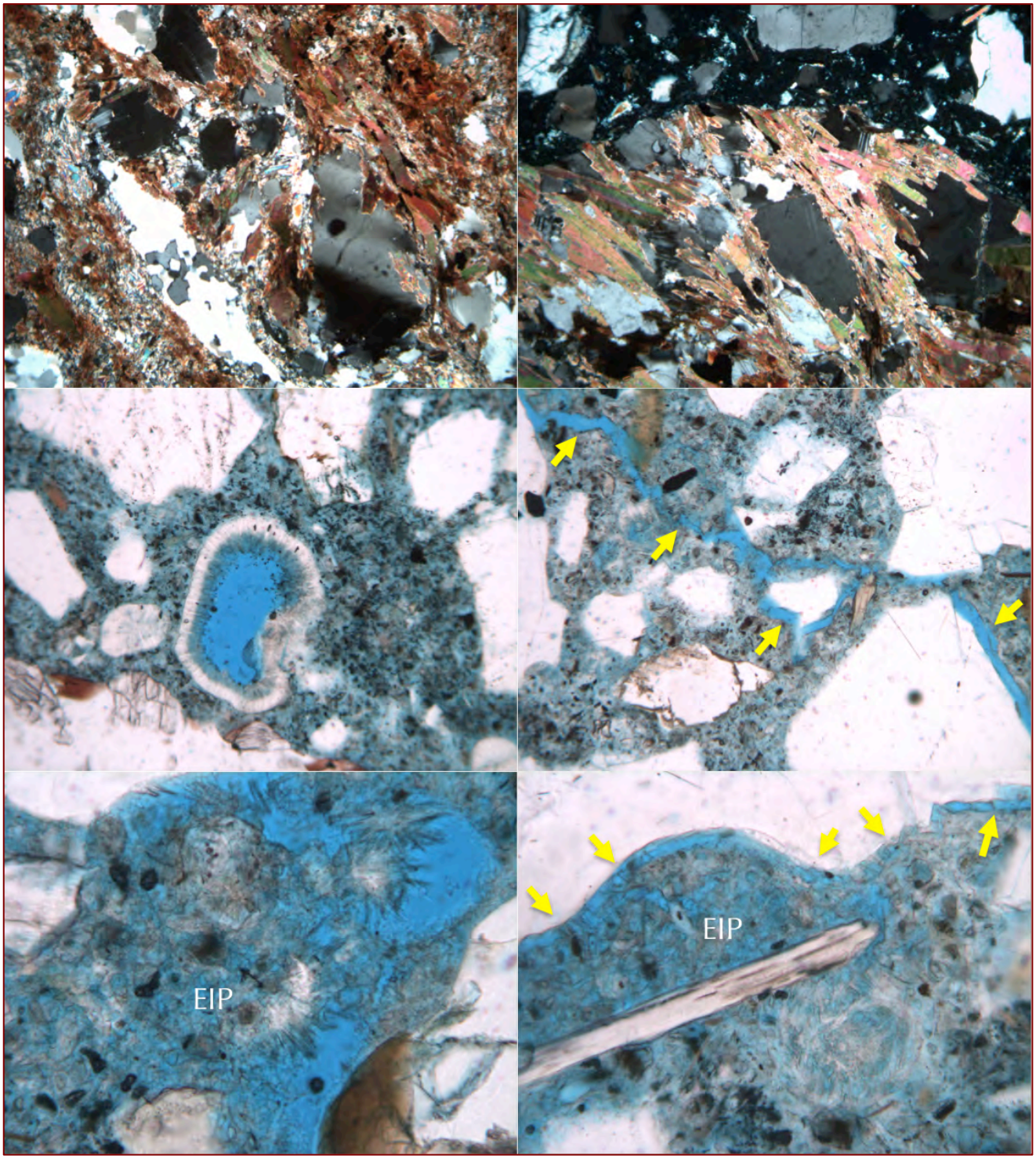

Figure 34: Thin Section# 5: Top row shows gneiss coarse aggregate. Middle row shows an ettringite-lined void and a microcrack (arrows). Bottom row shows EIP or ettringite infested paste, which is the breeding ground for internal sulfate attack. Field width of each photo is 0.25 mm for the top and middle row, and 0.04 mm for the bottom row.

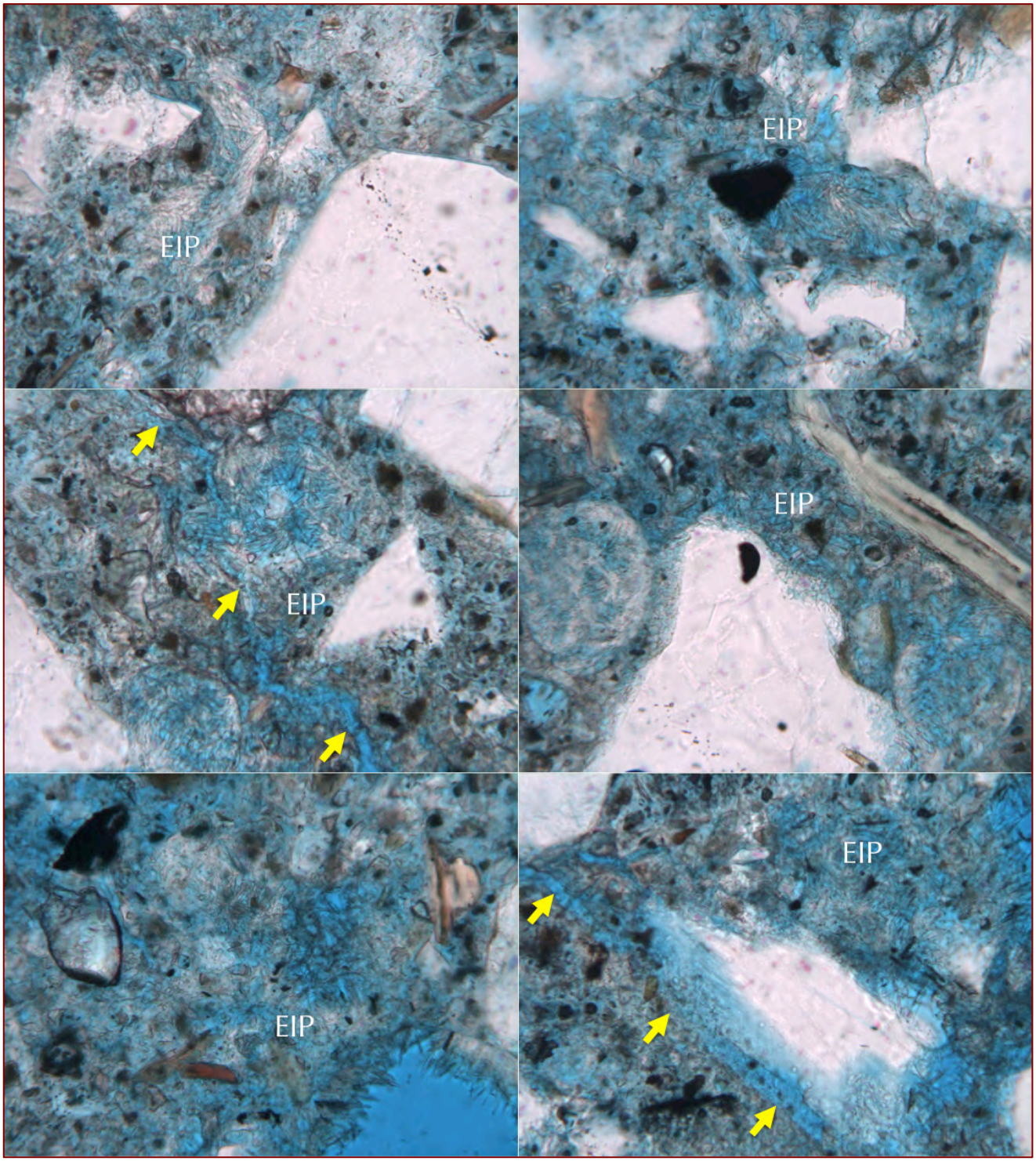

Figure 35: Thin Section# 5: EIP or ettringite infested paste is the breeding ground for internal sulfate attack that forms poorly crystalline ettringite in the confined spaces in paste, and becomes well crystalline when formed in an open void or a crack. Arrows show incipient crack development through EIP. Field width of each photo is 0.04 mm.

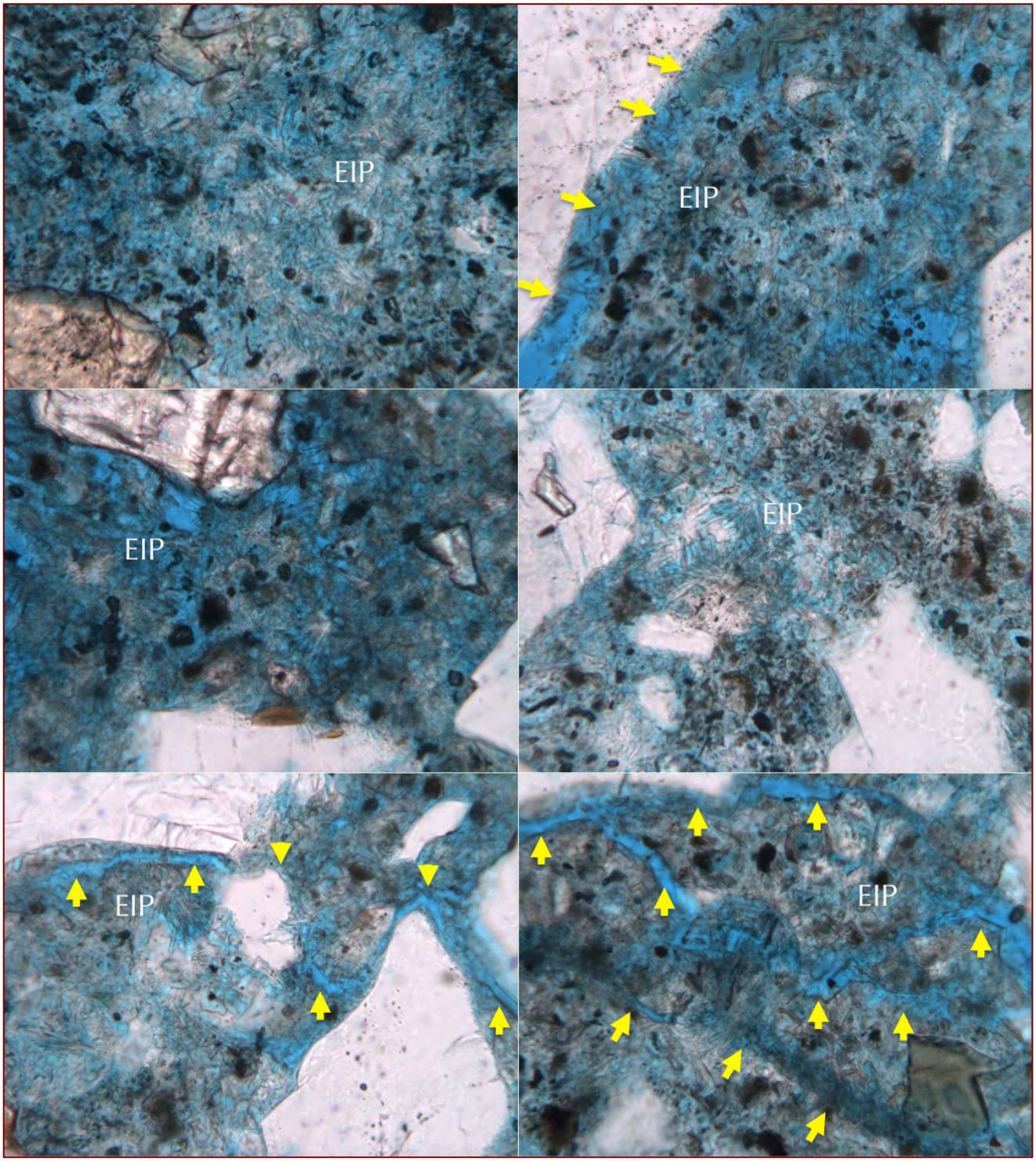

Figure 36: Thin Section# 5: EIP or ettringite infested paste is the breeding ground for internal sulfate attack that forms poorly crystalline ettringite in the confined spaces in paste, and becomes well crystalline when formed in an open void or a crack. Arrows in the top right photo show ettringite formation along an aggregate-paste interface. Arrows in the bottom row show incipient crack development through EIP. Field width of each photo is 0.04 mm.

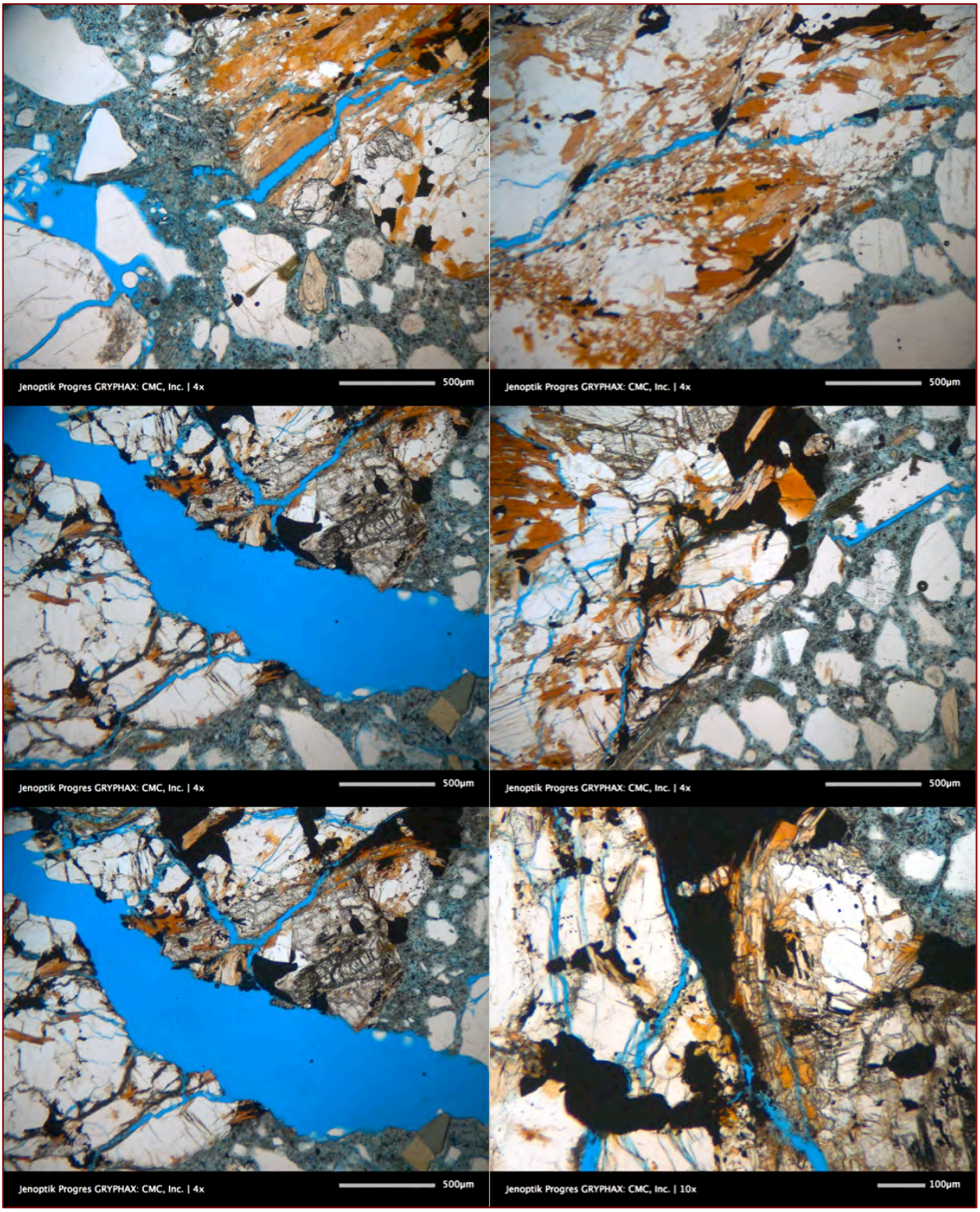

Figure 37: Thin Section# 6: Microcracking in and around concrete aggregate particles shown by arrows. Such extensive cracking of aggregates are testaments of expansion due to pyrrhotite oxidation.

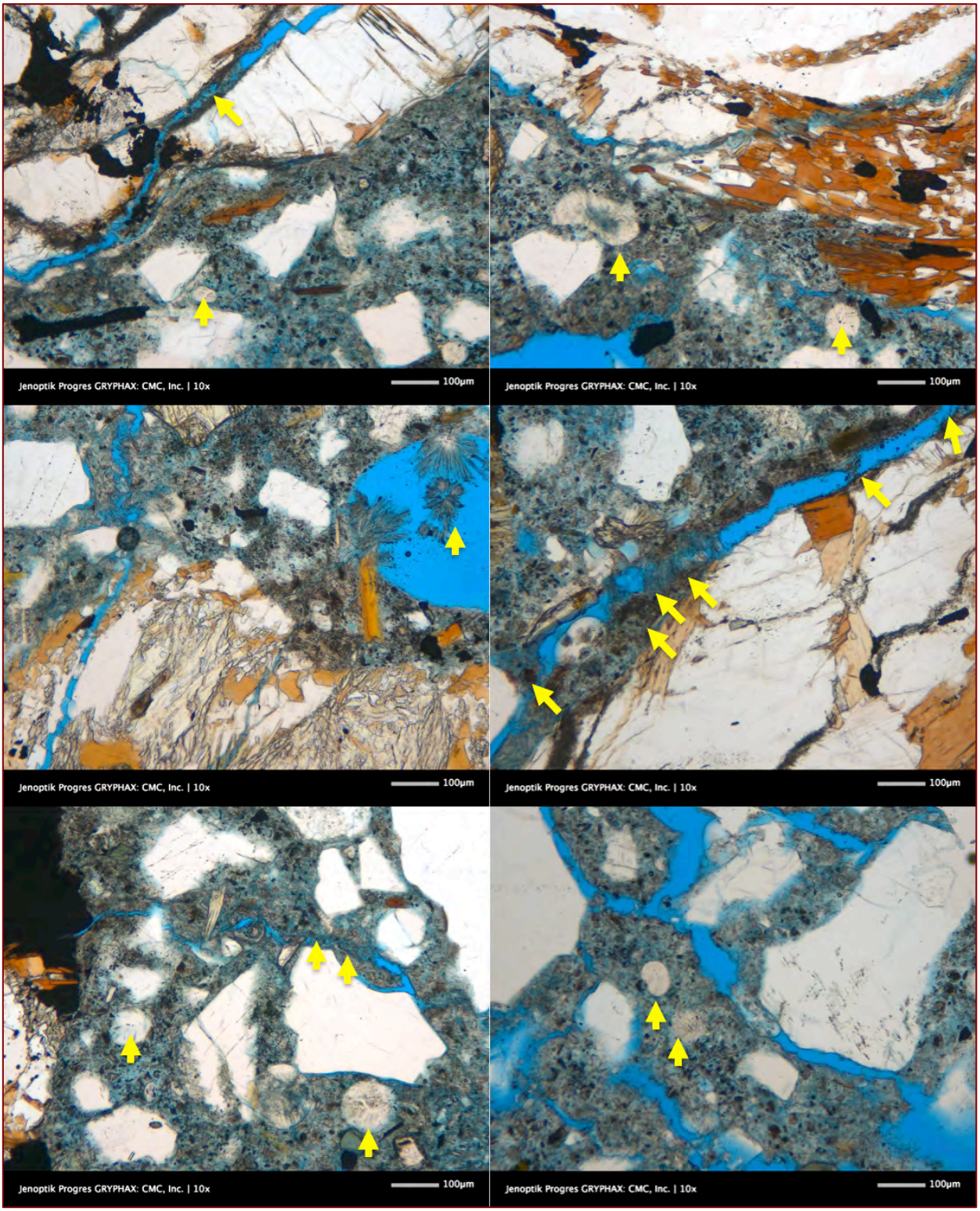

Figure 38: Thin Section# 6: Microcracking in and around concrete aggregate particles and in surrounding paste, and, secondary ettringite deposits in voids and cracks (shown by arrows). Middle row right photo shows 'bridges' of fine fibrous ettringite across the crack walls along aggregate-paste interface.

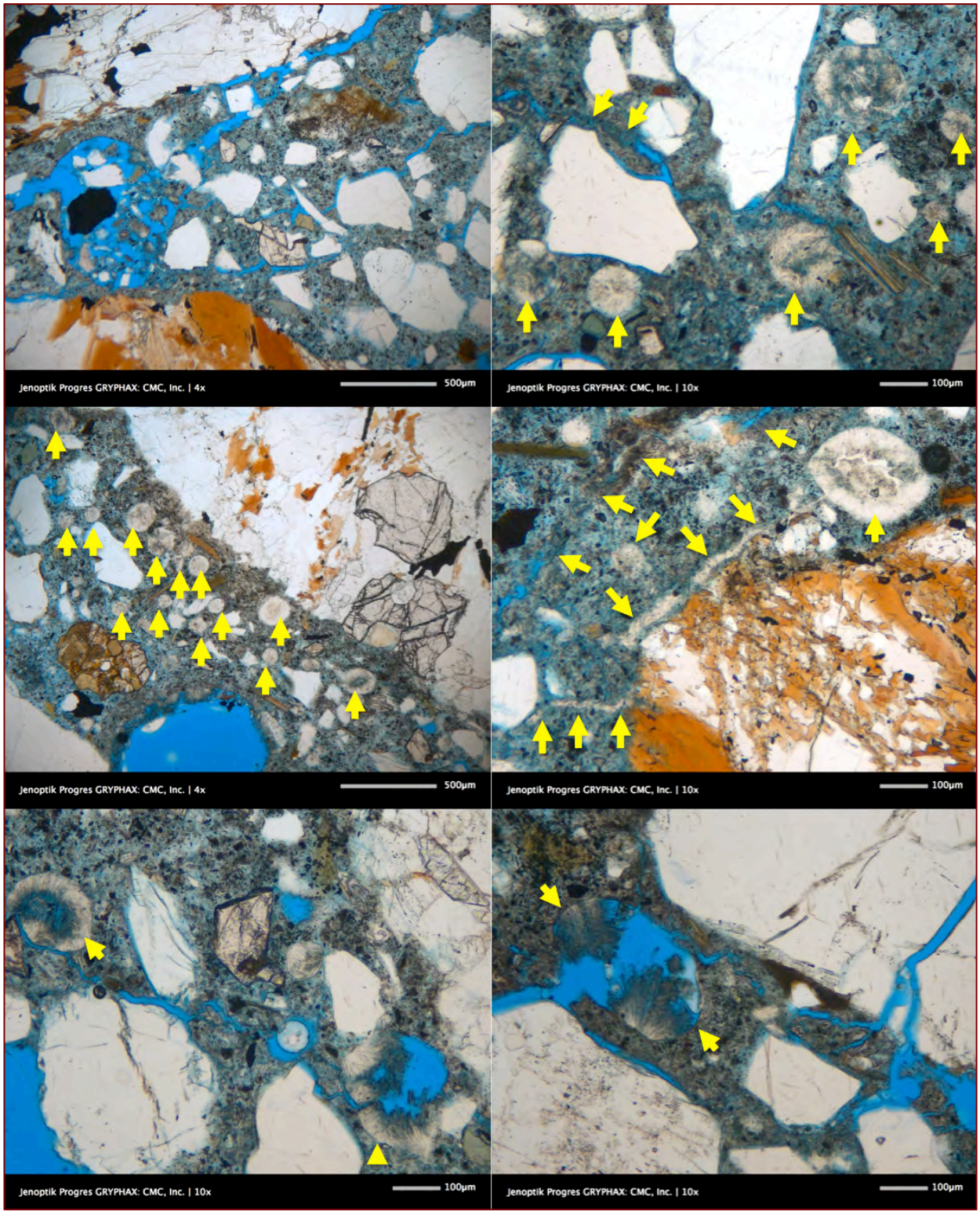

Figure 39: Thin Section# 6: Microcracking in and around concrete aggregate particles and in surrounding paste, and, secondary ettringite deposits in voids and cracks (shown by arrows). The second row of this figure shows most spectacular ettringite-filled air-voids (left) and cracks (right) in Thin Section# 6 taken from interior of the core.

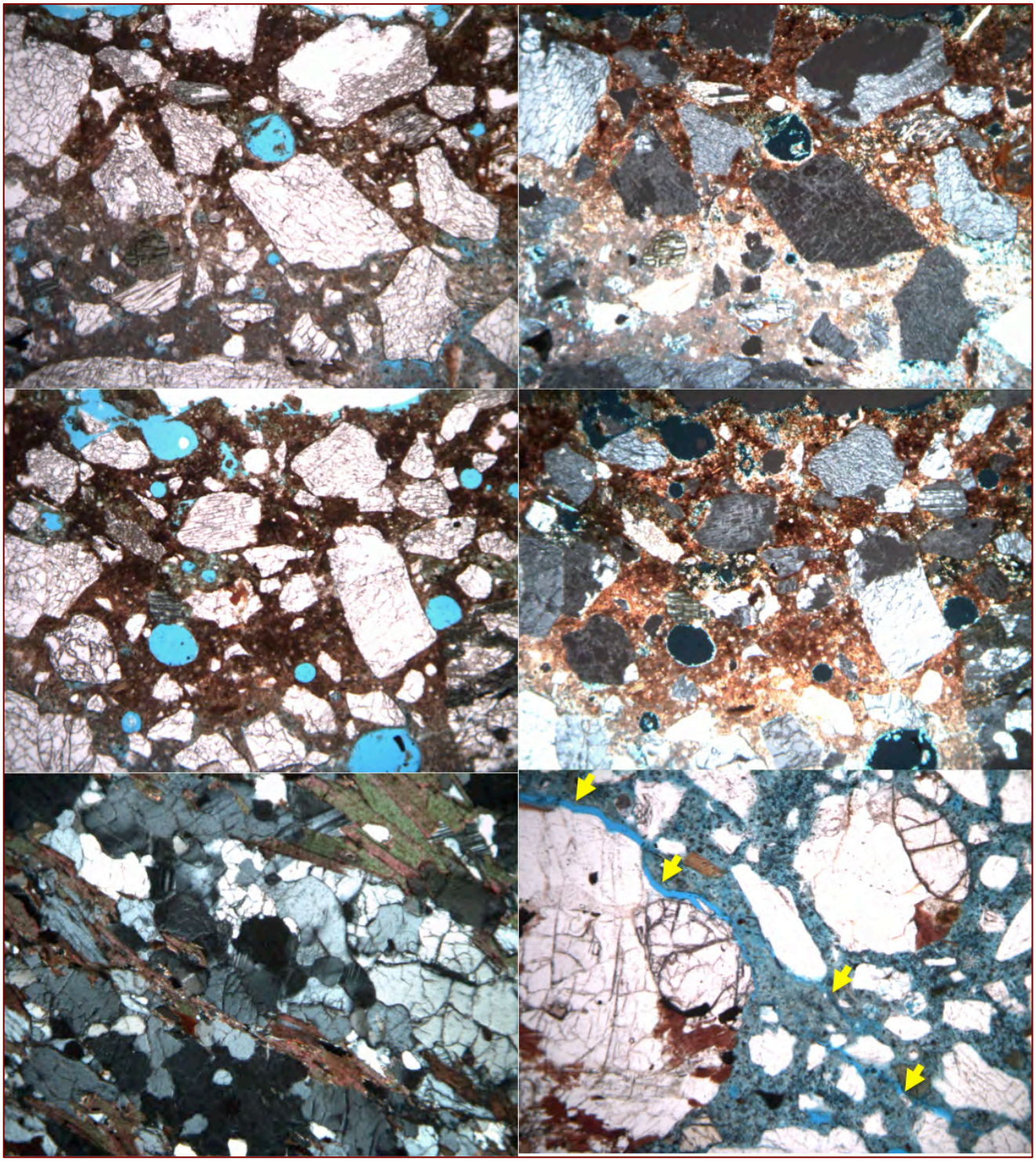

Figure 40: Thin Section# 7: Top and bottom row shows reddish brown weathered dark gray exterior surface end of the core (wall) that has carbonated paste. Bottom left photo shows a gneiss coarse aggregate having alternating bands of biotite and quartzo-feldspathic minerals. Bottom right photo shows cracking in the mortar fraction. Field width of each photo is 0.25 mm.

COARSE AGGREGATE

Coarse aggregate is crushed stone which is a mixture of a predominant dark gray metamorphic garnetiferous quartzo-feldspathic and micaceous gneiss and a subordinate light brown quartz-feldspar-mica gneiss (having a higher quartz content than the dark gray gneiss) both having a nominal maximum size of 3/4 in. (19 mm) and showing the typical gneissose texture of alternating bands of quartz-albitic feldspar and micaceous (mostly biotite and less muscovite) minerals that often contain pyrope garnet poikiloblast. Particles are angular, dense, hard, and medium to dark gray, gneissose-textured, equidimensional to elongated, variably altered, uncoated, and variably cracked. Coarse aggregate particles are well-graded and well-distributed. There is no evidence of alkali-aggregate reactions of coarse aggregate particles in the concrete. However, particles have been unsound during their service in the concrete due to observed cracking and microcracking in many particles often extending into paste that are determined to be due to oxidation of pyrrhotite minerals in these particles.

FINE AGGREGATE

Fine aggregate is natural siliceous sand having a nominal maximum size of 3/8 in. (9.5 mm). Particles contain major amounts of quartz and quartzite, and subordinate amounts of feldspar, mica, ferruginous rock, and mafic minerals. Particles are variably colored, subangular to subrounded, dense, hard, equidimensional to elongated, unaltered, uncoated, and uncracked. Fine aggregate particles are well-graded and well-distributed. There is no evidence of alkali-aggregate reaction of fine aggregate. Particles are sound during their service in the concrete.

Properties and Compositions of Aggregates	Wall Core
Coarse Aggregates	
Types	Crushed Stone
Nominal maximum size (in.)	3/4 in. (19 mm)
Rock Types	Mixture of a predominant dark gray metamorphic garnetiferous quartzo-feldspathic and micaceous gneiss and a subordinate light brown quartz-feldspar-mica gneiss
Angularity, Density, Hardness, Color, Texture, Sphericity	Angular, dense, hard, medium to dark gray, massive textured, equidimensional to elongated
Cracking, Alteration, Coating	Variably altered, Uncoated, and variably cracked
Grading & Distribution	Well-graded and Well-distributed
Soundness	Sound
Alkali-Aggregate Reactivity	None
Fine Aggregates	
Types	Natural siliceous sand
Nominal maximum size (in.)	3/8 in. (9.5 mm)
Rock Types	Major amounts of quartz and quartzite, and subordinate amounts of feldspar, mica, ferruginous rock, and mafic minerals

Properties and Compositions of Aggregates	Wall Core
Cracking, Alteration, Coating	Variably colored, subangular to subrounded, dense, hard, equidimensional to elongated
Grading & Distribution	Well-graded and Well-distributed
Soundness	Sound
Alkali-Aggregate Reactivity	None

Table 1: Properties of coarse and fine aggregates of concrete.

PASTE

Properties and composition of hardened cement paste are summarized in Table 2. Paste at the near-surface carbonated zones is beige-toned, but interior body is medium gray, dense and hard; freshly fractured surfaces have subvitreous lusters and subconchoidal textures. Residual and relict Portland cement particles are present and estimated to constitute 8 to 10 percent of the paste volume. Hydration of Portland cement is normal. The textural and compositional features of the paste are indicative of a cement content estimated to be 6 to 6$^1/_2$ bags of Portland cement per cubic yard. The concrete has an estimated water-cement ratio (*w/c)* more or less similar throughout the body and is estimated to be from 0.40 to 0.45. There is evidence of deleterious secondary ettringite deposits found in the core. Bonds between the coarse and fine aggregate particles and paste are tight to moderately tight to weak. There is clear evidence of microcracking due to deleterious reactions. The overall quality and condition of the concrete in the wall core is judged to be poor and unsound with evidence of chemical deterioration due to internal sulfate attack. The interior concrete is moderately dense and consolidated but cracked extensively in micro to macro scales due to pyrrhotite oxidation and internal sulfate attack.

Properties and Compositions of Paste	Wall Core
Color, Hardness, Porosity, Luster	Gray, dense and hard, Subtranslucent vitreous
Residual Portland Cement Particles	Normal, 8 to 10 percent by paste volume
Calcium hydroxide from cement hydration	Normal, 10 to 14 percent by paste volume
Pozzolans, Slag, etc.	None
Water-cement ratio (*w/c*), estimated	0.40 to 0.45
Cementitious materials contents, estimated (equivalent to bags of cement per cubic yard)	6 to 6$^1/_2$
Secondary Deposits	Poorly crystalline secondary ettringite infested paste (EIP) as well as relatively well crystalline secondary ettringite lining and filing many air-voids and sometimes in cracks
Depth of Carbonation, mm	40 to 50 mm from inside surface of wall, and 20 to 30 mm from outside surface
Microcracking	Present
Aggregate-paste Bond	Tight to moderately tight to weak (gaps)
Bleeding, Tempering	None
Chemical deterioration	Internal sulfate attack, ettringite infested paste, high sulfate content of paste all due to oxidation of pyrrhotite in crushed

Properties and Compositions of Paste	Wall Core
	gneiss coarse aggregate during service

Table 2: Composition and properties of paste.

AIR

Air occurs as: (a) numerous fine, discrete, spherical and near-spherical voids having sizes of 1 mm; and (b) a few coarse near-spherical and irregularly shaped voids that are characteristic of entrapped air. Concrete is air-entrained having an estimated air content of 6 to 7 percent (Figure 19).

SEM-EDS STUDIES

Figures 41 through 50 provide SEM-EDS analyses of concrete to investigate the following:

1. Composition of iron sulfide minerals in aggregates – from X-ray elemental map, backscatter electron image, X-ray elemental maps, and energy-dispersive x-ray fluorescence spectroscopy - Figures 43 and 44;
2. Composition of paste to determine high sulfur (SO_3) level from infestation of poorly crystalline ettringite in paste from released sulfates from aggregates – Figures 42, 45, and 46;
3. Microstructure of unsound pyrrhotite-bearing aggregate including cracking and extension of cracks from unsound aggregates to paste – Figures 45 and 50;
4. Secondary ettringite crystallization along aggregate-paste interfaces – from backscatter and secondary electron images, X-ray elemental maps, and energy-dispersive x-ray fluorescence spectroscopy – Figures 42, 47 to 50;
5. Secondary ettringite crystallization in air-voids – Figures 41, 42;
6. Gaps around aggregate due to expansion of sulfate-contaminated paste – Figure 46

All these microstructural and microchemical studies are helpful for:

1. Identifying iron sulfide mineral present in aggregate, e.g., low S/Fe atomic ratio than pyrite to indicate pyrrhotite;
2. Evidence of oxidation of pyrrhotite from low S/Fe atomic ratio compared to non-oxidized stoichiometric S/Fe ratio of pyrrhotite;
3. Evidence of unsoundness of pyrrhotite-bearing aggregate from expansion and cracking;
4. Evidence of internal sulfate attack in paste from high sulfur (as SO_3) level of paste compared to normal Portland cement paste, due to secondary ettringite infestation in confined areas in paste;
5. Evidence of internal sulfate attack in paste from gaps around aggregates due to expansion of paste and secondary ettringite crystallization along aggregate-paste interfaces.

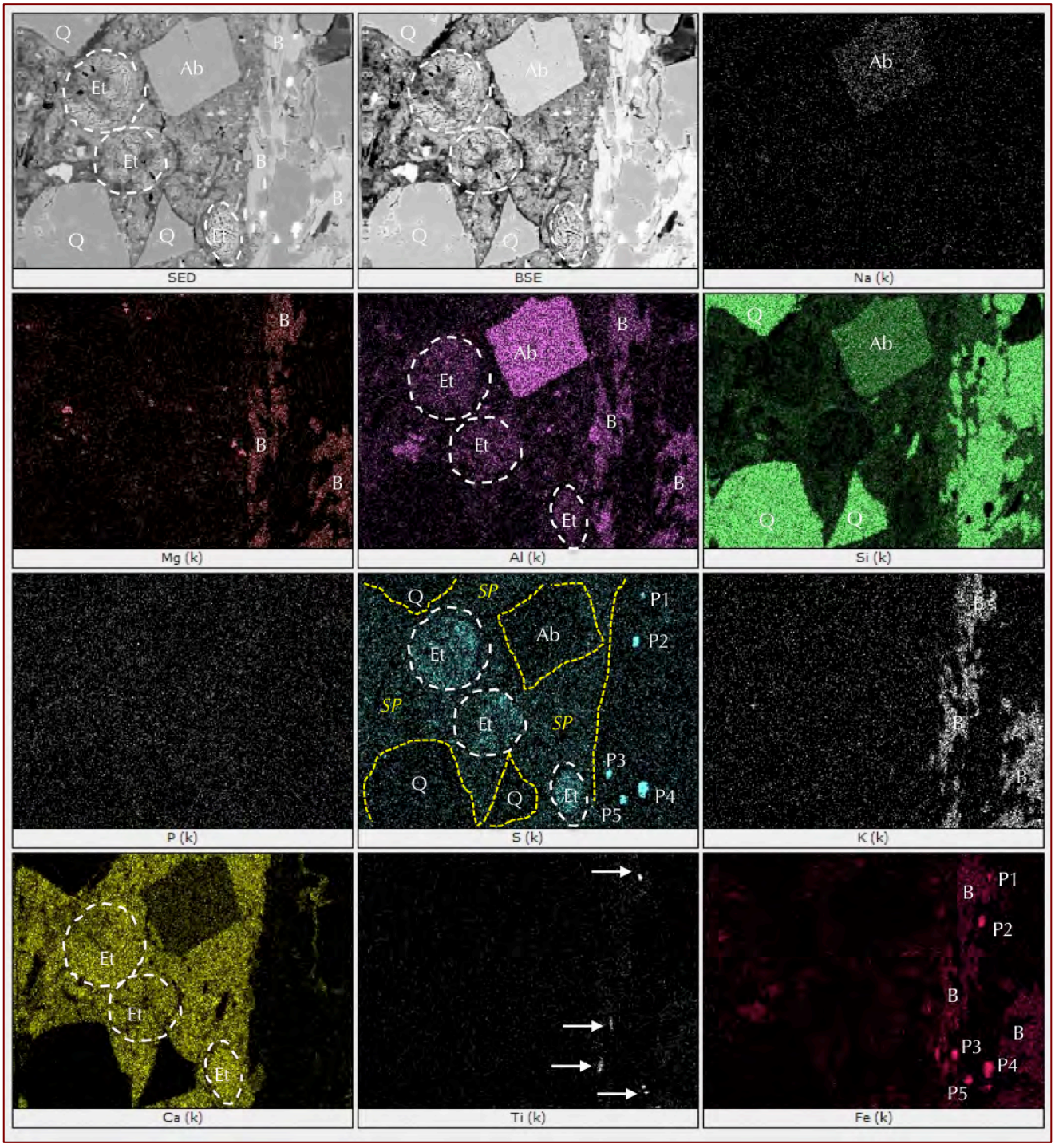

Figure 41: X-ray elemental maps of various elements (K-lines) showing: (a) three ettringite (Et) filled air-voids that are highlighted in respective maps of Ca, Al, and S the three main elements in ettringite, (b) albitic feldspar (Ab) in gneiss from Na-Al-Si maps, (c) quartz (Q) sand particles from characteristic Si-maps, (d) biotite (B) flakes in gneiss from characteristic Fe-Mg-K-Si-Al maps, (e) sulfate-contaminated paste (*SP*) in S-map having higher S-concentrations than aggregates (but lower sulfur than etringite-filled voids), (f) five pyrrhotite (P1 to P5) grains in aggregate highlighted in Fe and S maps, and (g) a few tiny iron-titanium (ilmenite) grains marked by arrows in Ti-map.

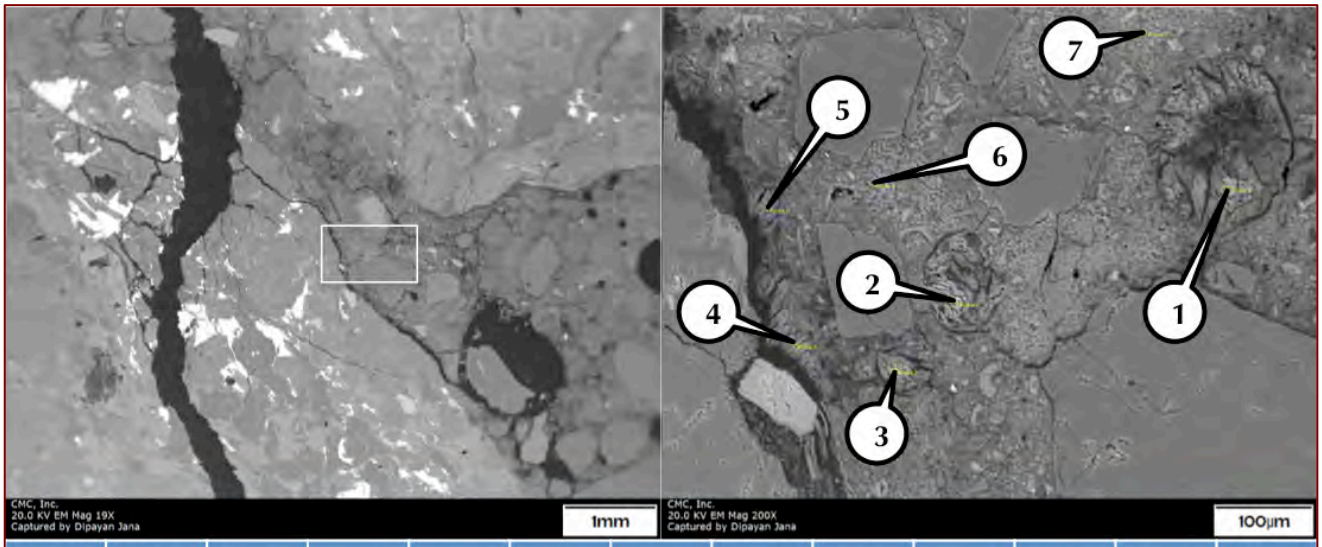

Probe	CaO	SiO_2	Al_2O_3	Na_2O	MgO	SO_3	K_2O	P_2O_5	TiO_2	FeO	Total	Phase
1	57.58	13.90	10.48	0.00	0.00	15.12	0.19	2.72	0.00	0.00	99.99	Ettringite
2	49.67	13.42	13.80	0.00	0.00	19.14	0.02	3.20	0.00	0.74	99.25	Ettringite
3	52.65	15.97	11.32	0.00	0.00	15.82	0.00	3.30	0.00	0.94	99.06	Ettringite
4	51.69	13.34	12.02	0.00	0.00	18.08	0.36	2.96	0.34	1.20	98.79	Ettringite
5	49.43	17.27	13.98	0.00	0.00	14.27	0.72	3.21	0.00	1.13	98.88	Ettringite
6	55.32	29.24	2.06	0.00	0.00	5.02	0.20	3.25	0.59	4.32	95.68	Paste
7	55.24	29.16	2.45	0.00	0.00	5.08	0.63	2.67	0.18	4.58	95.41	Paste

Figure 42: Secondary electron image (top left), enlarged view of the boxed area in the top left shown in the top right, and X-ray elemental analyses of various phases (bottom Table) showing compositions of secondary ettringite crystallization in three air-voids (Probe Nos. 1 through 3), in aggegate-paste interface (Probe Nos. 4 and 5) and compositions of paste (Probe Nos. 6 and 7). In all Probes, analyses were done at the tips of the callouts. The top left photo shows a pyrrhotite-bearing crushed gneiss coarse aggregate particle with extensive macro and microcracking (highlighted in dark), and, pyrrhotite and other iron inclusions (highlighted in bright areas in aggregates). Paste in Probe Nos. 6 and 7 show sulfate contents (as SO_3) of 5 percent, which are significantly higher than normal less than 1% sulfate (as SO_3) in a paste commonly found in Portland cement concretes containing no iron sulfide contaminants. Clearly, release of sulfate from pyrrhotite has contaminated the paste to promote internal sulfate attack with manifestation of additional cracking in the paste and along aggregate-paste interfaces, above and beyond cracking in the unsound aggregates from pyrrhotite oxidation.

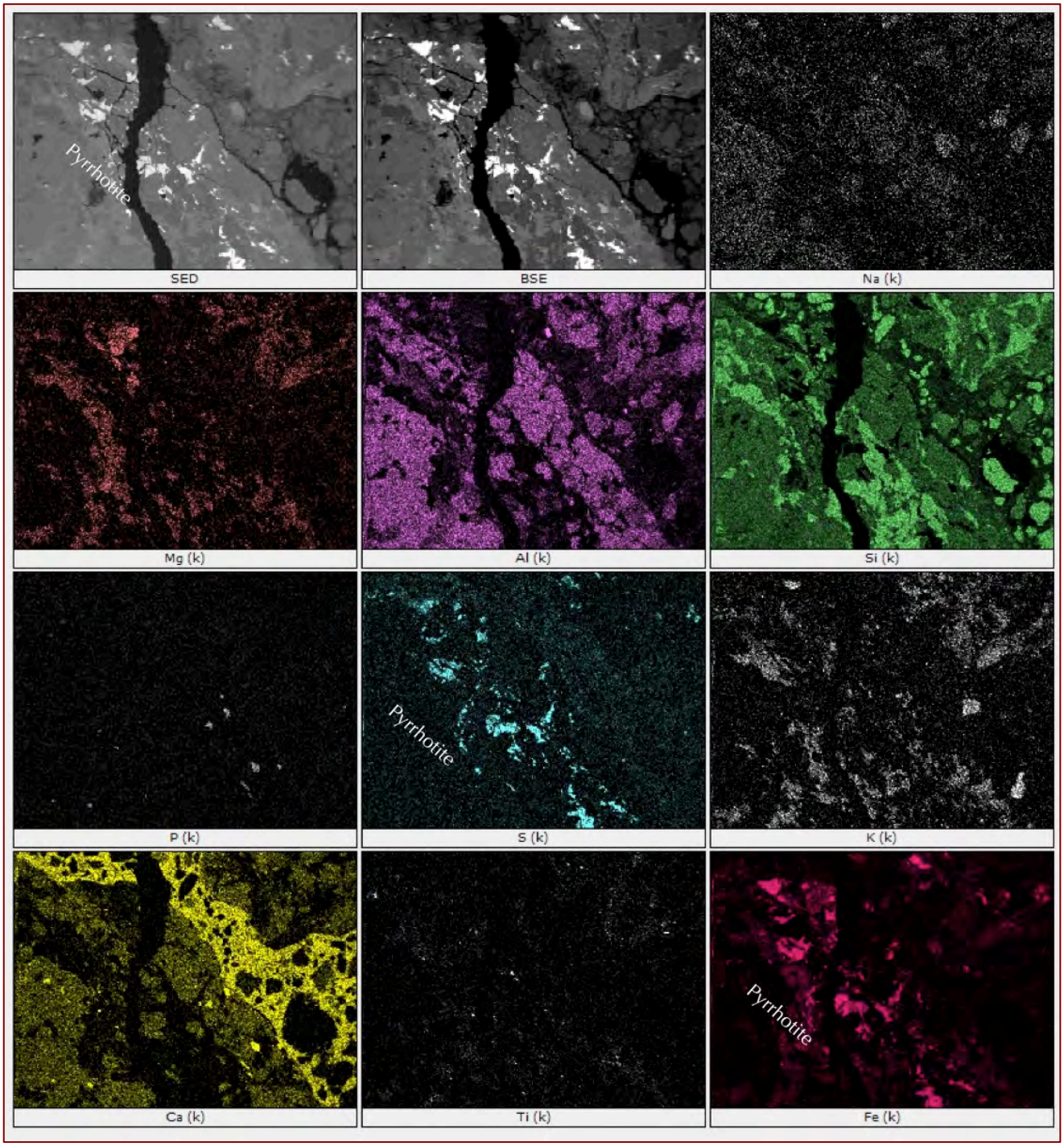

Figure 43: X-ray elemental maps of various elements (K-lines) showing pyrrhotite inclusions in a crushed gneiss coarse aggregate particle (shown in Figure 34) that is characterized by high sulfur and iron in respective elemental maps. Paste between two gneiss aggregate particles show characteristic high calcium and silica in respective maps. The bright spots in the Mg, Al, Na, K, and Si maps show biotite mica in gneiss; very bright areas in the Si map in paste are from quartz sand particles in paste.

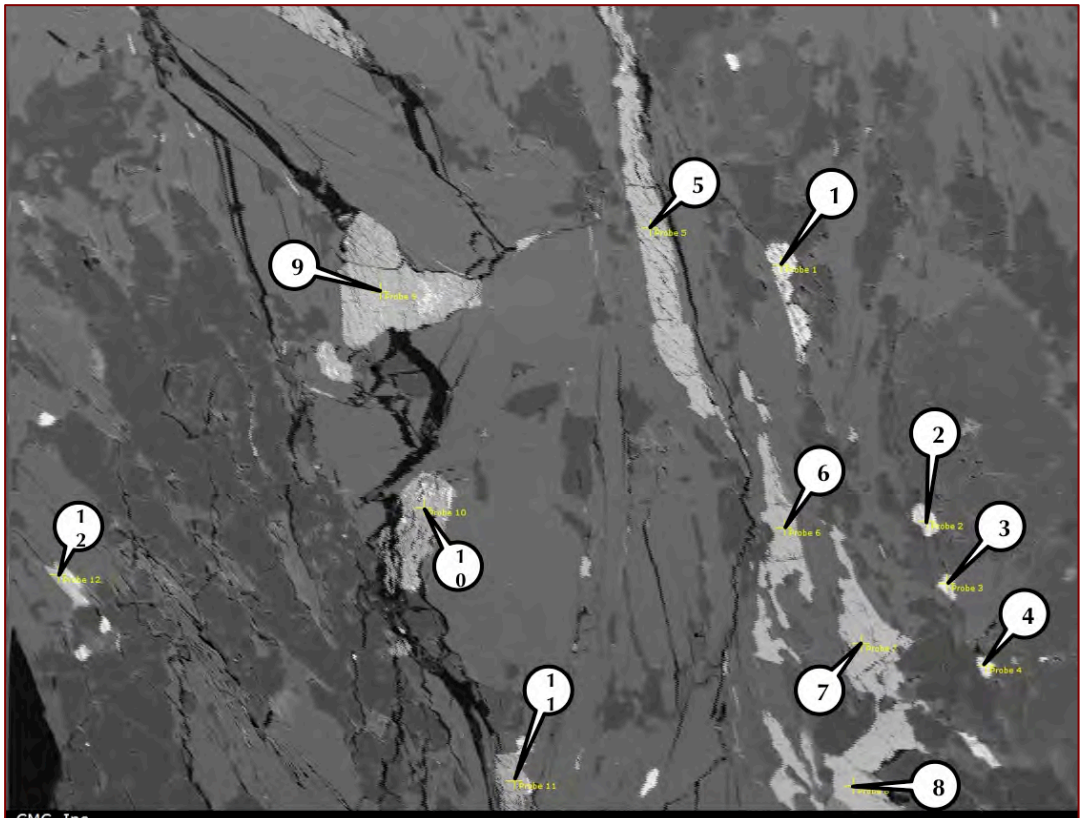

Probe	Ca	Si	Al	Na	Mg	S	K	P	Ti	Fe	O	S/Fe	O/Fe	Phase
1	0.47	0.43	0.33	0.00	0.00	27.41	0.10	0.79	0.09	70.34	0.02	0.39	0.00	Pyrrhotite
2	0.14	0.00	0.17	0.01	0.00	30.91	0.12	0.43	0.00	68.21	0.01	0.45	0.00	Pyrrhotite
3	0.00	0.33	0.00	0.01	0.00	30.94	0.42	0.82	0.58	66.90	0.00	0.46	0.00	Pyrrhotite
4	19.79	42.03	21.88	0.07	0.00	2.87	0.21	4.39	0.13	0.44	8.18	6.52	18.59	?
5	0.30	0.84	0.76	0.00	0.00	0.76	0.12	0.91	44.62	51.26	0.43	0.01	0.01	Fe-Ti-Oxide
6	0.28	1.19	0.01	0.00	0.00	0.67	0.00	1.55	43.53	50.84	1.93	0.01	0.04	Fe-Ti-Oxide
7	0.06	0.59	0.00	0.00	0.00	1.05	0.00	0.89	43.86	52.94	0.60	0.02	0.01	Fe-Ti-Oxide
8	0.29	1.00	0.04	0.00	0.00	1.09	0.47	0.93	44.04	50.46	1.68	0.02	0.03	Fe-Ti-Oxide
9	5.11	1.24	0.07	0.00	0.00	2.42	0.08	1.16	0.00	88.75	1.18	0.03	0.01	Fe-Oxide/hydroxide
10	6.54	2.16	0.12	0.00	0.00	1.06	0.10	1.01	0.00	88.24	0.75	0.01	0.01	Fe-Oxide/hydroxide
11	0.33	31.14	12.09	0.00	6.35	2.72	14.30	2.79	4.83	19.17	6.29	0.14	0.33	Biotite
12	4.19	0.36	0.56	0.00	0.00	5.57	0.00	1.17	0.00	87.73	0.41	0.06	0.00	Fe-Oxide/hydroxide

Figure 44: Secondary electron image (top) and X-ray elemental analyses (bottom) of various iron minerals in a crushed gneiss coarse aggregate particle showing three different types of opaque iron minerals: (a) iron sulfide (pyrrhotite) having high Fe and S (S/Fe ratio <0.5 indicating oxidaiton) in the blue rows in the Table, (b) iron-titanium oxides (rutile, ilmenite) having high Fe and Ti in the green rows, and Fe-oxide or hydroxide having very high Fe in orange rows. All three opaqaue iron minerals show similar bright areas in the secondary and backscatter electron images.

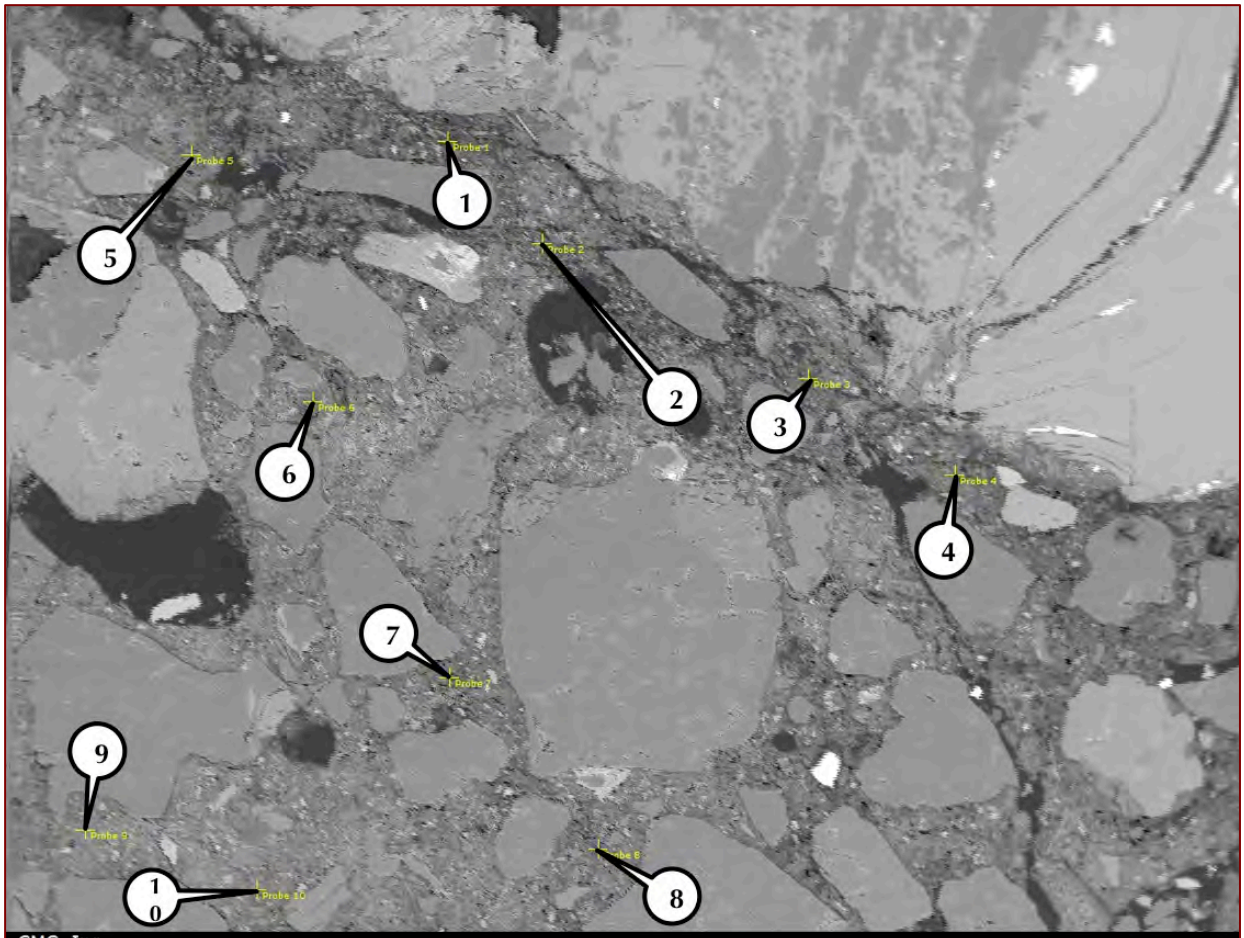

Probe	CaO	SiO_2	Al_2O_3	Na_2O	MgO	SO_3	K_2O	P_2O_5	TiO_2	FeO	Total	Phase
1	10.27	74.06	2.53	0.00	0.00	4.87	0.42	7.49	0.12	0.25	99.76	Quartz+
2	32.70	33.94	6.99	0.00	0.35	4.16	5.54	3.09	2.36	10.87	89.13	Paste
3	55.14	26.88	3.65	0.00	0.00	6.34	0.36	3.70	0.42	3.51	96.49	Paste
4	55.12	26.24	3.80	0.00	0.00	5.59	0.00	4.26	0.41	4.57	95.42	Paste
5	56.25	22.64	3.33	0.00	0.00	5.33	0.24	2.91	0.82	8.49	91.52	Paste
6	53.38	27.65	4.40	0.00	0.26	6.57	0.13	4.33	0.00	3.27	96.72	Paste
7	50.98	30.41	4.97	0.00	0.00	6.13	0.27	4.46	0.00	2.78	97.22	Paste
8	0.00	87.60	0.45	0.00	0.00	4.68	0.00	6.41	0.85	0.00	99.99	Quartz
9	54.52	22.60	3.98	0.00	0.92	4.70	0.32	2.74	0.80	9.41	90.58	Paste
10	52.90	30.13	2.50	0.00	0.00	5.79	0.00	3.87	0.85	3.96	96.04	Paste

Figure 45: : Secondary electron image (top) and and X-ray elemental analyses (bottom) of various areas of paste showing sulfate contents (as SO_3) of 4.1 to 6.5 percent, which are significantly higher than normal less than 1% sulfate (as SO_3) in a paste commonly found in Portland cement concretes containing no iron sulfide contaminants. Clearly, release of sulfate from pyrrhotite has contaminated the paste to promote internal sulfate attack with manifestation of additional cracking in the paste and along aggregate-paste interfaces, above and beyond cracking in the unsound aggregates from pyrrhotite oxidation.

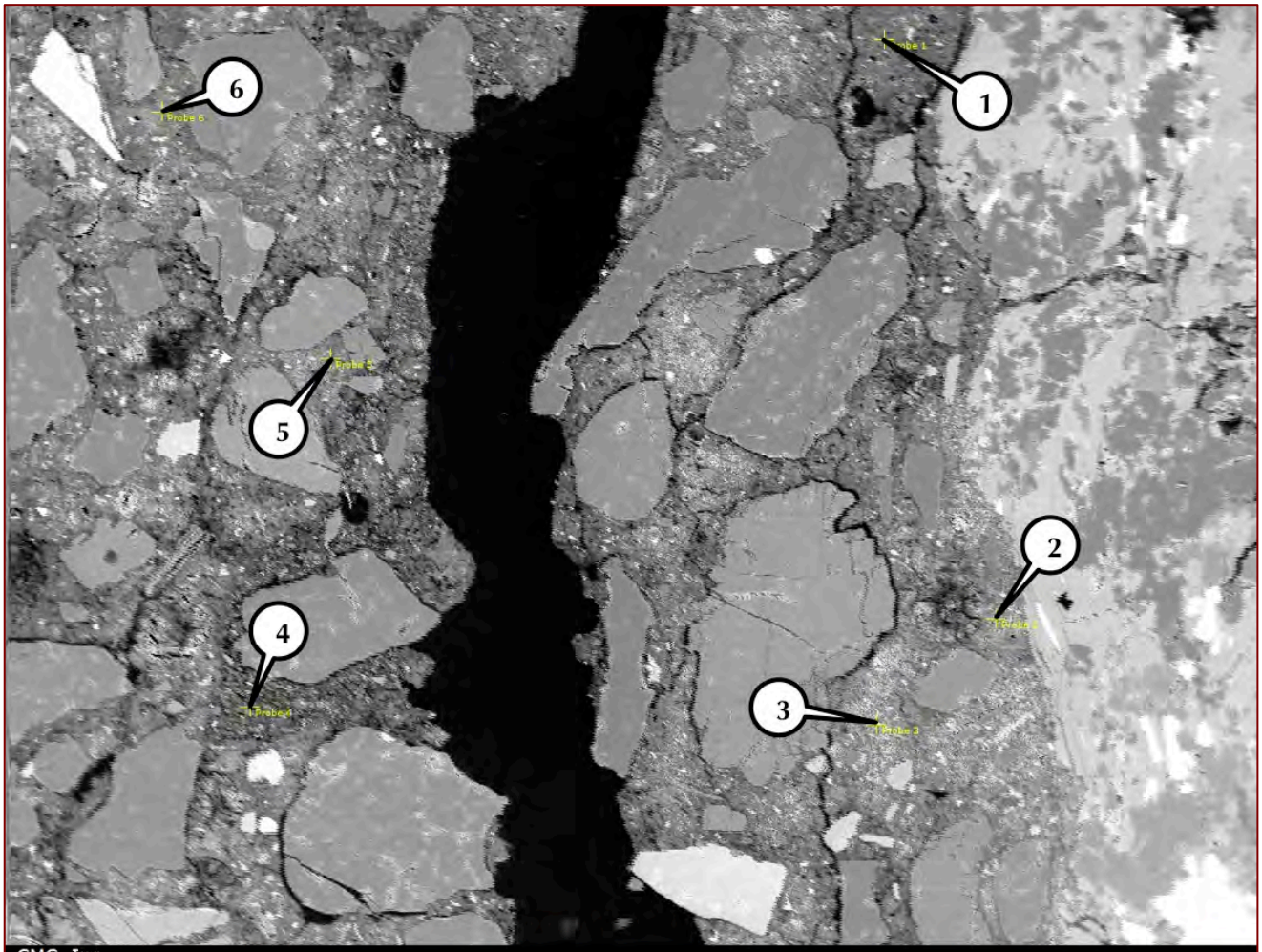

Probe	CaO	SiO_2	Al_2O_3	Na_2O	MgO	SO_3	K_2O	P_2O_5	TiO_2	FeO	Total	Phase
1	50.49	31.00	3.52	0.00	0.00	6.12	0.88	3.35	0.50	4.14	95.86	Paste
2	43.50	18.58	14.66	0.00	0.00	15.09	1.14	2.98	0.06	3.98	96.01	Paste+ Ettringite
3	51.53	25.95	4.15	0.00	0.60	6.65	0.33	3.53	0.31	6.93	93.05	Paste
4	12.87	56.00	18.98	0.45	0.00	4.04	1.04	6.61	0.00	0.00	99.99	Paste+ Feldspar
5	35.38	14.73	10.99	0.00	13.15	5.03	0.44	2.80	1.64	15.83	84.16	Paste
6	8.66	73.76	8.98	1.19	0.03	3.01	0.38	3.50	0.05	0.42	99.56	Paste+ Quartz

Figure 46: Backscatter electron image (top) and X-ray elemental analyses (bottom) of various areas of paste showing gaps around fine aggregates that are common in many DEF-affected concretes due to expansion of paste due to internal sulfate attacks. Compositional analyses of paste *per se* in Probe Nos. 1, 3, and 5 show sulfate contents (as SO_3) from 5 to 6.6 percent, which are significantly higher than normal less than 1% sulfate (as SO_3) in a paste commonly found in Portland cement concretes containing no iron sulfide contaminants. Clearly, release of sulfate from pyrrhotite has contaminated the paste to promote internal sulfate attack with manifestation of additional cracking in the paste and along aggregate-paste interfaces, above and beyond cracking in the unsound aggregates from pyrrhotite oxidation.

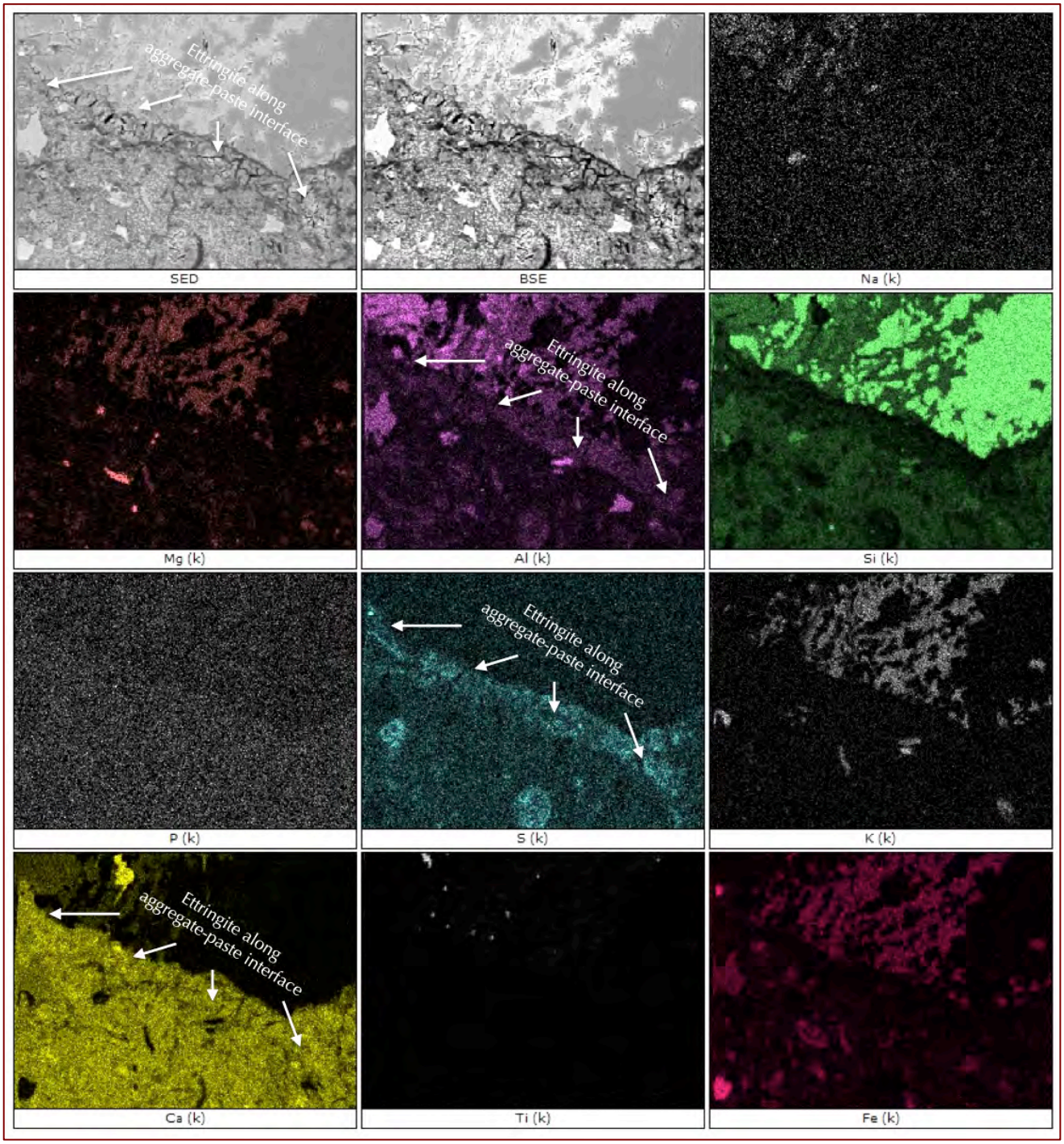

Figure 47: X-ray elemental maps of various elements (K-lines) showing secondary ettringite crystallization along aggregate-paste interface that is characterized by high sulfur, aluminum, and calcium in respective elemental maps.

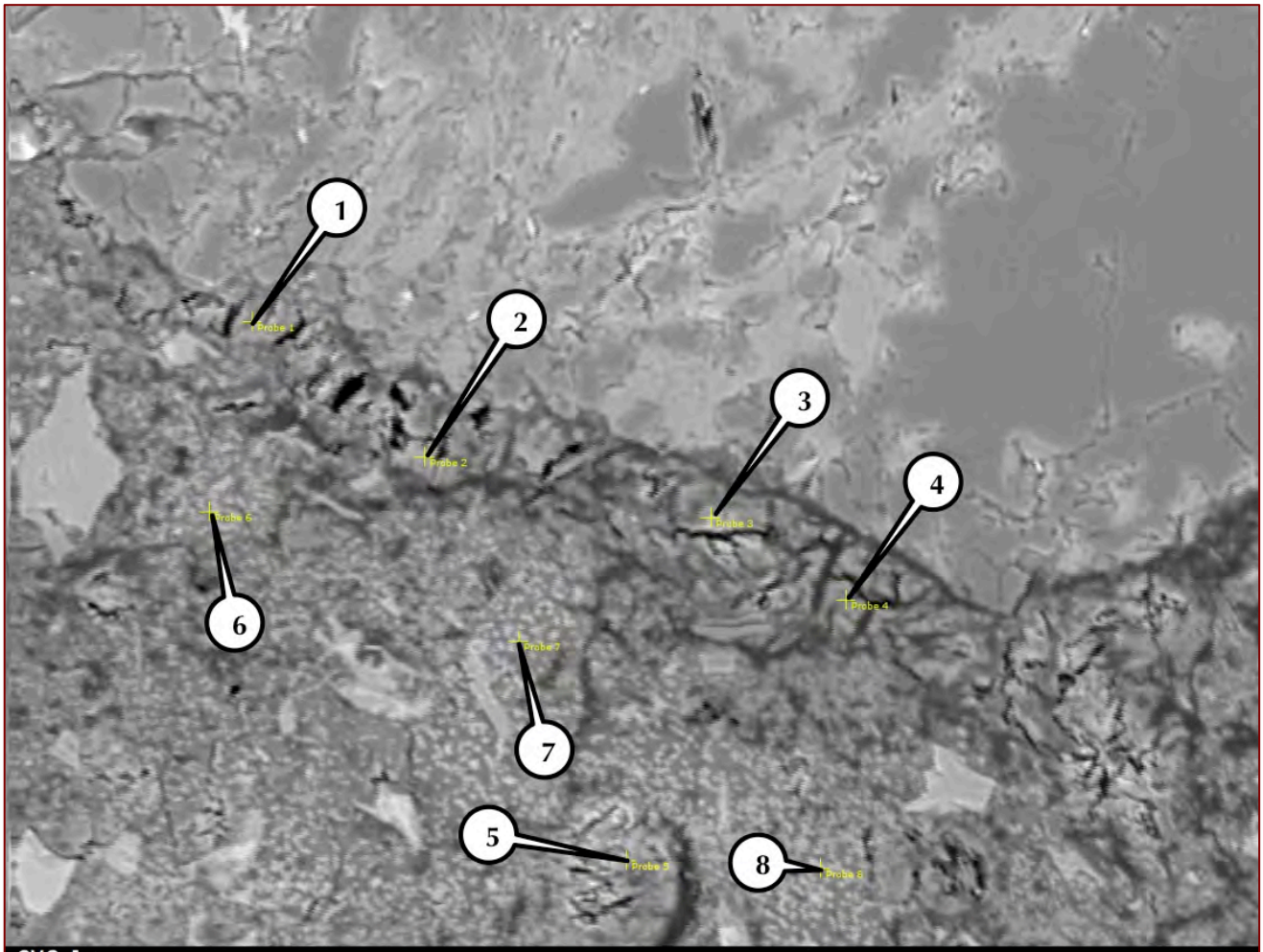

Probe	CaO	SiO_2	Al_2O_3	Na_2O	MgO	SO_3	K_2O	P_2O_5	TiO_2	FeO	Total	Phase
1	54.91	15.54	8.59	0.00	0.00	15.70	0.52	3.77	0.00	0.96	99.03	
2	56.12	20.52	9.88	0.00	0.00	7.78	0.00	3.95	0.35	1.40	98.60	Ettringite along A-P Interface
3	60.78	18.92	6.80	0.00	0.00	8.27	0.63	3.78	0.42	0.40	99.60	
4	51.75	19.78	14.24	0.00	0.00	10.32	0.55	3.01	0.00	0.33	99.65	
5	56.92	15.51	7.56	0.00	0.00	15.20	0.50	3.79	0.00	1.10	99.48	Ettringite in a void
6	55.88	27.63	2.38	0.00	0.00	5.11	0.01	3.59	0.29	5.11	94.89	Paste
7	56.64	28.46	1.98	0.00	0.01	4.83	0.08	3.42	0.56	4.03	95.98	Paste
8	53.76	17.73	13.14	0.00	0.00	10.59	0.53	3.73	0.08	0.43	99.56	Paste

Figure 48: Backscatter electron image (top) and and X-ray elemental analyses (bottom) of secondary ettringite crystalization along aggregate-paste interface showing characteristic Ca-Al-S compositions of ettringite and sulfate-contaminated calcium aluminum silicate hydrate paste.

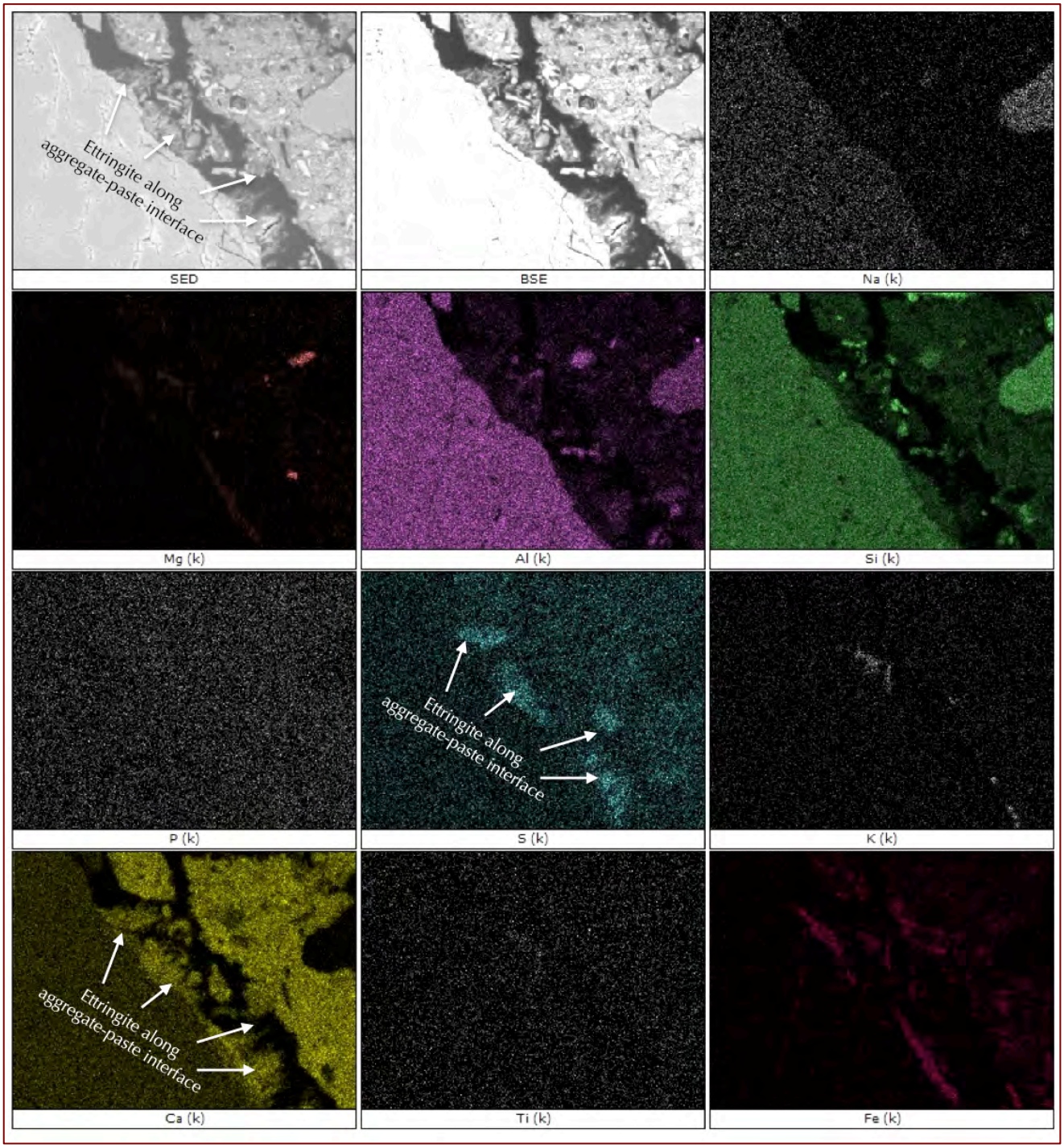

Figure 49: X-ray elemental maps of various elements (K-lines) showing secondary ettringite crystallization along aggregate-paste interface that is characterized by high sulfur, aluminum, and calcium in respective elemental maps.

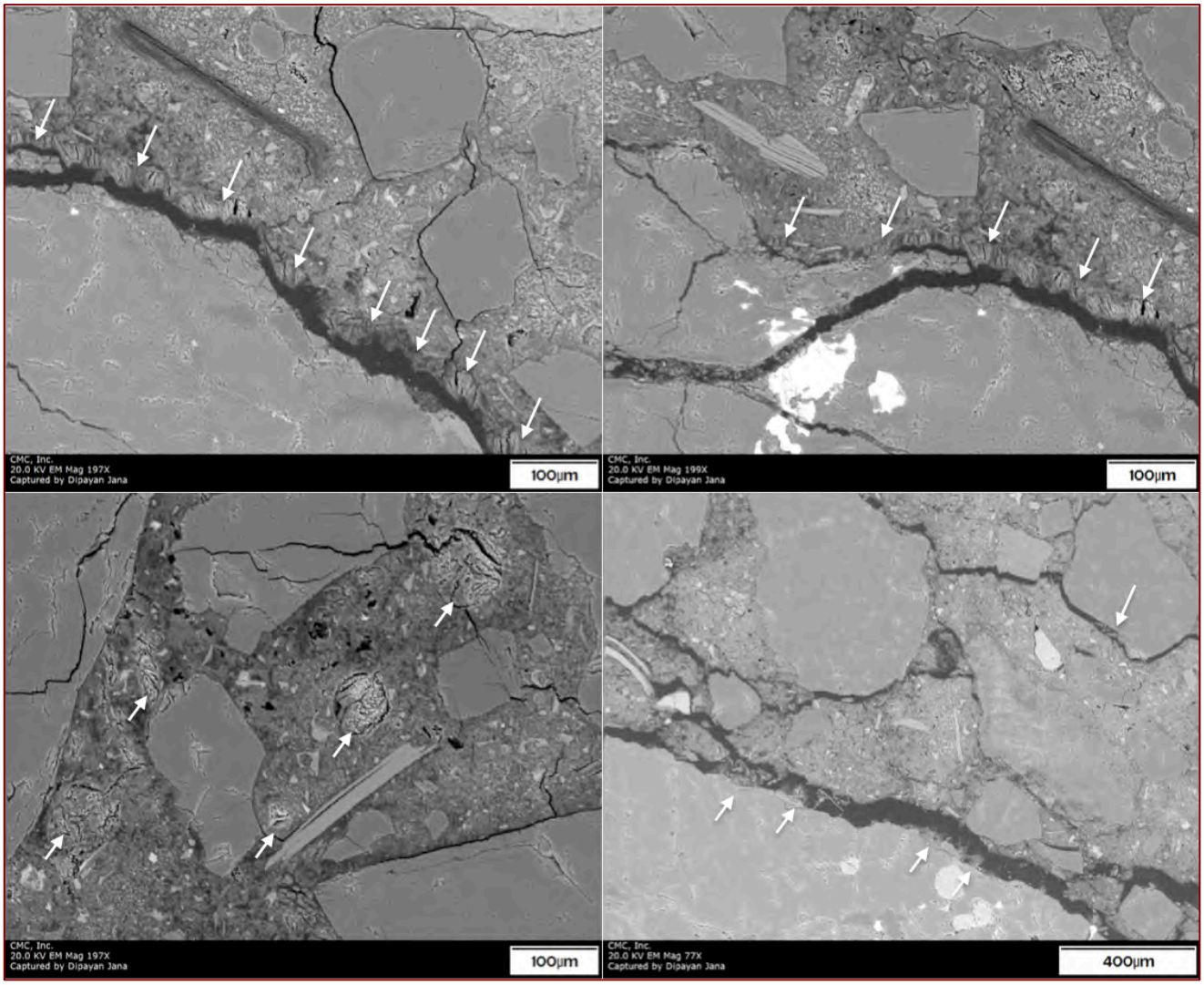

Figure 50: Secondary electron images showing secondary ettringite crystallization in microcracks along aggregate-paste interfaces, and in air-voids (bottom left photo). All these features are testiments of having moisture in a sulfate-contaminated paste.

The following conclusions are drawn from the SEM-EDS analyses:

a) SEM-EDS studies found secondary ettringite crystallization mostly in air-voids and only occasionally in microcracks including in gaps around aggregates and at aggregate-paste interfaces, which are not as common as in other DEF-distressed concretes. Most of the microcracks are empty and gaps around aggregates due to paste expansion are not as frequent as in other DEF-affected concretes.

b) However, EDS analyses of sulfate contents of paste are in the range of 4 to 6.5% (as SO_3), which is noticeably higher than less than 1% sulfate (SO_3) commonly found in the paste of a normal Portland cement concrete prepared using a Portland cement containing 3 percent sulfate at a similar water-cement ratio and cement content of the present core but containing no iron sulfide contaminant. Clearly, high sulfate content of paste detected from EDS analyses is consistent with the overall high bulk sulfate content of concrete, indicating sulfate release from pyrrhotite oxidation.

c) SEM-EDS analyses found three different optically opaque iron species in gneiss, e.g., iron sulfide (pyrrhotite), oxidation products of pyrrhotite measured in the EDS as iron oxide (determined in XRD as ferrihydrite), and iron-titanium oxide (rutile and ilmenite).

d) High sulfate content of paste, high bulk sulfate content (1.45%) of concrete, yet the absence of abundant secondary ettringite in many microcracks and gaps around aggregates except more profuse crystallization in air voids – all these chemical and microstructural features indicate that perhaps microcracking due to paste expansion by internal sulfate attack occurred from poorly crystallized ettringite or perhaps in a colloidal form within the confined spaces in paste, which is not as frequently diagnosed even in SEM as in other DEF-affected concretes having well-crystallized delayed ettringite in cracks, gaps, and voids.

MICROSTRUCTURAL EVIDENCE OF PYRRHOTITE-OXIDATION & RELATED CRACKING

a. Visible and invisible cracking in pyrrhotite-bearing crushed gneiss aggregates, many extending from aggregates to paste (Figures 30 to 33, 37 to 39);
b. Lower S/Fe ratio (< 0.50) of oxidized pyrrhotite in SEM-EDS analyses than that from stoichiometry of non-oxidized pyrrhotite (Figures 44)

MICROSTRUCTURAL EVIDENCE OF INTERNAL SULFATE ATTACK BY RELEASED SULFATES

a. High sulfate (SO_3) content in paste (Figures 42, 45, 46, 48)
b. Ettringite infected paste – the breeding ground for internal sulfate attack (Figures 32 to 36)
c. Secondary ettringite crystallization in microcracks (Figures 42, 47 to 50)
d. Secondary ettringite crystallization in aggregate-paste interfaces (Figures 38, 39, 42, 47 to 50)
e. Gaps around aggregates due to expansion of paste (Figure 45)

XRD & XRF OF UNSOUND COARSE AGGREGATE FOR SULFIDE MINERALOGY, OXIDATION PRODUCTS, AND SULFUR (SO_3) CONTENTS

Figure 51 provides results of X-ray diffraction patterns, semi-quantitative proportions of different minerals, and X-ray fluorescence analyses of a representative dark gray crushed gneiss coarse aggregate and a light brown crushed gneiss coarse aggregate carefully extracted from the core by removing all adhered paste to show the presence of pyrrhotite only in the dark gray particle instead of any other sulfide mineral (inset at the top right photo shows one such particle with a pyrrhotite grain shown by an arrow) and its oxidation product ferrihydrite in both particles. Dominant minerals of aggregates are quartz, albitic feldspar, pyrope garnet, and biotite for garnetiferous quartzo-feldspathic and micaceous gneiss rock type. Extracted aggregates were pulverized and pressed to pellet to use for both XRD and XRF studies. Table 3 provided bulk compositions of aggregates and sulfur (as SO_3) levels from XRF.

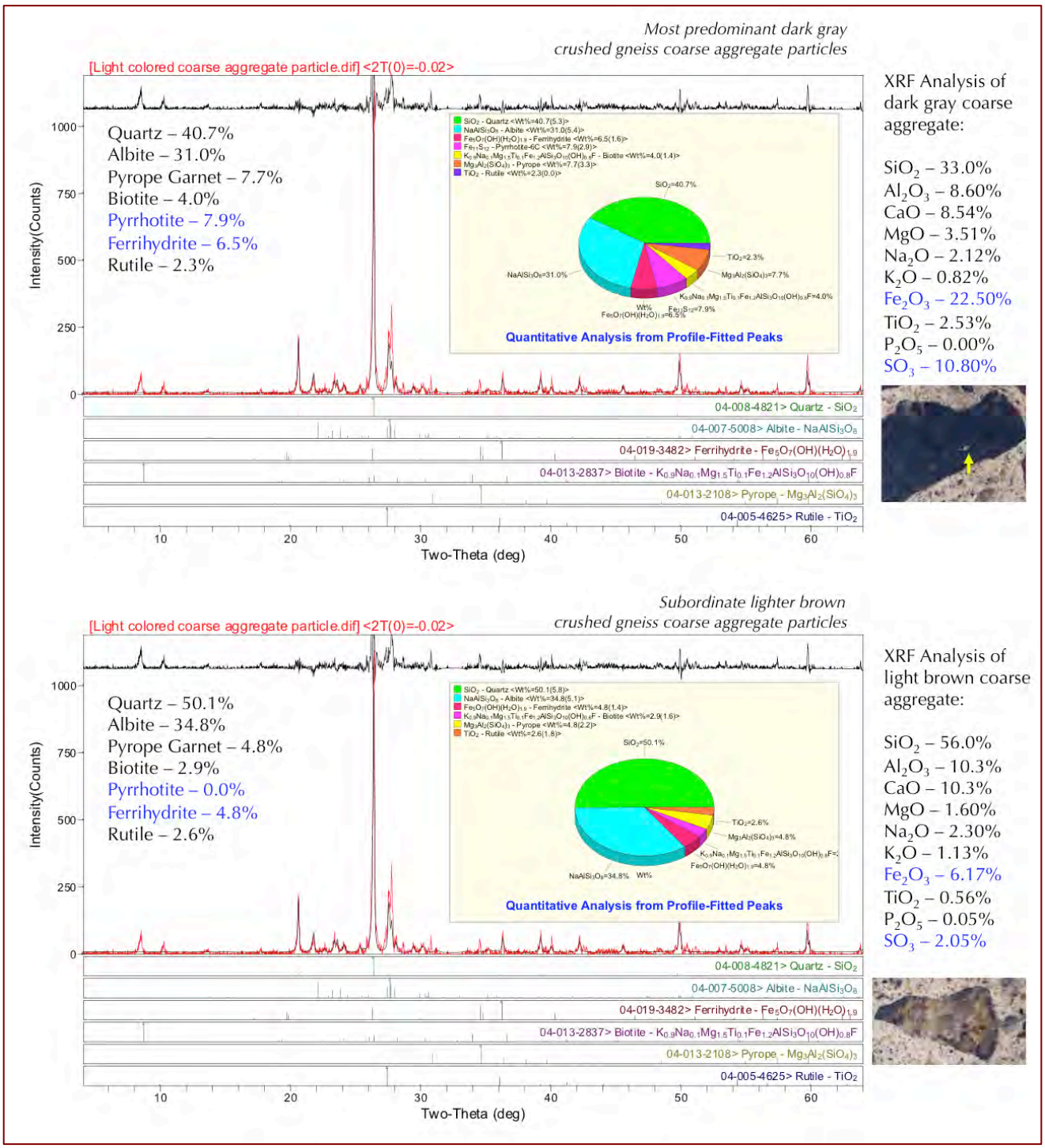

Figure 51: X-ray diffraction patterns, quantitative proportions of minerals, and X-ray fluorescence analyses of a representative dark gray crushed gneiss coarse aggregate (top) and a light brown crushed gneiss coarse aggregate (bottom) showing the presence of pyrrhotite only in the dark gray particle (inset at the top right shows one such particle with a pyrrhotite grain shown by an arrow) and its oxidation product ferrihydrite in both particles, and the presence of pyrope garnet.

Oxide (wt.%) from XRF	Dark Gray Crushed Gneiss Coarse Aggregate	Light Brown Crushed Gneiss Coarse Aggregate	Bulk Concrete
SiO_2	33.0	56.0	54.5
Al_2O_3	8.60	10.30	10.60
Fe_2O_3	22.50	6.17	7.29
CaO	8.54	10.30	8.92
MgO	3.51	1.60	3.12
K_2O	0.82	1.13	1.75
TiO_2	2.53	0.56	1.00
P_2O_5	-	0.05	0.09
SO_3	10.80	2.05	1.45
Balance	7.66	9.57	9.89
Total	100.0	100.0	100.0
Mineralogy from XRD	**Dark Gray Crushed Gneiss Coarse Aggregate**	**Light Brown Crushed Gneiss Coarse Aggregate**	**Bulk Concrete**
Quartz	40.7	50.1	54.3
Feldspar (Albite)	31.0	34.8	33.2
Pyrope Garnet	7.7	4.8	0.0
Biotite	4.0	2.9	5.1
Pyrrhotite	7.9	0.0	0.9
Ferrihydrite	6.5	2.3	5.1
Rutile	2.3	2.6	1.5
Calcite	0.0	0.0	1.5

Table 3: Results of XRF and XRD analyses of coarse aggregate particles for sulfide mineralogies and oxidation products of iron sulfide, XRF analyses of bulk concrete for sulfate (SO_3) content, and XRD analyses of bulk concrete to show the presence of ferrihydrite in bulk concrete from oxidation of pyrrhotite.

XRD & XRF OF BULK CONCRETE FOR SULFATE LEVEL IN CONCRETE

The wall concrete showed abundant secondary ettringite crystallization lining or filing many air-voids. Any Portland cement concrete exposed to moisture during service form secondary ettringite deposits lining and filling air voids. To establish the source of secondary ettringite i.e. from Portland cement's sulfate and/or from oxidation of pyrrhotite-bearing aggregates require determination of sulfate levels in concrete i.e. if the level is higher than that expected from a typical Portland cement concrete where sulfate (as SO_3) content in cement is around 3 weight percent, giving about 0.45 percent sulfate in concrete for a usual cement content of 15 percent by mass of a normal weight concrete. Excess sulfate in concrete above 0.45 percent from cement's contribution would correspond to the pyrrhotite-aggregate source if no other sulfate source were present.

To determine the sulfate (SO_3) level of bulk concrete, a thin slice of concrete was sectioned through the entire length of the core and pulverized and pressed into a pellet to do XRF analysis, which showed 1.45 percent sulfate (SO_3) by weight of concrete i.e. more than 3 times sulfate than that normally contributed from Portland cement. Clearly, some of the secondary ettringite crystallization in air-voids is derived from sulfates other than cement having the most likely source from oxidation of pyrrhotite in coarse aggregate. XRD analysis of the concrete pellet showed similar mineralogies (plus calcite) as in coarse aggregates including the presence of ferrihydrite.

ION CHROMATOGRAPHY FOR POTENTIAL SULFATE RELEASE OF AGGREGATES IN ACCELERATED OXIDATION TEST

Pyrrhotite-bearing crushed gneiss coarse aggregate particles were carefully extracted from the core and cleaned of all adhering paste to be crushed and immersed in a strong oxidant (35% hydrogen peroxide) solution. Four dark gray gneiss and one light brown gneiss particle were extracted. A separate crushed gneiss aggregate from a different project with no known iron sulfide mineral from XRD study was included as a 'control' sample.

For each extracted aggregate, after crushing, two 4-gram aliquots were selected for determining released sulfate contents at two different days. Each sample was immersed in a 25-mL hydrogen peroxide (35%) solution, then at the end of run filtered all solid residues with a 25-micron filter paper, the filtrate was then re-filtered through a 0.45-micron filter paper. The filtrate thus prepared is then diluted with distilled water to 250 mL to be analyzed in IC.

Figure 52 shows normalized amounts of sulfates released from various crushed gneiss coarse aggregate particles extracted from the core and submersed in 35% hydrogen peroxide solution for various days, along with no release of any sulfate from the control aggregate without any sulfide. The bottom photo in Figure 52 incorporated results of accelerated oxidation tests of quarried rocks by Wille and Zhong (2016) as well as the present studies of released sulfates at various days.

As seen in both photos, all pyrrhotite-bearing aggregates show noticeable release of sulfates in an oxidizing environment even after service in concrete, compared to a control aggregate of no sulfide. Apparently, released sulfates have contaminated the paste, and formed the seeds for internal sulfate attack by reactions with cement hydration products.

Compared to the study of Wille and Zhong (2016), this study showed a large range of released sulfate from different crushed gneiss coarse aggregate particles, indicating various amounts of pyrrhotite present in the aggregate particles. One light brown gneiss showed a much higher amount of released sulfate than the four dark gray gneiss, even though XRD analysis of another light brown gneiss did not detect any pyrrhotite, which, again, indicates a rather large variation in pyrrhotite contents amongst crushed gneiss particles.

Due to these clear signals of sulfates released from pyrrhotite-bearing aggregates, accelerated oxidation test of potential pyrrhotite-bearing aggregates followed by ion chromatography of filtrate to determine the sulfate contents are helpful techniques for evaluation of quarried aggregates for potential pyrrhotite-related distress by internal sulfate attacks.

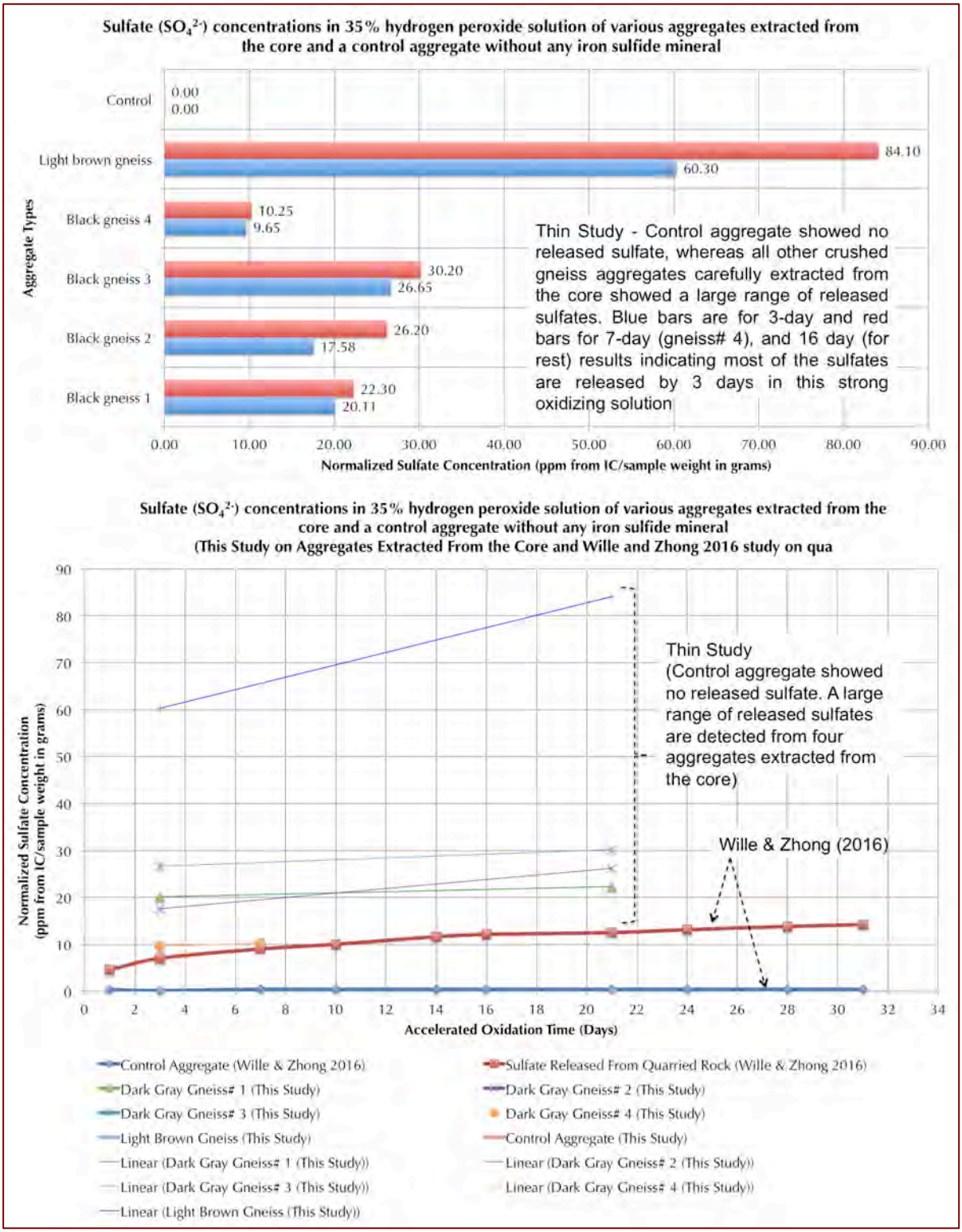

Figure 52: Results of accelerated oxidation test of five crushed gneiss coarse aggregate particles (four dark gray and one light brown gneiss) carefully extracted from the core and cleaned of all adhering paste to be crushed and immersed in a strong oxidant (35% hydrogen peroxide) solution for several days. Bottom graph included results of Wille and Zhong (2016) of quarried stones all showing sulfate release from pyrrhotite-bearing aggregates. Compared to Wille and Zhong (2014) this study showed a large range of released sulfates from extracted crushed gneiss coarse aggregate.

DISCUSSION

IRON SULFIDE MINERALS IN CONCRETE AGGREGATES[1]

Iron sulfide minerals (e.g., pyrite FeS_2, or pyrrhotite $Fe_{1-x}S$, x varies from 0 to 0.125) occurring mostly as 'accessory' minerals in many concrete aggregates are known to cause various deteriorations in concrete in service. **Oxidation of iron sulfide minerals in concrete** can cause various deteriorations from **unsightly staining** on the exposed surface to **popouts** of near-surface unsound aggregates (Jana 2008) and associated local fracturing to in extreme cases severe **cracking, microcracking, and loss of strength** of concrete from **internal sulfate attacks** by reactions between released sulfate and hydrogen ion (sulfuric acid) from oxidation reactions with cement hydration products – all resulting in expansive reactions leading to structural instability. The mineral pyrrhotite has been found to be the most reactive and detrimental to the durability of concrete. If a suspicion arises regarding a possible pyrrhotite-related distress in a concrete structure then identification of the type of iron sulfide mineral responsible for the distress, and quantification of the total sulfur content in the pyrrhotite-bearing aggregate would be prudent to determine whether the mineral may have an effect on the durability of concrete.

Background

Iron sulfide minerals occur commonly as minor, but significant accessory minerals in a variety of rocks. Pyrite is the most common of all sulfide minerals. It is a common accessory mineral in igneous, metamorphic, and sedimentary rocks, and is a major phase in many sulfide ore bodies. In hand sample, this mineral has a metallic luster and pale yellow color. Microscopically, pyrite is a cubic isotropic mineral with a yellowish-white color in reflected light (Deer et al., 1992). Pyrite, with the chemical formula FeS_2, is composed of 46.6% Fe and 53.5% S.

Pyrrhotite is the second most common iron sulfide in nature, found as a primary accessory mineral in ultra-mafic and mafic rocks, metamorphosed igneous and sedimentary rocks, and as a secondary mineral in hydrothermal deposits. It is mostly found with other iron sulfides, particularly pentlandite ($(Fe,Ni)_9S_8$), but also commonly found associated with pyrite, marcasite (orthorhombic FeS_2), magnetite (Fe_3O_4) and chalcopyrite ($CuFeS_2$) (Deer et al, 1992; Belzile et al, 2004). These different minerals can all coexist within a grain of pyrrhotite or in contact with the grain (Uytenbogaardt, Burke, 1971). In hand sample, this mineral has a metallic luster and bronze brown, yellow, or reddish color. Microscopically, pyrrhotite is a monoclinic or pseudohexagonal anisotropic mineral with a pink cream or skin color in reflected light (Deer et al, 1992). Pyrrhotite has an unbalanced chemical formula $Fe_{1-x}S$, with × ranging from 0 (FeS) to 0.125 (Fe_7S_8).

[1] Excerpts from American Concrete Institute's technical notes on pyrrhotite-related distress in concrete, plus author's own addition.

Mechanism of Distress by: (1) Oxidation of Iron Sulfides (Primary Expansion Causing Surface Staining, Popout, Cracking), (2) Release of Sulfates and Internal Sulfate Attack (Secondary Expansion Causing Further Cracking)

It is well known from the literature that sulfide minerals are unstable in oxidizing conditions. According to Divet and Davy (1996), high pH conditions, such as those found in concrete, enhance iron sulfide oxidation. Upon exposure to water and oxygen, sulfide minerals (pyrite, pyrrhotite) oxidize to form acidic, iron oxides/hydroxides, and sulfate-rich by-products with an increase in solid volumes from the sulfide minerals to their oxidized products (Belzile et al. 2004, Rodrigues et al. 2012). The oxidation of ferrous iron (Fe^{2+}) produces ferric ions (Fe^{3+}) that can precipitate out of solution to form ferric hydroxide, if pH is not too low. Fe^{2+} is oxidized and precipitated as ferric oxyhydroxides, principally **ferrihydrite** [$Fe(OH)_3$] and **goethite** [FeO(OH)]. The sulfuric acid (sulfate and hydrogen ion, H_2SO_4) generated through oxidation reactions reacts with cement hydration products, e.g., with the portlandite [$Ca(OH)_2$], to form **gypsum** [$CaSO_4 \bullet 2H_2O$] (Grattan-Bellew and Eden 1975, Shayan 1998, Rodrigues et al. 2012), with calcium aluminate or monosulfoaluminate hydrates to form **ettringite [**$Ca_6Al_2(SO_4)_3(OH)_{12}{\cdot}26H_2O$**]**, or, **thaumasite** [$Ca_6[Si(OH)_6]_2(CO_3)_2(SO)_4)_2(H_2O)_{22}$] latter one if carbonate minerals are present. Both the processes of *oxidation of iron sulfides*, and *reactions between released sulfates and cement hydration products* are expansive in natures resulting in concrete deteriorations.

Figure 53 from various authors (e.g., Rodrigues et al. 2012, Oliveira et al., 2014, Willi and Zhoing 2016) summarizes mechanism of two-stage expansions resulting in concrete deterioration from: (a) *primary expansion due to oxidation of iron sulfide minerals to ferric oxyhydroxides, principally goethite and ferrihydrite and associated solid volumes' increases*, and (b) *secondary expansion due to internal sulfate attacks of released sulfate and hydrogen ions (sulfuric acid) from oxidation to cement hydration products*, e.g., calcium hydroxide and calcium sulfoaluminate hydrate to form gypsum (with a solid volume increase of 42) or more commonly due to formation of ettringite (with a solid volume increase of 172).

The above expansive mineral formation results in **rust staining and pop-outs at the aggregate site in milder cases most commonly associated with pyrite**, to **severe cracking and decreased strength due to internal sulfate attack in paste from released sulfates in the most severe cases associated with pyrrhotite**.

In the case of pyrrhotite, the degree of cracking damage correlates with the deterioration of the mineral and the quantity of resultant expansive sulfates in the paste. **Not all concretes with pyrrhotite in aggregates, however, result in deterioration**. As shown in the case studies in Table 4, the rate and extent of damage can be variable. The rate and severity of damage are dependent on a number of factors including: (a) the interaction between the particle and the surrounding host rock that forms the aggregate (Oliveira et al. 2014) and the concrete paste, (b) the concrete quality, (c) the environmental conditions to which the concrete element is exposed to (exposure to oxygen, moisture, and temperature), (d) crystal structure, (e) the mineral associations (more than one sulfide

minerals present), (f) concrete pH, (g) trace metal content, and (h) bacterial activity (Belzile et al. 2004). The extents of controlling factors are not yet fully understood in light of the limitations of reproducing the deterioration in the laboratory.

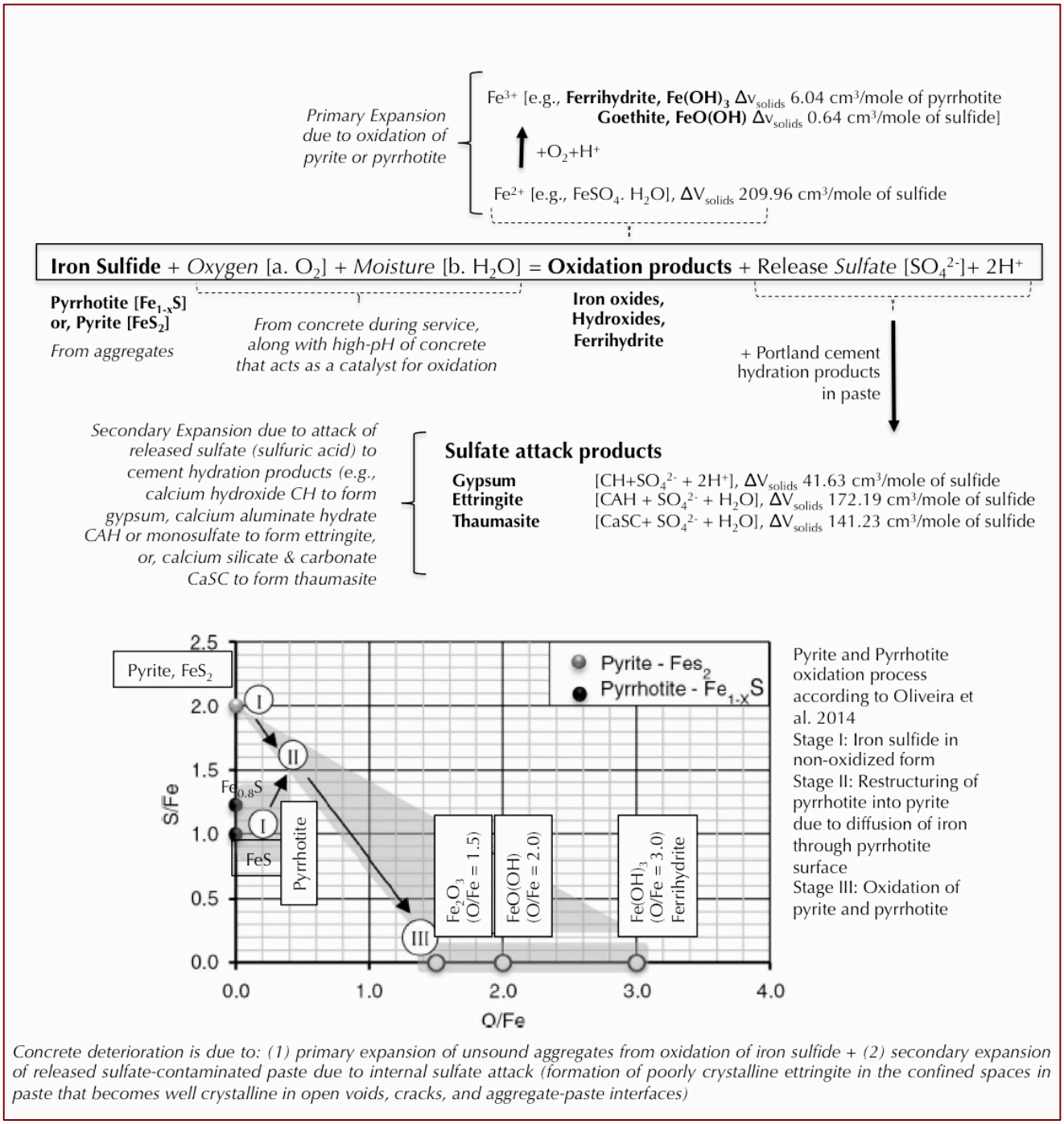

Figure 53: Mechanisms of oxidation of iron sulfide minerals in concrete according to various authors, and primary expansion due to oxidation of iron sulfide to various forms of iron oxides, hydroxides, ferrihydrite, followed by secondary expansions due to reactions between the released sulfates and hydrogen ions from oxidation reactions (sulfuric acid) and cement hydration products (calcium hydroxide, calcium aluminate, and monosulfoaluminate hydrate) to form ettringite (or thaumasite if carbonate ions are present).

Pyrrhotite Limit

Standardization of the amount of iron sulfide minerals that are considered acceptable in concrete aggregates is not well established. American, Canadian, British, and French standards for concrete aggregates mention iron sulfides and their related problems with use in concrete, but have not established acceptable limits of iron sulfide contents in aggregates. Limits have been established for total sulfur (S_T) by mass in French at 0.4%, European at 1%, or 0.1% if pyrrhotite is present. The limits as to the amount of pyrrhotite that would lead to damage has not been identified to date; this may be quite difficult because the reactivity of pyrrhotite may vary according to its crystallographic characteristics, while many factors are involved in this deleterious mechanism. No precise guidelines or methods have been proposed to evaluate the potential reactivity of sulfide containing aggregates.

Recently, an extensive investigation was carried out over a four-year period by researchers from four Canadian organizations aimed at developing an evaluation protocol for iron sulfide bearing aggregate (Rodrigues et al., 2016). The resulting recommended protocol involved a three-phase testing program including (a) measurement of total sulfur, (b) oxygen consumption determination, and (c) accelerated mortar bar expansion test. Limits are proposed for each phase of the protocol, but are in need of additional validation. These tests can be used as a general screening, but would need to be supplemented by further testing to identify the sulfate sulfur and the sulfate mineral type. Significant research is still needed to identify appropriate limits.

CASE STUDIES OF CONCRETE DETERIORATION DUE TO OXIDATION OF IRON SULFIDE MINERALS IN AGGREGATES

Examples of deterioration of concrete structures due to oxidation corrosion of iron sulfate minerals, with pyrrhotite date back to 1955, and span a range of aggregate types. Structural damage to buildings due to pyrite or pyrrhotite breakdown has been observed in many places around the world since the mid-1950s, including Ireland, Wales, Spain, Canada, Namibia, and Japan. In the United States, pyrite-induced swelling has been observed in Ohio, West Virginia, Pennsylvania, Missouri, Kansas, and Kentucky, and more recently thousands of homes in Connecticut have been affected by pyrrhotite in concrete foundations.

Following are summaries of cases studies on concrete deterioration around the world that are described due to unsoundness of aggregates containing iron sulfide minerals, all of which have concluded that expansions associated with oxidation of iron sulfide minerals followed by additional expansions associated with internal sulfate attacks between the released sulfates and cement hydration products have caused the deterioration in form of map cracking, heaving, displacement of affected elements, and in severe cases of crumbling of concrete elements. The last row is for oxidation of pyritic shale in the substrate causing heaving of structural elements, or, blistering of floor tiles when pyritic is present in the concrete aggregates at the surface of floor slab, but all other case studies are from pyrrhotite-oxidation related damages.

• Locality (References)	• Pyrrhotite containing rocks • Associated sulfide minerals	• Average sulfur content in aggregate • Pyrrhotite content	• Structure affected • Type of Damage • Time taken to manifest the damage	Proposed Mechanisms of Distress
• *Oslo, Norway* (Moum and Rosenqvist 1959)	• Sedimentary rocks (alum shales some with slight metamorphism) • Pyrite occurred with pyrrhotite	• 6% (highly variable), all shales that weathered 'explosively' due to oxidation contained more than 0.2% sulfur as monoclinic pyrrhotite. • Pyrrhotite content is related to rate of alteration of pyrite and rate of weathering of shale	• Foundation • Upheaval of foundation, cracking, crumbling, yellowish deposit of jarosite [$KFe_3(OH)_6(SO_4)_2$] and brown-iron oxide (Fe_2O_3. nH_2O) on weathered shales. • Within 9 months	Swelling of shale due to oxidation of pyrrhotite and internal sulfate attack from released sulfate; reactivity of alum shale and resultant damage increased with increasing pyrrhotite content, with no occurrence of damage when alum shale was free of pyrrhotite; acidic and sulfate-rich water percolated through alum shale has caused acid attack and internal sulfate attack in concrete
• *Trois-Rivières area, Quebec, Canada* (Tagnit-Hamou, et.al. 2005; Rodrigues, et.al. 2012; Duchesne and Benoit 2013)	• Quarried intrusive igneous rock anorthositic gabbro (norite) with different degrees of metamorphism • Pyrite and chalcopyrite. Only pyrrhotite showed signs of oxidation but pyrite and chalcopyrite were largely unaffected. A thin coating of iron carbonate (siderite) on sulfides provided carbonates to promoted thaumasite form of attack in addition to internal sulfate attack from pyrrhotite oxidation	• As low as 0.30% to 2.92% total sulfur by mass of aggregate in pyrrhotite-bearing coarse aggregates that have caused damage, all damaged concrete exceeded the European limit of 0.1% sulfur in aggregate when pyrrhotite is present by 3 times to as high as 30 times. • Less than 5 to 10 percent total sulfide minerals by volume, average 75% of sulfide minerals was pyrrhotite and lesser pyrite and chalcopyrite from a study of 223 house basements containing varying amounts of iron sulfide in gabbro coarse aggregate	• Residential foundations and commercial buildings. • Map cracking (cracks up to 40 mm in width) and yellowish or brownish staining), popouts of oxidized pyrrhotite with white rim of secondary reaction products, and open cracks more pronounced at the corners of the foundation blocks • More than 1000 to as high as estimated 4000 residential and commercial buildings were affected within 3 to 5 years after construction	Oxidation of sulfide minerals (mainly pyrrhotite) in anorthositic gabbro coarse aggregate in concrete has: (a) formed various "rust" minerals (e.g., ferric oxyhydroxides such as goethite FeO(OH), limonite, and ferrihydrite) and (b) released sulfuric acid/sulfates, which then reacted with cement hydration products resulting in further expansive formation of gypsum, ettringite, and thaumasite in concrete. Oxidation of pyrrhotite followed by internal sulfate attack of cement paste is the main mechanism of concrete deterioration.
• *Northeastern Connecticut, USA* (Wille and Zhong 2016)	• Foliated schist and gneissic metamorphic rocks, granofels, foliated quartz diorite in a hydrothermally altered vein from a particular quarry in Willington, CT (Becker's quarry). • Pyrrhotite as the predominant iron sulfide mineral present in metamorphic rocks containing quartz, plagioclase feldspar, micas, and garnet	• Average 2.54% sulfur in pyrrhotite-bearing quarry aggregate • Pyrrhotite was not detected in XRD analysis of quarry aggregate by Wille and Zhong due to possible presence below the 5% detection limit of XRD	• Residential foundations. • Map cracking, crumbling, deformation of wall, reddish-brown discoloration, whitish formation of secondary ettringite and thaumasite in the vicinity of surface cracks. Cores from foundation walls of houses showed noticeably lower compressive strengths (some no strength due to complete crumbling) compared to the cores from slabs, indicating possible effect of more oxidation in wall than slab and hence more damage in wall than slab • 10 to 20 years after construction, estimated	Primary expansion due to oxidation of pyrrhotite followed by secondary expansion due to internal sulfate attack by released sulfates

• Locality (References)	• Pyrrhotite containing rocks • Associated sulfide minerals	• Average sulfur content in aggregate • Pyrrhotite content	• Structure affected • Type of Damage • Time taken to manifest the damage	Proposed Mechanisms of Distress
			34,000 homes are at risk	
• *Catalan Pyrenees, Spain* (Araujo et al. 2008)	• Schist containing quartz, muscovite mica, chlorite and non-expansive illitic clay. • Pyrite and Pyrrhotite	• 2% sulfur (as SO_3 from XRF) in schist. • Predominantly pyrrhotite (S/Fe ratio 0.62 as opposed to 1.15 of pyrite) but XRD also detected some pyrite	• Tórán Dam • Map cracking and non-recoverable movements, more dramatic expansion in the downstream face of the dam for upstream displacement of the crest	Oxidation of pyrite and pyrrhotite forming surface stains of greyish brown iron hydroxides (goethite) and lighter-green potassium iron sulfates (jarosite), gypsum efflorescence from sulfate attack; and causing expansions, e.g., 6.04 cm^3/mol from primary expansion from oxidation of iron sulfides followed by 172.19 cm^3/mol from internal sulfate attack by reaction between released sulfates and cement phases
• *Central Pyrenees, Spain* (Ayora et al. 1998; Oliveira et al. 2014)	• Schist containing bands of pyrrhotite that created planes of weakness and present cracks that serve as preferential paths for entrance of oxygen thus aggregates containing pyrrhotite bands with cracks showed much more pronounced oxidation than the aggregates without cracks. • Pyrite	• Median sulfur (SO_3) content of 1.42% for rocks from a quarry that have known to cause severe damage when used as aggregate in dam	• Graus and Tavascan Dams • Map cracking, damage in downstream face and galleries of the Graus Dam due to severe cracking and movement	Alteration from acidic solution produced by weathering and oxidation of pyrrhotite in aggregates followed by expansion due to internal sulfate attack and formation of ettringite and gypsum. Characteristic ratios of 2.44 for the Fe/O ratio and of 2.63 for the S/O ratio in pyrrhotite marked critical limits that produced the activation and acceleration of pyrrhotite oxidation leading to an increase of expansive reactions and risk of structural damage.
• *Ottawa, Quebec City, Matane, and Montreal, Canada* (Quigley and Vogan 1970; Berard 1970; Berube et al. 1986; Penner et al. 1972) • *Ireland* • *Wales* (Hawkins and Pinches 1987) • *Marcellus Shale, USA* (Hoover and Lehmann 2009) • *Chattanooga Shale, Kentucky, USA* (Anderson 2008) • SW England in Cornwall and Devon	• Black shale containing pyrite (not pyrrhotite). Pyrite is most common in metamorphic and sedimentary rocks as either a primary mineral or a fine, widespread impregnation of subsequent origin. • Pyrite is frequently found in association with coal and shale deposits • Mundic (means mine waste) concrete blocks used in the foundations of thousands of 20th century homes in SW England, blocks were prepared using mine waste rocks as aggregates containing pyrite that has caused serious damage (Mundic decay) in foundations	The minimum amount of pyrite that will cause heaving problems is not known with certainty. Some reports describe difficulties with contents as low as 0.1 per cent by weight. In the Ottawa area heaving problems have been encountered only in rock formations with much higher pyrite contents, although a systematic sampling program has not been carried out. Pyrite weathering is a chemical-micro-biological oxidation process; some of the oxidation reactions are solely chemical, others are attributed to autotrophic bacteria of the ferrobacillus-thiobacillus group, and still others are both chemical and micro-biological.	• Foundation, basement floor above weathered pyritic substrate. Pyrite weathering was identified as early as 1950 as a major foundation problem in the U.S.A. in buildings dating back to 1920. • Pyrite oxidation in the Chattanooga Shale has caused serious foundation problems in numerous buildings and structures in Estill County, KY. • Heaving of pyritic substrate causes cracking, lifting of concrete floor slabs; differences in levels across floor slabs; cracking, buckling lifting of elements resting on the concrete floor slabs, doors, stairs, fixtures; cracking, bulging, movement of internal or external walls. • Blistering and de-bonding of vinyl tile from concrete floor is reported due to oxidation of pyritic aggregates at the surface of concrete floor (Shayan 1988)	Oxidation of pyrite in shale or coal causes formation of *gypsum* from reactions between (a) sulfates or sulfuric acid released from pyrite oxidation and calcium hydroxide component of cement hydration (if pyritic rock is used as aggregate in concrete), and/or (b) between sulfuric acid from oxidation and associated calcite in pyritic rocks cause heaving and associated volume changes. When calcite converts to gypsum, the volume increases by a factor of 2, but of greater importance is the force associated with the growth of gypsum crystals, which can be very high. When gypsum grows in rock under buildings it tends to form needle-like crystals that force the layers apart, resulting in much greater heave than would occur with simple volume expansion during formation. Another oxidation product found in all weathered pyritic materials is jarosite, $KFe_3(SO_4)_2(OH)_6$, recognized by its bright yellow-brown color. The calculated volume increase from pyrite to jarosite is 115 per cent, which is another main contributor to volume increase and heaving.

Table 4: Case studies on concrete deterioratios due to oxidation of iron sulfide minerals in aggregates.

PYRRHOTITE EPIDEMIC IN EASTERN CONNECTICUT

Figure 54 shows regional spread of the latest reported incident of widespread outbreak of deterioration of concrete due to pyrrhotite oxidation in the aggregate along northeastern Connecticut with many hundreds of homes being affected. Figures 55 through 58 show various manifestations of distress in the affected homes from various sources. Typical visual deterioration was in the form of map cracking, some causing deformation of the wall, extensive longitudinal to random cracking of the wall, reddish-brown discoloration, and whitish formation in the vicinity of surface cracking most of which are shown in Figures 55 to 58. Currently, much of the information available on this problem is limited to newspaper articles but the cause of deterioration has been confirmed by an investigation conducted at the University of Connecticut (Wille and Zhong, 2016) as oxidation of pyrrhotite present in the aggregate. In contrast to the problems encountered in Quebec, manifestation of the damage in Connecticut has taken as much as 10 to 20 years.

Most of the damage to date has been linked to one quarry operating in Willington, CT. The geology in the vicinity of the quarry is made up of metamorphic rocks predominately from two to three formations. The formations are comprised predominantly of foliated schists and gneissic rock, granofels, and a foliated quartz diorite. Quartz, plagioclase or oligoclase are primary minerals with micas, and noted are garnet and graphite as common accessory minerals. Iron sulfides are found predominately as pyrrhotite.

Wille and Zhong (2016) did an extensive mechanical, mineralogical, microstructural and chemical tests on the core samples taken from 7 houses and did visual inspection of 14 additional houses, from which the primary findings they found are:

a) Ubiquitous in all cases of concrete deterioration are the presence of pyrrhotite in aggregates and their oxidation products, such as goethite [FeO(OH)], and ferrihydrite [$Fe(OH)_3$];
b) Sodium sulfate and hydrated forms of sodium sulfate (thenardite and mirabilite) based white efflorescence deposits at the vicinity of surface cracks;
c) Porous paste and aggregate-paste interfaces, abundance of secondary ettringite crystallization in aggregate-paste interfaces and other open spaces; cracking is often associated with these open spaces and either within the voids or extends into cement paste
d) Oxidation of pyrrhotite in the presence of water and oxygen is reported to have caused the distress by expansive formation of ferrihydrite, and subsequent release of sulfate to paste, sulfate-aluminate reactions with aluminate phases in paste, and expansive formation of secondary ettringite crystals.
e) In the presence of carbonate ions secondary thaumasite crystallization is also noted.

In light of the present study it is concluded that the above finding of Wille and Zhong (2016) are all in the same line as the present study. Additionally, this study found formation of poorly crystalline secondary ettringite in the confined areas in paste as ettringite infested paste to be the breeding ground for internal sulfate attack that has

caused the expansion and cracking. Relatively well formed secondary ettringite in voids and cracks are the result of exposure to moisture of sulfate-contaminated paste. All these information are primarily obtained from optical microscopy, which is an indispensable tool for this type of investigation, which Wille and Zhong (2016) did not do. The host rock is garnetiferous quartzo-feldspathic gneiss (again, determined from optical microscopy) containing pyrrhotite having sulfur (as SO_3) levels from 2 percent in light brown gneiss to as high as 10 percent in predominant dark gray gneiss particles, giving a total bulk sulfate (SO_3) content of 1.45 percent in the concrete, which is more than 3 times the sulfate in a normal Portland cement concrete without any iron sulfide contaminant. As high as 8 percent pyrrhotite is found from XRD analysis of dark gray gneiss. Pyrrhotite oxidation has readily released sulfates and contaminated the Portland cement paste as detected from high (4 to 6.5%) sulfate contents in paste as opposed to normal less than 1% sulfate found in the paste of a Portland cement concrete containing no iron sulfide contaminants. Ready release of sulfate has promoted internal sulfate attack and subsequent secondary expansion of paste with additional cracking.

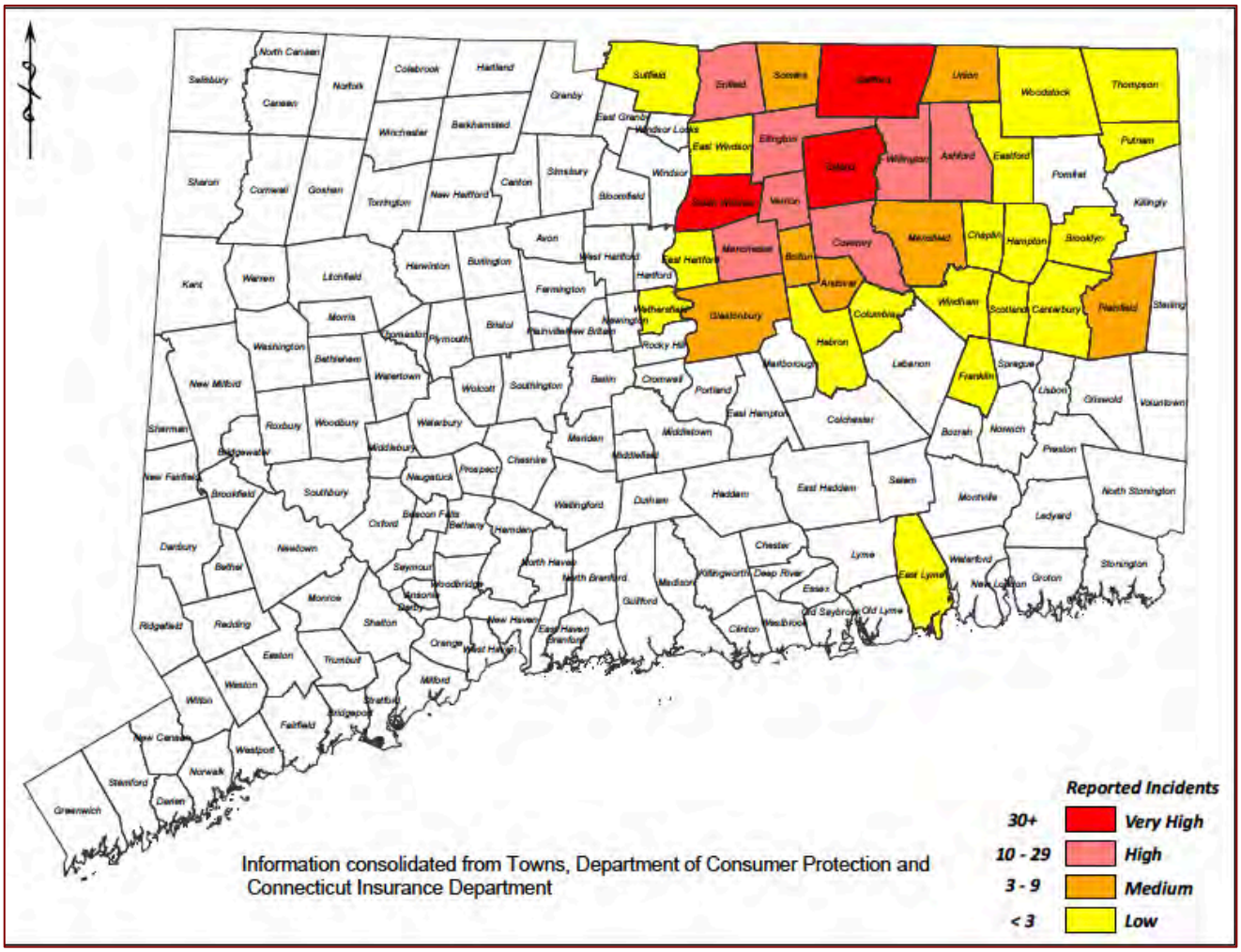

Figure 54: Reported incidences of pyrrhotite-related concrete deterioration in northeastern Connecticut. Note the present residential house in Ellington falls under high-risk zone for concrete containing aggregates reportedly supplied from the Becker's quarry.

Figure 55: Cracking of concrete foundations in Connecticut due to oxidation of pyrrhotite bearing aggregates in concrete. Notice wide cracks in the top row as well as a network of numerous fine cracks in the wall in the bottom right row all from pyrrhotite oxidation and associated expansion of concrete.

Figure 56: Cracking of concrete foundations in Connecticut due to oxidation of pyrrhotite bearing aggregates in concrete. Notice dark reddish brown rust staining on the wall and associated cracking in the top row from pyrrhotite oxidation and formation of ferric oxy-hydroxide oxidation products (goethite, limonite, ferrihydrite rust minerals). Notice wide cracks in the 2nd through 4th rows from pyrrhotite oxidation and associated expansion of concrete.

Figure 57: Cracking of concrete foundation in Connecticut due to oxidation of pyrrhotite bearing aggregates in concrete. Notice wide cracks in the foundation walls, extensive cracking of walls in the top left photo all reportedly from pyrrhotite oxidation and associated expansion of concrete.

Figure 58: Cracking of concrete foundation in Connecticut due to oxidation of pyrrhotite bearing aggregates in concrete. Notice extensive cracking of foundation in all photos reportedly from pyrrhotite oxidation and associated expansion of concrete.

CONCLUSIONS

Oxidation of pyrrhotite in concrete aggregates has caused severe damage to concrete foundations in several thousands of residential and commercial buildings in Quebec, Canada, in three concrete dams in Central Pyrenees, Spain, and anticipated to have deteriorated several thousands of residential foundations in eastern Connecticut that have reportedly received concrete containing pyrrhotite-bearing aggregates from the Becker's quarry in Ellington, CT. The amount of pyrrhotite required to cause damage has been found to be as low as 0.3% (total sulfur by mass of aggregate). Recommendations in Europe limit the sulfur content of sulfide-containing aggregates to 1% sulfur by mass unless the presence of pyrrhotite is confirmed in which case the limit is just 0.1% sulfur by mass. Limits on the sulfur contents in aggregates have not yet been imposed in North America.

Based on comprehensive study of cracked foundation from the residential foundation of the current project situated within the pyrrhotite-infested zone, the following conclusions are drawn regarding the details of deterioration:

1. Observed cracking and reported crumbling of concrete foundation wall is determined to be due oxidation of unsound pyrrhotite grains in crushed quartzo-feldspathic and biotitic gneiss coarse aggregate particles in the presence of oxygen and moisture during service in concrete. The host rock for pyrrhotite mineralization used as coarse aggregate in concrete is the predominant dark gray garnetiferous quartzo-feldspathic and biotitic gneiss having alternating bands of quartz-feldspar and micaceous (mostly biotite less muscovite) minerals and garnet poikiloblast (i.e. containing inclusions) and lesser amounts of light brown (more oxidized rusty) gneiss having more quartz and less pyrrhotite than the dark gray stones.
2. Sulfur (as SO_3) contents in the pyrrhotite-bearing crushed gneiss aggregates are from 2 percent in light brown gneiss to as high as 10 percent in predominant dark gray gneiss particles, or perhaps even higher, giving a total bulk sulfate (SO_3) content of 1.45 percent in the concrete, which is more than 3 times the sulfate in a normal Portland cement concrete without any iron sulfide contaminant. As high as 8 percent pyrrhotite is found from XRD analysis of dark gray gneiss.
3. Oxidation of pyrrhotite has formed ferrihydrite with an expansion of unsound crushed gneiss coarse aggregate causing extensive cracking in many particles having cracks extending from affected the particles to paste. The typical gneissose texture of quarried aggregates has facilitated crack formation during expansion due to the presence of inherent planes of weakness along the micaceous bands in gneiss. Reddish brown rust stain found in many distressed foundations are due to pyrrhotite (and also pyrite) oxidation and formation of iron oxy-hydroxides (e.g., goethite, limonite) and ferrihydrites.
4. Evidence of pyrrhotite oxidation is confirmed from: (a) detection of ferrihydrite in XRD (however, no classic rust stain of iron oxy-hydroxides was found in the core received) as well as (b) from SEM-EDS studies of lower than stoichiometric S/Fe ratio of pyrrhotite (mostly <0.50). Microstructural evidence of

oxidation-related expansion of unsound aggregate is found from extensive cracking of many of these crushed gneiss coarse aggregate particles often extending into the paste.

5. Pyrrhotite oxidation has readily released sulfates and contaminated the Portland cement paste as detected from high (4 to 6.5%) sulfate contents in the SEM-EDS analyses of paste as opposed to normal less than 1% sulfate found in the paste of a Portland cement concrete containing no iron sulfide contaminants. Ready release of sulfate has promoted internal sulfate attack and subsequent secondary expansion of paste with additional cracking.
6. Sulfates released from pyrrhotite oxidation have reacted with cement hydration products (e.g., calcium hydroxide, calcium aluminate hydrate, calcium monosulfoaluminate) and formed poorly crystalline or perhaps colloidal form of ettringite within the confined spaces in paste with the resultant secondary expansion of paste and additional cracking within the paste and around aggregate-paste interfaces. Presence of excess sulfates, moisture, and open spaces of air-voids and cracks – all three conditions have facilitated dissolution and precipitation of well-crystallized fibrous secondary ettringite in voids and occasionally in cracks that were visible in optical microscopy and SEM analyses.
7. Evidence of internal sulfate attack in paste came first from the paste chemistry i.e. (a) very high sulfate (SO_3) content of paste from SEM-EDS studies, and then from various microstructural evidences in optical and scanning electron microscopy, e.g., (b) ettringite-infested paste containing poorly crystalline (perhaps some colloidal) form of ettringite, (c) well-formed secondary ettringite crystallization in aggregate-paste interfaces, microcracks, and air-voids, and (d) gaps between aggregates due to expansion of paste.
8. Relative roles of primary expansion of unsound aggregates due to pyrrhotite oxidation and secondary expansion of paste due to internal sulfate attack in the overall distress of foundation depend on various factors, e.g., proportion of pyrrhotite (and total available sulfate), moisture condition during service, consolidation and degree of impermeability of concrete to moisture ingress, etc.
9. In light of the observed severe cracking of the foundation wall all throughout the thickness, and its anticipated progress with potential worsening of condition with time, replacement of the wall is the only viable option with particular emphasis to avoid use of any aggregate from the subject quarry or elsewhere that contains pyrrhotite, at least anywhere near the amounts that have caused the cracking.
10. If the pyrrhotite-bearing crushed gneiss coarse aggregate found in this concrete was indeed from the Becker's quarry in Ellington, CT (as reported for other foundations undergoing similar pyrrhotite-oxidation-related distress), then due to the known geology of pyrrhotite mineralization in the hydrothermal vein in which this quarry is situated, and its known devastating effects when used in concrete from case studies of multiple homes (Wille and Zhong 2016) including the present one, use of crushed stone from this quarry for concrete aggregate should be abandoned, or should only be used after extensive evaluation of aggregates for the presence of pyrrhotite (e.g., from magnetic test, total sulfur test from XRF, XRD detection of pyrrhotite) and its potential release of sulfate in an accelerated oxidation test of aggregates.

11. Aggregate to be used in a new foundation must be verified for the possible presence of any unsound constituents, including iron sulfide minerals, e.g., (a) from XRD analysis of quarried stones to detect the amount and speciation of iron sulfide minerals present, (b) from XRF analysis to detect the total sulfur (as SO_3) content of quarried stones, (d) from accelerated oxidation test to detect the rate and level of sulfates that can be released from aggregates, and (e) even from a magnetic test to separate weakly magnetic pyrrhotite grains from other non-magnetic iron sulfide minerals. Since there is no established consensus on pyrrhotite limit above which potential for oxidation-related distress occur, in fact as low as 0.3% pyrrhotite in host rock has reportedly shown distress in concrete, the best solution is to avoid aggregates containing pyrrhotite without further laboratory verification of its potential unsoundness in concrete, such as from expansion of concrete prism tests.

REFERENCES

ACI Committee Report 201.2R, Guide to Durable Concrete, ACI Manual of Concrete Practice, Vol. 1, American Concrete Institute, 2008.

Anderson, W.H., Foundation Problems and Pyrite Oxidation in the Chattanooga Shale, Estill County, Kentucky, Kentucky Geological Survey Report of Investigation, 2008.

Araujo, G.S., Chinchon, S., and Aguado, A., Evaluation of the behavior of concrete gravity dams suffering from internal sulfate attack, *Revista ibracon de estruturas e materials* (Ibracon Structures and Materials Journal), Vol. 1, No. 1, pp 84-112, 2008.

ASTM C 856 "Standard Practice for Petrographic Examination of Hardened Concrete," Vol. 4.02, ASTM International, West Conshohocken, PA, 2014.

Ayora, C., Chinchon, S., Aguado, A. and Guirado, F. (1998). Weathering of iron sulfides and concrete alteration: thermodynamic model and observation in dams from Central Pyrenees, Spain. *Cement and Concrete Research*, Vol. 28, Issue 4, pp. 1223–1235.

Belzile, N., Y.W. Chen, M.F.Cai, and Y. Li. (2004). A review on pyrrhotite oxidation. J., *Geochem. Explor.*, Vol. 84, pp. 65–76.

Bérard, J., Black shale heaving at Ottawa, Canada: Discussion. Canadian Geotechnical Journal 1970. 7(2): 113-114.

Bérubé, M.A., Locat, J., Gélinas, P., Chagon, J.Y., and Lefrancois, P., Heaving of black shale in Québec City. Canadian Journal of Earth Sciences 1986. 23: 1774-1781.

Capitol Region Council of Governments (CRCOG) Meeting on July 2016

Casanova, I; Agulló, L.; Aguado, A. Aggregate Expansivity Due To Sulfide Oxidation - I. Reaction System And Rate Model, Cement And Concrete Research, Vol. 26, No. 7, 1996, P. 993-998.

Casanova, I.; Aguado, A.; Agulló, L. Aggregate Expansivity due to Sulfide Oxidation - II Physico-Chemical Modeling of Sulfate Attack, Cement and Concrete Research, vol. 27, no. 11, 1997, p. 1627-1632

Chinchón-Payá, S.; Aguado, A.; Chinchón, S., A comparative investigation of the degradation of pyrite and pyrrhotite under simulated laboratory conditions. Engineering Geology, v. 127, p. 75-80, 2012

Chinchón, J. S., Ayora, C., Aguado, A. and Guirado, F. (1995). Influence of weathering of iron sulfides contained in aggregates on concrete durability, *Cement and Concrete Research*, Vol. 25, No. 6, pp. 1264–1272.

Connecticut Geological and Natural History Survey, DEP, in cooperation with the U.S. Geological Survey, 2000, Bedrock Geology of Connecticut, data format: shape file, file name: bedrock, downloaded from: http://magic.lib.uconn.edu/cgi-bin/MAGIC_DBsearch2.pl? Geography=37800&Loc=0000 on 9/18/2003, scale 1:50,000.

Côté, F., Bérard, J., Roux, R. Cas de réactivité et de gonflement de remblais granulaires riches en shale pyriteux. Collection Environment et Géologie, APGGQ 1991. 12: 225-246. 93

Côté, F., Expansion de shales pyriteux. M.Sc. thesis, Département de genie mineral, École Polytechnique de Montréal, Montréal,Qué, 1990.

CSA A23.1-14/A23.2-14, Appendix P. "Concrete Materials and Methods of Concrete Construction/Test Methods and Standard Practices for Concrete," Canadian Standards Association, Mississauga, ON, Canada, 2014, pp.668.

Deer, W., Howie, R. and Zussman, J. (1992). An introduction to the rock-forming minerals. 2nd Edition. Pearson education limited, England, 696p.

Duchesne, J. and Fournier, B. (2011). Petrography of concrete deteriorated by weathering of sulphide minerals. *International Cement Microscopy Association Conference*, San Francisco, USA, April 2011. EN-12620 (2003) Aggregates for concrete.

Duchesne, J., Benoît, F., Deterioration of concrete by the oxidation of sulphide minerals in the aggregate. Journal of Civil Engineering and Architecture 2013. 7(8): 922-931.EN-12620 (2003) Aggregates for concrete.

Grattan-Bellew, P.E. and W.J. Eden. (1975). Concrete Deterioration and Floor Heave Due to Biogeochemical Weathering of Underlying Shale, *Canadian Geotechnical Journal*, Vol. 12, pp. 372–378.

Hawkins, A.B., and Pinches, G.M., Cause and significance of heave at Llandough Hospital, Cardiff—a case history of ground floor heave due to gypsum growth, Quarterly Journal of Engineering Geology and Hydrogeology, 20, 41-57, 1, 1987.

Hoover, S.E., and Lehmann, D., The expansive effects of concentrated pyritic zones within the Devonian Marcellus Shale Formation of North America, Quarterly Journal of Engineering Geology and Hydrogeology (2009) 42 (2): 157-164.

Jana, D., "Sample Preparation Techniques in Petrographic Examinations of Construction Materials: A State-of-the-art Review", *Proceedings of the 28th Conference on Cement Microscopy*, International Cement Microcopy Association, Denver, Colorado, pp. 23-70, 2006.

Jana, D., Concrete deterioration from pyrite staining, sewer gases, and chimney flue gases – Case studies showing microstructural similarities, Proc. of the 30th Conference on Cement Microscopy, International Cement Microscopy Association, Reno, Nevada, 2008.

Jana, D., DEF and ASR in Concrete – A Systematic Approach from Petrography, Proc. of the 30th Conference on Cement Microscopy, International Cement Microscopy Association, Reno, Nevada, 2008.

Lee, H., Cody, R.D., Cody, A.M., Spry, P.G., The formation and role of ettringite in Iowa highway concrete deterioration. Cement and Concrete Research 2005. 35: 332-343.

Mahoney, J., Aggregates Containing Pyrrhotite, Executive Director, Connecticut Transportation Institute, PowerPoint Presentation.

Marcelino, A.P., Calixto, J.M., Gumieri, A.G., Ferreira, M.C., Caldeira C.L., Silva, M.V., and Costa A.L., Evaluation of pyrite and pyrrhotite in concretes, *Revista ibracon de estruturas e materials* (Ibracon Structures and Materials Journal), Vol. 9, No. 3, 2016.

Moum, J., Rosenqvist, I.Th.. 1959. Sulfate Attack on Concrete in the Oslo Region, *Journal of the American Concrete Institute*, 56-18, pp. 257-264.

Oliveira, I., Cavalaro, S.H.P., Aguado, A. (2014). Evolution of pyrrhotite oxidation in aggregates for concrete, *Materiales De Construccion*, Vo. 64, Issue 316, e038.

Penner, E., Eden, W.J., Grattan-Bellew, Expansion of pyritic shales, NRC Publication archive, Canadian Building Digest, CBD 152, 1972.

Quigley, R.M., Vogan, R.W., Black shale heaving at Ottawa, Canada. Canadian Geotechnical Journal 1970. 7(2): 106-112.

Rodgers, John, compiler, 1985. Bedrock Geological Map of Connecticut: Connecticut Geological and Natural History Survey. Hartford, Connecticut. 2 sheets, scale 125,000.

Rodrigues, A., Duchesne, J., Fournier, B. 2015. A new accelerated mortar bar test to assess the potential deleterious effect of sulfide-bearing aggregate in concrete. *Cement and Concrete Research*, 73: 96-110.

Rodrigues, A., Duchesne, J., Fournier, B. 2016 : Quantitative assessment of the oxidation potential of sulfide-bearing aggregates in concrete using an oxygen consumption test. *Cement and Concrete Composites*, 67: 93-100.

Rodrigues, A., Duchesne, J., Fournier, B. et al. 2012. Mineralogical and chemical assessment of concrete damaged by oxidation of sulphide-bearing aggregates. *Cement and Concrete Research*, 42: 1336-47.

Rodrigues, A., Duchesne, J., Fournier, B., Durand, B., Shehata, M., Rivard, P. 2016. Evaluation protocol for concrete aggregates containing iron sulfide minerals. *ACI Materials Journal*, 113 (3): 349-359.

Shayan, A., Deterioration of a concrete surface due to the oxidation of pyrite contained in pyritic aggregate. Cement and Concrete Research 1988. 18: 723-730.

Tagnit-Hamou, A., M. Saric-Coric and P. Rivard. (2005). Internal deterioration of concrete by oxidation of pyrrhotitic aggregates, Cement and Concrete Research, Vol. 35, p. 99–107.

Uytenbogaardt. W., Burke, E.A.J.. Tables for Microscopic Identification of Ore Minerals. Amsterdam, Netherlands: Elsevier Publishing Company. Pp. 139, 1971.

Wille, K. and Zhong, R. 2016. "Investigating the deterioration of basement walls made of concrete in CT." University of Connecticut, Storrs, CT 06269. 93 p.

✪ ✪ ✪ END OF TEXT ✪ ✪ ✪

END OF REPORT[2]

[2] The CMC logo is made using a lapped polished section of a 1930's concrete from an underground tunnel in the U.S. Capitol.